

Performance of Missing Transverse Momentum Reconstruction in Proton-Proton Collisions at $\sqrt{s} = 7$ TeV with ATLAS

The ATLAS Collaboration

CERN, 1211 Geneva 23, Switzerland

December 6, 2011

Abstract. The measurement of missing transverse momentum in the ATLAS detector, described in this paper, makes use of the full event reconstruction and a calibration based on reconstructed physics objects. The performance of the missing transverse momentum reconstruction is evaluated using data collected in pp collisions at a centre-of-mass energy of 7 TeV in 2010. Minimum bias events and events with jets of hadrons are used from data samples corresponding to an integrated luminosity of about 0.3 nb^{-1} and 600 nb^{-1} respectively, together with events containing a Z boson decaying to two leptons (electrons or muons) or a W boson decaying to a lepton (electron or muon) and a neutrino, from a data sample corresponding to an integrated luminosity of about 36 pb^{-1} . An estimate of the systematic uncertainty on the missing transverse momentum scale is presented.

1 Introduction

In a collider event the missing transverse momentum is defined as the momentum imbalance in the plane transverse to the beam axis, where momentum conservation is expected. Such an imbalance may signal the presence of unseen particles, such as neutrinos or stable, weakly-interacting supersymmetric (SUSY) particles. The vector momentum imbalance in the transverse plane is obtained from the negative vector sum of the momenta of all particles detected in a pp collision and is denoted as missing transverse momentum, \vec{E}_T^{miss} . The symbol E_T^{miss} is used for its magnitude.

A precise measurement of the missing transverse momentum, E_T^{miss} , is essential for physics at the LHC. A large E_T^{miss} is a key signature for searches for new physics processes such as SUSY and extra dimensions. The measurement of E_T^{miss} also has a direct impact on the quality of a number of measurements of Standard Model (SM) physics, such as the reconstruction of the top-quark mass in $t\bar{t}$ events. Furthermore, it is crucial in the search for the Higgs boson in the decay channels $H \rightarrow WW$ and $H \rightarrow \tau\tau$, where a good E_T^{miss} measurement improves the reconstruction of the Higgs boson mass [1].

This paper describes an optimized reconstruction and calibration of E_T^{miss} developed by the ATLAS Collaboration. The performance achieved represents a significant improvement compared to earlier results [2] presented by ATLAS. The optimal reconstruction of E_T^{miss} in the ATLAS detector is complex and validation with data, in terms of resolution, scale and tails, is essential. A number of data samples encompassing a variety of event topologies are used. Specifically, the event samples used to assess the quality of the E_T^{miss} reconstruction are: min-

imum bias events, events where jets at high transverse momentum are produced via strong interactions described by Quantum Chromodynamics (QCD) and events with leptonically decaying W and Z bosons. This allows the full exploitation of the detector capability in the reconstruction and calibration of different physics objects and optimization of the E_T^{miss} calculation. Moreover, in events with $W \rightarrow \ell\nu$, where ℓ is an electron or muon, the E_T^{miss} performance can be studied in events where genuine E_T^{miss} is present due to the neutrino, thus allowing a validation of the E_T^{miss} scale. In simulated events, the genuine E_T^{miss} , $E_T^{\text{miss, True}}$, is calculated from all generated non-interacting particles in the event and it is also referred to as true E_T^{miss} in the following.

An important requirement on the measurement of E_T^{miss} is the minimization of the impact of limited detector coverage, finite detector resolution, the presence of dead regions and different sources of noise that can produce fake E_T^{miss} . The ATLAS calorimeter coverage extends to large pseudorapidities¹ to minimize the impact of high energy particles escaping in the very forward direction. Even so, there are inactive transition regions between different calorimeters that produce fake E_T^{miss} . Dead and noisy readout channels in the detector, if present, as

¹ ATLAS uses a right-handed coordinate system with its origin at the nominal interaction point (IP) in the centre of the detector and the z -axis coinciding with the axis of the beam pipe. The x -axis points from the IP to the centre of the LHC ring, and the y axis points upward. Cylindrical coordinates (r, ϕ) are used in the transverse plane, ϕ being the azimuthal angle around the beam pipe. The pseudorapidity is defined in terms of the polar angle θ as $\eta = -\ln \tan(\theta/2)$.

well as cosmic-ray and beam-halo muons crossing the detector, will produce fake E_T^{miss} . Such sources can significantly enhance the background from multi-jet events in SUSY searches with large E_T^{miss} or the background from $Z \rightarrow \ell\ell$ events accompanied by jets of high transverse momentum (p_T) in Higgs boson searches in final states with two leptons and E_T^{miss} . Cuts are applied to clean the data against all these sources (see Section 3), and more severe cuts to suppress fake E_T^{miss} are applied in analyses for SUSY searches, after which, for selected events with high- p_T jets, the tails of the E_T^{miss} distributions are well described by MC simulation [3].

This paper is organised as follows. Section 2 gives a brief introduction to the ATLAS detector. Section 3 and Section 4 describe the data and Monte Carlo samples used and the event selections applied. Section 5 outlines how E_T^{miss} is reconstructed and calibrated. Section 6 presents the E_T^{miss} performance for data and Monte Carlo simulation, first in minimum bias and jet events and then in Z and W events. The systematic uncertainty on the E_T^{miss} absolute scale is discussed in Section 7. Section 8 describes the determination of the E_T^{miss} scale in-situ using $W \rightarrow \ell\nu$ events. Finally, the conclusions are given in Section 9.

2 The ATLAS Detector

The ATLAS detector [1] is a multipurpose particle physics apparatus with a forward-backward symmetric cylindrical geometry and near 4π coverage in solid angle. The inner tracking detector (ID) covers the pseudorapidity range $|\eta| < 2.5$, and consists of a silicon pixel detector, a silicon microstrip detector (SCT), and, for $|\eta| < 2.0$, a transition radiation tracker (TRT). The ID is surrounded by a thin superconducting solenoid providing a 2 T magnetic field. A high-granularity lead/liquid-argon (LAr) sampling electromagnetic calorimeter covers the region $|\eta| < 3.2$. An iron/scintillator-tile calorimeter provides hadronic coverage in the range $|\eta| < 1.7$. LAr technology is also used for the hadronic calorimeters in the end-cap region $1.5 < |\eta| < 3.2$ and for both electromagnetic and hadronic measurements in the forward region up to $|\eta| < 4.9$. The muon spectrometer surrounds the calorimeters. It consists of three large air-core superconducting toroid systems, precision tracking chambers providing accurate muon tracking out to $|\eta| = 2.7$, and additional detectors for triggering in the region $|\eta| < 2.4$.

3 Data samples and event selection

During 2010 a large number of proton-proton collisions, at a centre-of-mass energy of 7 TeV, were recorded with stable proton beams as well as nominal magnetic field conditions. Only data with a fully functioning calorimeter, inner detector and muon spectrometer are analysed.

Cuts are applied to clean the data sample against instrumental noise and out-of-time energy deposits in the calorimeter (from cosmic-rays or beam-induced background). Topological clusters reconstructed in the calorimeters (see Section 5.1) at the electromagnetic energy (EM) scale² are used as the inputs to the jet finder [4]. In this paper the anti- k_t algorithm

[5], with distance parameter $R = 0.6$, is used for jet reconstruction. The reconstructed jets are required to pass basic jet-quality selection criteria. In particular events are rejected if any jet in the event with transverse momentum $p_T > 20$ GeV is caused by sporadic noise bursts in the end-cap region, coherent noise in the electromagnetic calorimeter or reconstructed from large out-of-time energy deposits in the calorimeter. These cuts largely suppress the residual sources of fake E_T^{miss} due to those instrumental effects which remain after the data-quality requirements.

The 2010 data sets used in this paper correspond to a total integrated luminosity [6, 7] of approximately 600 nb^{-1} for jet events and to 0.3 nb^{-1} for minimum bias events. Trigger and selection criteria for these events are described in Section 3.1. For the $Z \rightarrow \ell\ell$ and $W \rightarrow \ell\nu$ channels, the samples analysed correspond to an integrated luminosity of approximately 36 pb^{-1} . Trigger and selection criteria, similar to those developed for the W/Z cross-section measurement [8], are applied. These criteria are described in Sections 3.2 and 3.3.

3.1 Minimum bias and di-jet event selection

For the minimum bias events, only the early period of data taking, with a minimal pile-up contribution, is studied. Selected minimum bias events were triggered by the minimum bias trigger scintillators (MBTS), mounted at each end of the detector in front of the LAr end-cap calorimeter cryostats [9].

Events in the QCD jet sample are required to have passed the first-level calorimeter trigger, which indicates a significant energy deposit in a certain region of the calorimeter, with the most inclusive trigger with a nominal p_T threshold at 15 GeV. The event sample used in this analysis consists of two subsets of 300 nb^{-1} each, corresponding to two periods with different pile-up and trigger conditions³. One subset corresponds to the periods with lower pile-up conditions with, on average, 1 to 1.6 reconstructed vertices per event. The other subset corresponds to the periods with higher pileup conditions, where the peak number of visible inelastic interactions per bunch crossing goes up to 3. In the following, di-jet events are used, selected requiring the presence of exactly two jets with $p_T > 25$ GeV and $|\eta| < 4.5$. Jets are calibrated with the local hadronic calibration (see Section 5.1).

For each event, at least one good primary vertex is required with a z displacement from the nominal pp interaction point less than 200 mm and with at least five associated tracks. After selection, the samples used in the analysis presented here correspond to 14 million minimum bias events and 13 million di-jet events.

3.2 $Z \rightarrow \ell\ell$ event selection

Candidate $Z \rightarrow \ell\ell$ events, where ℓ is an electron or a muon, are required to pass an e/γ or muon trigger with a p_T threshold between 10 and 15 GeV, where the exact trigger selection varies

by electromagnetic showers. It does not correct for the lower energy hadron shower response nor for energy losses in the dead material.

³ Pile-up in the following refers to the contribution of additional pp collisions superimposed on the hard physics process.

² The EM scale is the basic calorimeter signal scale for the ATLAS calorimeters. It provides the correct scale for energy deposited

depending on the data period analysed. For each event, at least one good primary vertex, as defined above, is required.

The selection of $Z \rightarrow \mu\mu$ events requires the presence of exactly two good muons. A good muon is defined to be a muon reconstructed in the muon spectrometer with a matched track in the inner detector with transverse momentum above 20 GeV and $|\eta| < 2.5$ [10]. Additional requirements on the number of hits used to reconstruct the track in the inner detector are applied. The z displacement of the muon track from the primary vertex is required to be less than 10 mm. Isolation cuts are applied around the muon track.

The selection of $Z \rightarrow ee$ events requires the presence of exactly two identified electrons with $|\eta| < 2.47$, which pass the “medium” identification criteria [8, 11] and have transverse momenta above 20 GeV. Electron candidates in the electromagnetic calorimeter transition region, $1.37 < |\eta| < 1.52$, are not considered for this study. Additional cuts are applied to remove electrons falling into regions where the readout of the calorimeter was not fully operational.

In both the $Z \rightarrow ee$ and the $Z \rightarrow \mu\mu$ selections, the two leptons are required to have opposite charge and the reconstructed invariant mass of the di-lepton system, $m_{\ell\ell}$, is required to be consistent with the Z mass, $66 < m_{\ell\ell} < 116$ GeV.

With these selection criteria, about 9000 $Z \rightarrow ee$ and 13000 $Z \rightarrow \mu\mu$ events are selected. The estimated background contribution to these samples is less than 2% in both channels [8].

3.3 $W \rightarrow \ell\nu$ event selection

Lepton candidates are selected with lepton identification criteria similar to those used for the Z analysis. The differences for the selection of $W \rightarrow e\nu$ events are that the “tight” electron identification criteria [11, 8] are used and an isolation cut is applied on the electron cluster in the calorimeter to reduce contamination from QCD jet background. The event is rejected if it contains more than one reconstructed lepton. The E_T^{miss} , calculated as described in Section 5, is required to be greater than 25 GeV, and the reconstructed lepton- E_T^{miss} transverse mass, m_T , is required to be greater than 50 GeV.

With these selection criteria, about 8.5×10^4 $W \rightarrow e\nu$ and 1.05×10^5 $W \rightarrow \mu\nu$ events are selected. The background contribution to these samples is estimated to be about 5% in both channels [8].

4 Monte Carlo simulation samples

Monte Carlo (MC) events are generated using the PYTHIA6 program [12] with the ATLAS minimum bias tune (AMBT1) of the PYTHIA fragmentation and hadronisation parameters [13]. The generated events are processed with the detailed GEANT4 [14] simulation of the ATLAS detector.

The minimum bias MC event samples are generated using non-diffractive as well as single- and double-diffractive processes, where the different components are weighted according to the cross-sections given by the event generators.

The jet MC samples, generated using a 2-to-2 QCD matrix element and subsequent parton shower development, are used for comparison with the two subsets of data taken with different

pile-up conditions. In the earlier sample the fraction of events with at least two observed interactions is at most of the order of 8 – 10 %, while in the sample taken later in 2010 this fraction ranges from 10 % to more than 50 %. These samples are generated in the p_T range 8 – 560 GeV, in separated parton p_T bins to provide a larger statistics also in the high- p_T bins. Each sample is weighted according to its cross-section.

MC events for the study of SM backgrounds in $Z \rightarrow \ell\ell$ and $W \rightarrow \ell\nu$ analyses are also generated using PYTHIA6. The only exceptions are the $t\bar{t}$ background and the $W \rightarrow e\nu$ samples used in Section 8.2, which are generated with the MC@NLO program [15]. For the study of the total transverse energy of the events, samples produced with PYTHIA8 [16] are used as well.

MC samples were produced with different levels of pile-up in order to reflect the conditions in different data-taking periods. In particular, two event samples were used for jets: one was simulated with a pile-up model where only pile-up collisions originating from the primary bunch crossing are considered (in-time pile-up) and a second one was simulated with a realistic configuration of the LHC bunch group structure, where pile-up collisions from successive bunch crossings are also included in the simulation. In the case of events containing $Z \rightarrow \ell\ell$ or $W \rightarrow \ell\nu$, MC samples with in-time pile-up configuration are used, because these data correspond to periods where the contribution of out-of-time pileup is small.

The trigger and event selection criteria used for the data are also applied to the MC simulation.

5 E_T^{miss} reconstruction and calibration

The E_T^{miss} reconstruction includes contributions from energy deposits in the calorimeters and muons reconstructed in the muon spectrometer. The two E_T^{miss} components are calculated as:

$$E_{x(y)}^{\text{miss}} = E_{x(y)}^{\text{miss,calo}} + E_{x(y)}^{\text{miss,\mu}}. \quad (1)$$

Low- p_T tracks are used to recover low p_T particles which are missed in the calorimeters (see Section 5.3.1), and muons reconstructed from the inner detector are used to recover muons in regions not covered by the muon spectrometer (see Section 5.2). The two terms in the above equation are referred to as the calorimeter and muon terms, and will be described in more detail in the following sections. The values of E_T^{miss} and its azimuthal coordinate (ϕ^{miss}) are then calculated as:

$$E_T^{\text{miss}} = \sqrt{(E_x^{\text{miss}})^2 + (E_y^{\text{miss}})^2}, \quad \phi^{\text{miss}} = \arctan(E_y^{\text{miss}}, E_x^{\text{miss}}). \quad (2)$$

5.1 Calculation of the E_T^{miss} calorimeter term

In this paper, the E_T^{miss} reconstruction uses calorimeter cells calibrated according to the reconstructed physics object to which they are associated. Calorimeter cells are associated with a reconstructed and identified high- p_T parent object in a chosen order: electrons, photons, hadronically decaying τ -leptons, jets

and muons. Cells not associated with any such objects are also taken into account in the E_T^{miss} calculation. Their contribution, named $E_T^{\text{miss,CellOut}}$ hereafter, is important for the E_T^{miss} resolution [17].

Once the cells are associated with objects as described above, the E_T^{miss} calorimeter term is calculated as follows (note that the $E_{x(y)}^{\text{miss,calo},\mu}$ term is not always added, as explained in Section 5.2, and for that reason it is written between parentheses):

$$E_{x(y)}^{\text{miss,calo}} = E_{x(y)}^{\text{miss,e}} + E_{x(y)}^{\text{miss,\gamma}} + E_{x(y)}^{\text{miss,\tau}} + E_{x(y)}^{\text{miss,jets}} + E_{x(y)}^{\text{miss,softjets}} + (E_{x(y)}^{\text{miss,calo},\mu}) + E_{x(y)}^{\text{miss,CellOut}} \quad (3)$$

where each term is calculated from the negative sum of calibrated cell energies inside the corresponding objects, as:

$$E_x^{\text{miss,term}} = - \sum_{i=1}^{N_{\text{cell}}^{\text{term}}} E_i \sin \theta_i \cos \phi_i, \quad E_y^{\text{miss,term}} = - \sum_{i=1}^{N_{\text{cell}}^{\text{term}}} E_i \sin \theta_i \sin \phi_i \quad (4)$$

where E_i , θ_i and ϕ_i are the energy, the polar angle and the azimuthal angle, respectively. The summations are over all cells associated with specified objects in the pseudorapidity range $^4 |\eta| < 4.5$.

Because of the high granularity of the calorimeter, it is crucial to suppress noise contributions and to limit the cells used in the E_T^{miss} sum to those containing a significant signal. This is achieved by using only cells belonging to three-dimensional topological clusters, referred as topoclusters hereafter [18], with the exception of electrons and photons for which a different clustering algorithm is used [11]. The topoclusters are seeded by cells with deposited energy $^5 |E_i| > 4\sigma_{\text{noise}}$, and are built by iteratively adding neighbouring cells with $|E_i| > 2\sigma_{\text{noise}}$ and, finally, by adding all neighbours of the accumulated cells.

The various terms in Equation 3 are described in the following:

- $E_{x(y)}^{\text{miss,e}}$, $E_{x(y)}^{\text{miss,\gamma}}$, $E_{x(y)}^{\text{miss,\tau}}$ are reconstructed from cells in clusters associated to electrons, photons and τ -jets from hadronically decaying τ -leptons, respectively;
- $E_{x(y)}^{\text{miss,jets}}$ is reconstructed from cells in clusters associated to jets with calibrated $p_T > 20$ GeV;
- $E_{x(y)}^{\text{miss,softjets}}$ is reconstructed from cells in clusters associated to jets with $7 \text{ GeV} < p_T < 20 \text{ GeV}$;
- $E_{x(y)}^{\text{miss,calo},\mu}$ is the contribution to E_T^{miss} originating from the energy lost by muons in the calorimeter (see Section 5.2);
- the $E_{x(y)}^{\text{miss,CellOut}}$ term is calculated from the cells in topoclusters which are not included in the reconstructed objects.

All these terms are calibrated independently as described in Section 5.3. The final $E_{x(y)}^{\text{miss}}$ is calculated from Equation 1 adding the $E_{x(y)}^{\text{miss},\mu}$ term, described in Section 5.2.

5.2 Calculation of the E_T^{miss} muon term

The E_T^{miss} muon term is calculated from the momenta of muon tracks reconstructed with $|\eta| < 2.7$:

$$E_{x(y)}^{\text{miss},\mu} = - \sum_{\text{muons}} p_{x(y)}^\mu \quad (5)$$

where the summation is over selected muons. In the region $|\eta| < 2.5$, only well-reconstructed muons in the muon spectrometer with a matched track in the inner detector are considered (combined muons). The matching requirement considerably reduces contributions from fake muons (reconstructed muons not corresponding to true muons). These fake muons can sometimes be created from high hit multiplicities in the muon spectrometer in events where some particles from very energetic jets punch through the calorimeter into the muon system.

In order to deal appropriately with the energy deposited by the muon in the calorimeters, $E_{x(y)}^{\text{miss,calo},\mu}$, the muon term is calculated differently for isolated and non-isolated muons, with non-isolated muons defined as those within a distance $\Delta R = \sqrt{(\Delta\eta)^2 + (\Delta\phi)^2} < 0.3$ of a reconstructed jet in the event:

- The p_T of an isolated muon is determined from the combined measurement of the inner detector and muon spectrometer, taking into account the energy deposited in the calorimeters. In this case the energy lost by the muon in the calorimeters ($E_{x(y)}^{\text{miss,calo},\mu}$) is not added to the calorimeter term (Equation 3) to avoid double counting of energy.
- For a non-isolated muon, the energy deposited in the calorimeter cannot be resolved from the calorimetric energy deposits of the particles in the jet. The muon spectrometer measurement of the muon momentum after energy loss in the calorimeter is therefore used, so the $E_{x(y)}^{\text{miss,calo},\mu}$ term is added to the calorimeter term (Equation 3). Only in cases in which there is a significant mis-match between the spectrometer and the combined measurement, the combined measurement is used and a parameterized estimation of the muon energy loss in the calorimeter [10] is subtracted.

For higher values of pseudorapidity ($2.5 < |\eta| < 2.7$), outside the fiducial volume of the inner detector, there is no matched track requirement and the muon spectrometer p_T alone is used for both isolated and non-isolated muons.

Aside from the loss of muons outside the acceptance of the muon spectrometer ($|\eta| > 2.7$), muons can be lost in other small inactive regions (around $|\eta| = 0$ and $|\eta| \sim 1.2$) of the muon spectrometer. The muons which are reconstructed by segments matched to inner detector tracks extrapolated to the muon spectrometer are used to recover their contributions to E_T^{miss} in the $|\eta| \sim 1.2$ regions [10].

Although the core of the E_T^{miss} resolution is not much affected by the muon term, any muons which are not reconstructed, badly measured, or fake, can be a source of fake E_T^{miss} .

5.3 Calibration of E_T^{miss}

The calibration of E_T^{miss} is performed using the scheme described below, where the cells are calibrated separately according to their parent object:

⁴ This η cut is chosen because the MC simulation does not describe data well in the very forward region.

⁵ σ_{noise} is the Gaussian width of the EM cell energy distribution measured in randomly triggered events far from collision bunches.

- The $E_T^{\text{miss},e}$ term is calculated from reconstructed electrons passing the “medium” electron identification requirements, with $p_T > 10$ GeV and calibrated with the default electron calibration [8].
- The $E_T^{\text{miss},\gamma}$ term is calculated from photons reconstructed with the “tight” photon identification requirements [11], with $p_T > 10$ GeV at the EM scale. Due to the low photon purity, the default photon calibration is not applied.
- The $E_T^{\text{miss},\tau}$ term is calculated from τ -jets reconstructed with the “tight” τ -identification requirements [19], with $p_T > 10$ GeV, calibrated with the local hadronic calibration (LCW) scheme [20]. The LCW scheme uses properties of clusters to calibrate them individually. It first classifies calorimeter clusters as electromagnetic or hadronic, according to the cluster topology, and then weights each calorimeter cell in clusters according to the cluster energy and the cell energy density. Additional corrections are applied to the cluster energy for the average energy deposited in the non-active material before and between the calorimeters and for unclustered calorimeter energy.
- The $E_T^{\text{miss},\text{softjets}}$ term is calculated from jets (reconstructed using the anti- k_T algorithm with $R=0.6$) with $7 < p_T < 20$ GeV calibrated with the LCW calibration.
- The $E_T^{\text{miss},\text{jets}}$ term is calculated from jets with $p_T > 20$ GeV calibrated with the LCW calibration and the jet energy scale (JES) factor [21] applied. The JES factor corrects the energy of jets, either at the EM-scale or after cluster calibration, back to particle level. The JES is derived as a function of reconstructed jet η and p_T using the generator-level information in MC simulation.
- The $E_T^{\text{miss},\text{CellOut}}$ term is calculated from topoclusters outside reconstructed objects with the LCW calibration and from reconstructed tracks as described in Section 5.3.1.

Note that object classification criteria and calibration can be chosen according to specific analysis criteria, if needed.

5.3.1 Calculation of the $E_T^{\text{miss},\text{CellOut}}$ term with a track-cluster matching algorithm

In events with W and Z boson production, the calibration of the $E_T^{\text{miss},\text{CellOut}}$ term is of particular importance because, due to the low particle multiplicity in these events, this E_T^{miss} contribution balances the W/Z boson p_T to a large extent [17]. An energy-flow algorithm is used to improve the calculation of the low- p_T contribution to E_T^{miss} ($E_T^{\text{miss},\text{CellOut}}$). Tracks are added to recover the contribution from low- p_T particles which do not reach the calorimeter or do not seed a topocluster. Furthermore the track momentum is used instead of the topocluster energy for tracks associated to topoclusters, thus exploiting the better calibration and resolution of tracks at low momentum compared to topoclusters.

Reconstructed tracks with $p_T > 400$ MeV, passing track quality selection criteria such as the number of hits and χ^2 of the track fit, are used for the calculation of the $E_T^{\text{miss},\text{CellOut}}$ term. All selected tracks are extrapolated to the second layer of the electromagnetic calorimeter and very loose criteria are used for association to reconstructed objects or topoclusters, to avoid

double counting. If a track is neither associated to a topocluster nor a reconstructed object, its transverse momentum is added to the calculation of $E_T^{\text{miss},\text{CellOut}}$. In the case where the track is associated to a topocluster, its transverse momentum is used for the calculation of the $E_T^{\text{miss},\text{CellOut}}$ and the topocluster energy is discarded, assuming that the topocluster energy corresponds to the charged particle giving the track. It has to be noticed that there is a strong correlation between the number of particles and topoclusters, so, in general no neutral energy is lost replacing the topocluster by a track, and the neutral topoclusters are kept in most of the cases. If more than one topocluster is associated to a track, only the topocluster with the largest energy is excluded from the E_T^{miss} calculation, assuming that this energy corresponds to the track.

6 Study of E_T^{miss} performance

In this section the distributions of E_T^{miss} in minimum bias, di-jet, $Z \rightarrow \ell\ell$ and $W \rightarrow \ell\nu$ events from data are compared with the expected distributions from the MC samples. The performance of E_T^{miss} in terms of resolution and scale is also derived.

Minimum bias, di-jet events and $Z \rightarrow \ell\ell$ events are used to investigate the E_T^{miss} performance without relying on MC detector simulation. In general, apart from a small contribution from the semi-leptonic decay of heavy-flavour hadrons in jets, no genuine E_T^{miss} is expected in these events. Thus most of the E_T^{miss} reconstructed in these events is a direct result of imperfections in the reconstruction process or in the detector response.

6.1 E_T^{miss} performance in minimum bias and di-jet events

The distributions of E_x^{miss} , E_y^{miss} , E_T^{miss} and ϕ^{miss} for data and MC simulation are shown in Figure 1 for minimum bias events. The distributions are shown only for events with total transverse energy (see definition at the end of this section) greater than 20 GeV in order to reduce the contamination of fake triggers from the MBTS. Figure 2 shows the distributions of the same variables for the di-jet sample. The di-jet sample corresponding to the periods with higher pileup conditions (see Section 3.1) is used. The MC simulation expectations are superimposed, normalized to the number of events in the data.

In di-jet events a reasonable agreement is found between data and simulation for all basic quantities, while there is some disagreement in minimum bias events, attributed to imperfect modelling of soft particle activity in the MC simulation. The better agreement between data and MC simulation in the ϕ^{miss} distribution for the di-jet sample can be partly explained by the fact that the E_T^{miss} is not corrected for the primary vertex position; the primary vertex position in data is better reproduced by the MC simulation for the di-jet sample than in the case of the minimum bias sample.

Events in the tails of the E_T^{miss} distributions have been carefully checked, in order to understand the origin of the large measured E_T^{miss} . The tails are not completely well described by MC simulation, but, both in data and in MC simulation they are

in general due to mis-measured jets. In minimum bias events there are more events in the tail in MC simulation and this can be due to the fact that the MC statistics is larger than in data. In di-jet events, there are more events in the tail in data. More MC events would be desirable. In di-jet events there are 19 events with $E_T^{\text{miss}} > 110$ GeV in the data. The majority of them (13 events) are due to mis-measured jets, where in most of the cases at least one jet points to a transition region between calorimeters. Two events are due to a combination of mis-measured jets with an overlapping muon, and one event is due to a fake high- p_T muon. Finally two events look like good $b\bar{b}$ candidates, and one event has one reconstructed jet and no activity in the other hemisphere.

The events with fake E_T^{miss} due to mis-measured jets and jets containing leptonic decays of heavy hadrons can be rejected by a cut based on the azimuthal angle between the jet and E_T^{miss} , $\Delta\phi(\text{jet}, E_T^{\text{miss}})$. Since the requirement of event cleaning depends on the physics analysis, the minimal cleaning cut is applied and careful evaluation of tail events is performed in this paper. Analyses that rely on a careful understanding and reduction of the tails of the E_T^{miss} distribution (e.g. SUSY searches such as Ref. [3]) have performed more detailed studies to characterize the residual tail in events containing high- p_T jets. These analyses use tighter jet cleaning cuts, track-jet matching, and angular cuts on $\Delta\phi(\text{jet}, E_T^{\text{miss}})$ to further reduce the fake E_T^{miss} tail. In Ref. [3] a fully data-driven method (described in detail in Ref. [17]) was then employed to determine the residual fake E_T^{miss} background.

The contributions from jets, soft jets and topoclusters not associated to the reconstructed objects and muons are shown in Figure 3 for the di-jet events. The data-MC agreement is good for all of the terms contributing to E_T^{miss} . The tails observed in the muon term are mainly due to reconstructed fake muons and to one cosmic-ray muon, which can be rejected by applying a tighter selection for the muons used in the E_T^{miss} reconstruction, based on χ^2 criteria for the combination, isolation criteria and requirements on the number of hits in muon chambers used for the muon reconstruction.

In the following some distributions are shown for the total transverse energy, $\sum E_T$, which is an important quantity to parameterise and understand the E_T^{miss} performance. It is defined as:

$$\sum E_T = \sum_{i=1}^{N_{\text{cell}}} E_i \sin \theta_i \quad (6)$$

where E_i and θ_i are the energy and the polar angle, respectively, of calorimeter cells associated to topoclusters within $|\eta| < 4.5$. Cell energies are calibrated according to the scheme described in Section 5.3 for E_T^{miss} .

The data distributions of $\sum E_T$ for minimum bias and di-jet events from the subset corresponding to lower pileup conditions (see Section 3.1) are compared to MC predictions from two versions of PYTHIA in Figure 4. The left-hand distributions show comparisons with the ATLAS tune of PYTHIA6. The right-hand distributions show the comparisons with the default tune of PYTHIA8. Due to the limited number of events simulated, the distribution for the di-jet PYTHIA8 MC sample is not smooth, and is zero in the lowest $\sum E_T$ bin populated by data. This is not understood, also if it can be partly explained

by the fact that the low $\sum E_T$ region is populated by events from the jet MC sample generated in the lowest parton p_T bin (17–35 GeV), which is the most suppressed by the di-jet selection (a factor about 20 more than other samples) and has a large weight, due to cross-section. Moreover the PYTHIA8 jet MC sample in the 8–17 GeV parton p_T bin is not available. In the case of the minimum bias sample, due to the very limited number of events simulated (about a factor 25 less respect to data), the tails in the PYTHIA8 MC distribution are strongly depleted.

The PYTHIA8 MC [16] version used in this paper has not yet been tuned to the ATLAS data. The current tune [22] uses the CTEQ 6.1 parton distribution functions (PDF) instead of the MRST LO** as used in PYTHIA6, and its diffraction model differs, including higher- Q^2 diffractive processes. The comparison of the mean values and the shapes of the two different MC distributions with data seems to indicate that a better agreement is obtained with the PYTHIA8 but, due to the reduced PYTHIA8 MC statistics, no firm conclusion can be drawn. In the rest of the paper, the PYTHIA6 MC samples with the ATLAS tune are used for comparison with data; this version is used as the baseline for PYTHIA MC samples for 2010 data analyses.

6.2 E_T^{miss} performance in $Z \rightarrow \ell\ell$ events

The absence of genuine E_T^{miss} in $Z \rightarrow \ell\ell$ events, coupled with the clean event signature and the relatively large cross-section, means that it is a good channel to study E_T^{miss} performance.

The distributions of E_T^{miss} and ϕ^{miss} for data and MC simulation are shown in Figure 5 for $Z \rightarrow ee$ and $Z \rightarrow \mu\mu$ events. The contributions due to muons are shown for $Z \rightarrow \mu\mu$ events in Figure 6. Both the contributions from energy deposited in calorimeter cells associated to muons, taken at the EM scale, and the contributions from reconstructed muons are shown. For $Z \rightarrow ee$ events, the contributions from electrons, jets, soft jets and topoclusters outside the reconstructed objects are shown separately in Figure 7. The peak at zero in the distribution of the jet term corresponds to events where there are no jets with p_T above 20 GeV, and the small values (< 20 GeV) in the distribution are due to events with two jets whose transverse momenta balance. The MC simulation expectations, from $Z \rightarrow \ell\ell$ events and from the dominant SM backgrounds, are superimposed. Each MC sample is weighted with its corresponding cross-section and then the total MC expectation is normalized to the number of events in data. Reasonable agreement between data and MC simulation is observed in all distributions.

Events in the tails of the E_T^{miss} distributions in Figure 5 have been carefully checked. The 22 events with the highest E_T^{miss} values, above 60 GeV, have been examined in detail to check whether they are related to cosmic-ray muon background, fake muons, badly measured jets or jets pointing to dead calorimeter regions. The events in the tails are found to be compatible with either signal candidates, including $t\bar{t}$, WW and WZ diboson events, all involving real E_T^{miss} , or events in which the E_T^{miss} vector is close to a jet in the transverse plane. The latter category of events can arise from mis-measured jets, and be rejected at the analysis level with cuts on $\Delta\phi(\text{jet}, E_T^{\text{miss}})$ (see Section 6.1).

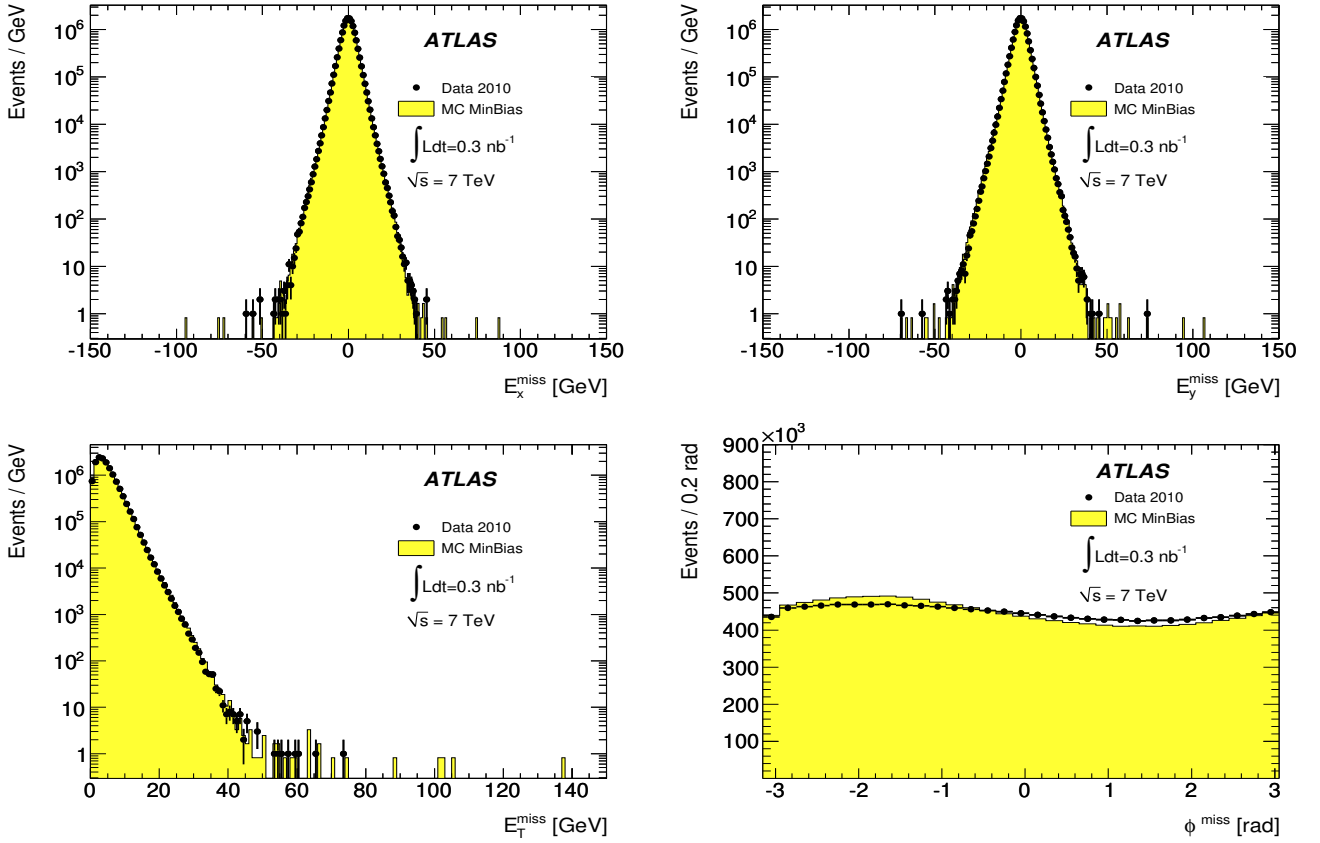


Fig. 1. Distribution of E_x^{miss} (top left), E_y^{miss} (top right), E_T^{miss} (bottom left), ϕ^{miss} (bottom right) as measured in a data sample of minimum bias events. The expectation from MC simulation, normalized to the number of events in data, is superimposed.

6.2.1 Measuring E_T^{miss} response in $Z \rightarrow \ell\ell$ events

From the event topology [17] in events with $Z \rightarrow \ell\ell$ decay one can define an axis in the transverse plane such that the component of E_T^{miss} along this axis is sensitive to detector resolution and biases. The direction of this axis, A_Z , is defined by the reconstructed momenta of the leptons:

$$A_Z = (\mathbf{p}_T^{\ell^+} + \mathbf{p}_T^{\ell^-}) / |\mathbf{p}_T^{\ell^+} + \mathbf{p}_T^{\ell^-}| \quad (7)$$

where \mathbf{p}_T^{ℓ} are the vector transverse momenta of the lepton and anti-lepton. The direction of A_Z thus reconstructs the direction of motion of the Z boson. The perpendicular axis in the transverse plane, A_{AZ} , is a unit vector placed at right angles to A_Z , with positive direction anticlockwise from the direction of the Z boson.

The mean value of the projection of E_T^{miss} onto the longitudinal axis, $\langle E_T^{\text{miss}} \cdot A_Z \rangle$, is a measure of the E_T^{miss} scale, as this axis is sensitive to the balance between the leptons and the hadronic recoil. Figure 8 shows the value of $\langle E_T^{\text{miss}} \cdot A_Z \rangle$ as a function of p_T^Z . These mean values are used as a diagnostic to validate the E_T^{miss} reconstruction algorithms. If the leptons perfectly balanced the hadronic recoil, regardless of the net momentum of the lepton system, then the $E_T^{\text{miss}} \cdot A_Z$ would be zero, independent of p_T^Z . Instead, $\langle E_T^{\text{miss}} \cdot A_Z \rangle$ displays a small bias in

both the electron and muon channels which is reasonably reproduced by the MC simulation. The observed bias is slightly negative for low values of p_T^Z , suggesting either that the p_T of the lepton system is overestimated or that the magnitude of the hadronic recoil is underestimated. The same sign and magnitude of bias is seen in both electron and muon channels, suggesting that the hadronic recoil, here dominated by $E_T^{\text{miss, CellOut}}$ and by soft jets, is the source of bias. The component of the E_T^{miss} along the perpendicular axis, $E_T^{\text{miss}} \cdot A_{AZ}$, displays no bias, and, indeed there is no mechanism for generating such a bias.

In Figure 9 the dependences of $\langle E_T^{\text{miss}} \cdot A_Z \rangle$ on p_T^Z are shown separately for events with $Z \rightarrow \ell\ell$ produced in association with zero jets or with at least one jet, with the jet definition as described in Section 3.1. The figure demonstrates that there is a negative bias in $\langle E_T^{\text{miss}} \cdot A_Z \rangle$ for events with zero jets, which increases with p_T^Z up to 6 GeV. A similar bias is observed in both electron and muon channels, hence it is interpreted as coming from imperfections in the calibration of the soft hadronic recoil (the $E_T^{\text{miss, CellOut}}$ and the $E_T^{\text{miss, softjets}}$ terms). In events with at least one jet there is a small positive bias in the electron channel at high p_T^Z , which is visible also in the muon channel for p_T^Z in the region 15-20 GeV.

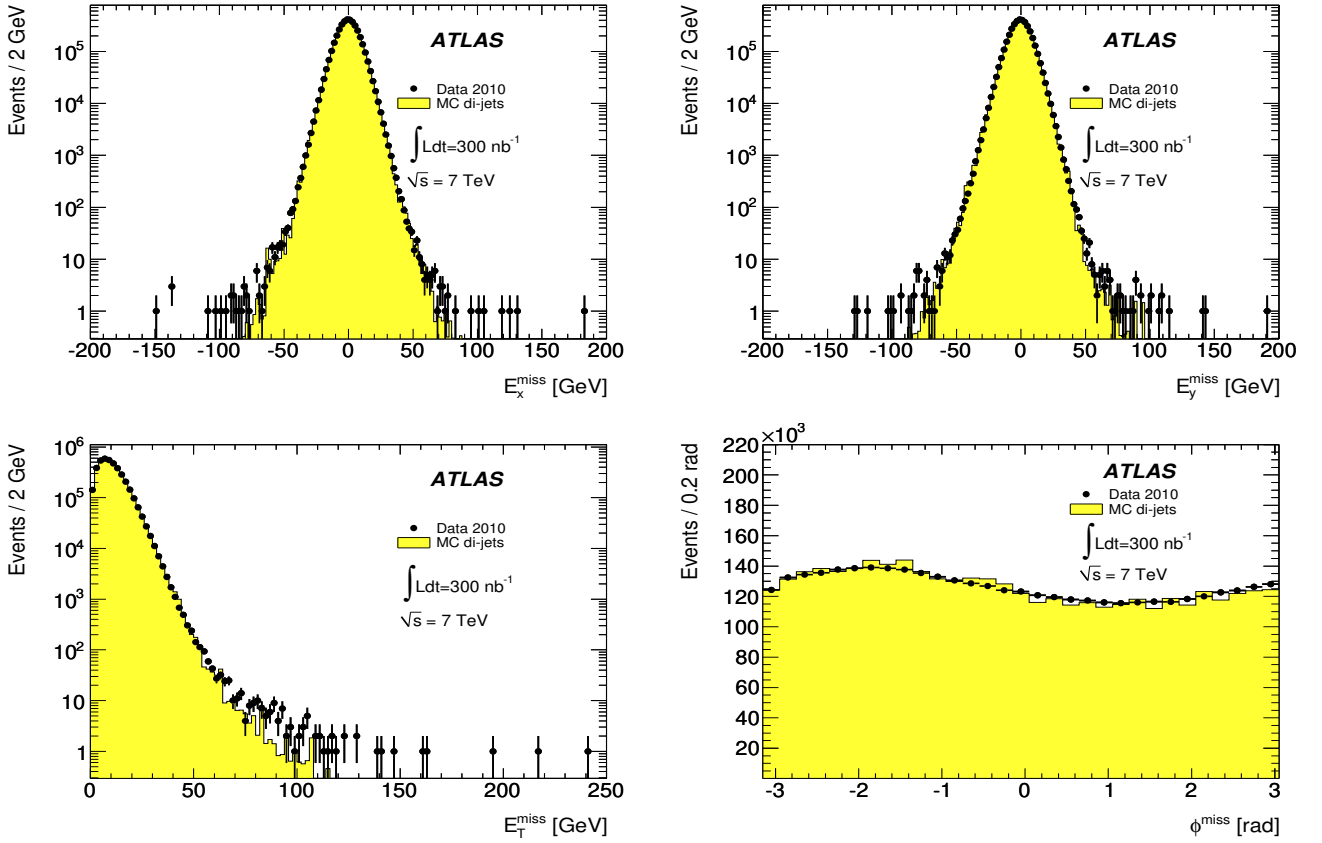


Fig. 2. Distribution of E_x^{miss} (top left), E_y^{miss} (top right), E_T^{miss} (bottom left), ϕ^{miss} (bottom right) as measured in the data sample of di-jet events. The expectation from MC simulation, normalized to the number of events in data, is superimposed. The events in the tails are discussed in the text.

Figure 10 shows $\langle E_T^{\text{miss}} \cdot A_Z \rangle$ for $Z \rightarrow \ell\ell$ events where there are neither high p_T nor soft jets, for two cases of E_T^{miss} reconstruction: calculating the $E_T^{\text{miss,CellOut}}$ term with the track-cluster matching algorithm (see Section 5.3.1) or calculating this term from the calorimeter topoclusters only (denoted as E_T^{miss} no tracks). The plots show a lower bias for the case with the track-cluster matching algorithm, indicating that it improves the reconstruction of the $E_T^{\text{miss,CellOut}}$ term.

6.3 E_T^{miss} performance in $W \rightarrow \ell\nu$ events

In this section the E_T^{miss} performance is studied in $W \rightarrow e\nu$ and $W \rightarrow \mu\nu$ events. In these events genuine E_T^{miss} is expected due to the presence of the neutrino, therefore the E_T^{miss} scale can be checked.

The distributions of E_T^{miss} and ϕ^{miss} in data and in MC simulation are shown in Figure 11 for $W \rightarrow e\nu$ and $W \rightarrow \mu\nu$ events. The contributions due to muons are shown for $W \rightarrow \mu\nu$ events in Figure 12. Both, the E_T^{miss} contribution from energy deposited in calorimeter cells associated to muons, taken at the EM scale, and the E_T^{miss} contribution from reconstructed muons are shown. The contributions given by the electrons, jets, soft jets and topoclusters outside reconstructed

objects are shown in Figure 13 for $W \rightarrow e\nu$ events. The MC expectations are also shown, both from $W \rightarrow \ell\nu$ events, and from the dominant SM backgrounds. The MC simulation describes all of the quantities well, with the exception that very small data-MC discrepancies are observed in the distribution of the $E_T^{\text{miss,e}}$ at low E_T^{miss} values. This can be attributed to the QCD jet background, which would predominantly populate the region of low E_T^{miss} [8], but which is not included in the MC expectation shown.

6.3.1 E_T^{miss} linearity in $W \rightarrow \ell\nu$ MC events

The expected E_T^{miss} linearity, which is defined as the mean value of the ratio: $(E_T^{\text{miss}} - E_T^{\text{miss, True}})/E_T^{\text{miss, True}}$, is shown as a function of $E_T^{\text{miss, True}}$ in Figure 14 for $W \rightarrow e\nu$ and $W \rightarrow \mu\nu$ MC events. The mean value of this ratio is expected to be zero if the reconstructed E_T^{miss} has the correct scale. In Figure 14, it can be seen that there is a displacement from zero which varies with the true E_T^{miss} . The bias at low $E_T^{\text{miss, True}}$ values is about 5% and is due to the finite resolution of the E_T^{miss} measurement. The reconstructed E_T^{miss} is positive by definition, so the relative difference is positive when the $E_T^{\text{miss, True}}$ is small.

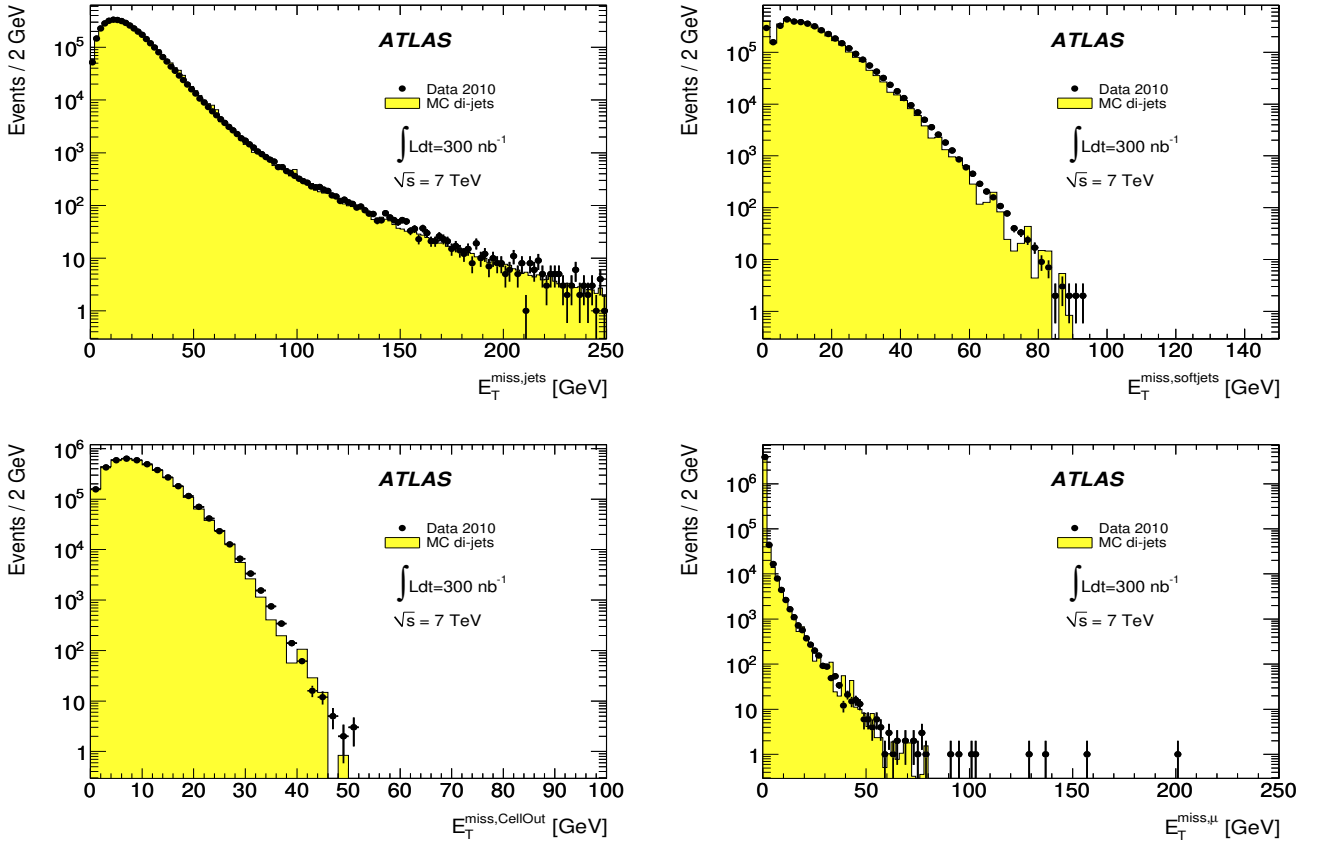


Fig. 3. Distribution of E_T^{miss} computed with cells from topoclusters in jets (top left), in soft jets (top right), from topoclusters outside reconstructed objects (bottom left) and from reconstructed muons (bottom right) for data for di-jet events. The expectation from MC simulation, normalized to the number of events in data, is superimposed. The events in the tail of the $E_T^{\text{miss},\mu}$ distribution are discussed in the text.

The effect extends up to 40 GeV. The bias is in general larger for $W \rightarrow \mu\nu$ events than for $W \rightarrow e\nu$ events. Considering only events with $E_T^{\text{miss, True}} > 40$ GeV, the E_T^{miss} linearity is better than 1% in $W \rightarrow e\nu$ events, while there is a non-linearity up to about 3% in $W \rightarrow \mu\nu$ events. This may be explained by an underestimation of the $E_T^{\text{miss, calo}, \mu}$ term, in which too few calorimeter cells are associated to the reconstructed muon.

6.4 E_T^{miss} resolution

A more quantitative evaluation of the E_T^{miss} performance can be obtained from a study of the $(E_x^{\text{miss}}, E_y^{\text{miss}})$ resolutions as a function of $\sum E_T$. In $Z \rightarrow \ell\ell$ events, as well as in minimum bias and QCD jet events, no genuine E_T^{miss} is expected, so the resolution of the two E_T^{miss} components is measured directly from reconstructed quantities, assuming that the true values of E_x^{miss} and E_y^{miss} are equal to zero. The resolution is estimated from the width of the combined distribution of E_x^{miss} and E_y^{miss} (denoted $(E_x^{\text{miss}}, E_y^{\text{miss}})$ distribution) in bins of $\sum E_T$. The core of the distribution is fitted, for each $\sum E_T$ bin, with a Gaussian over twice the expected resolution obtained from previous studies [17] and the fitted width, σ , is examined as a function of

$\sum E_T$. The E_T^{miss} resolution follows an approximately stochastic behaviour as a function of $\sum E_T$, which can be described with the function $\sigma = k \cdot \sqrt{\sum E_T}$, but deviations from this simple law are expected in the low $\sum E_T$ region due to noise and in the very large $\sum E_T$ region due to the constant term.

Figure 15 (left) shows the resolution from data at $\sqrt{s} = 7$ TeV for $Z \rightarrow \ell\ell$ events, minimum bias and di-jet events as a function of the total transverse energy in the event, obtained by summing the p_T of muons and the $\sum E_T$ in calorimeters, calculated as described in Section 6.1. If the resolution is shown as a function of the $\sum E_T$ in calorimeters, a difference between $Z \rightarrow ee$ and $Z \rightarrow \mu\mu$ events is observed due to the fact that $\sum E_T$ includes electron momenta in $Z \rightarrow ee$ events while muon momenta are not included in $Z \rightarrow \mu\mu$ events.

The resolution of the two E_T^{miss} components is fitted with the simple function given above. The fits are acceptable and are of similar quality for all different channels studied. This allows to use the parameter k as an estimator for the resolution and to compare it in various physics channels in data and MC simulation. There is a reasonable agreement in the E_T^{miss} resolution in the different physics channels, as can be seen from the fit parameters k reported in the figure. The k parameter has fit values ranging from $0.42 \text{ GeV}^{1/2}$ for $Z \rightarrow \ell\ell$ events to $0.51 \text{ GeV}^{1/2}$ for di-jet events. The E_T^{miss} resolution is better in $Z \rightarrow \ell\ell$ events

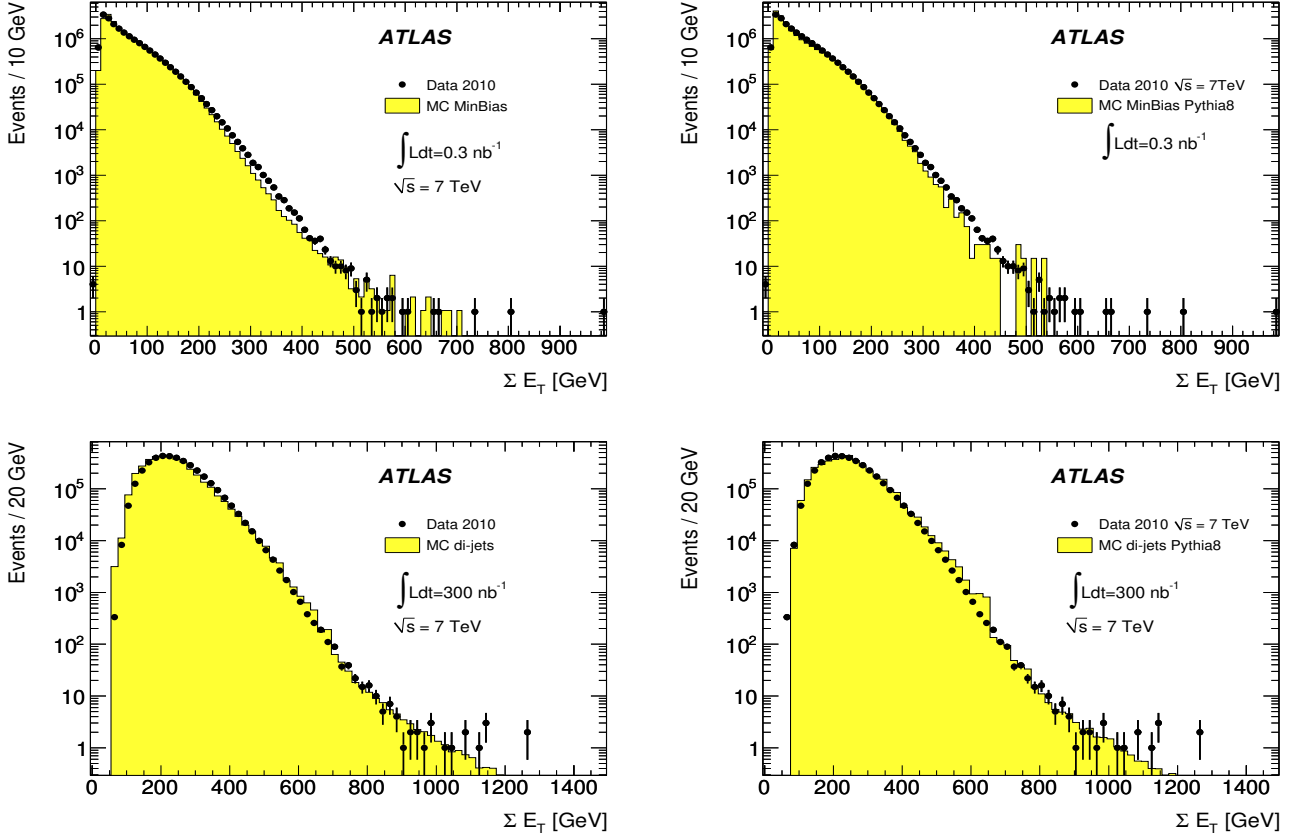


Fig. 4. Distribution of ΣE_T as measured in a data sample of minimum bias events (top) and di-jet events (bottom) selecting two jets with $p_T > 25$ GeV. The expectation from MC simulation, normalized to the number of events in data, is superimposed. On the left PYTHIA6 (ATLAS tune) is compared with the data. On the right PYTHIA8 is compared with the data.

because the lepton momenta are measured with better precision than jets.

In Figure 15 (right) the E_T^{miss} resolution is shown for MC events. In addition to the $Z \rightarrow \ell\ell$, minimum bias and di-jet events, the resolution is also shown for $W \rightarrow \ell\nu$ MC events. In W events the resolution of the two E_T^{miss} components is estimated from the width of $(E_x^{\text{miss}} - E_x^{\text{miss, True}}, E_y^{\text{miss}} - E_y^{\text{miss, True}})$ in bins of ΣE_T , fitted with a Gaussian as explained above. There is a reasonable agreement in the E_T^{miss} resolution in the different MC channels studied with the fitted value of k ranging from $0.42 \text{ GeV}^{1/2}$ for $Z \rightarrow \ell\ell$ events to $0.50 \text{ GeV}^{1/2}$ for di-jet events. As observed for data, the E_T^{miss} resolution is better in $Z \rightarrow \ell\ell$ events and slightly better in $W \rightarrow \ell\nu$ events, due to the presence of the leptons which are more precisely measured.

The resolution in MC minimum bias events is slightly worse than in data. This is probably due to imperfections of the modelling of soft particle activity in MC simulation, while there is a good data-MC agreement in the resolution for other channels.

7 Evaluation of the systematic uncertainty on the E_T^{miss} scale

For any analysis using E_T^{miss} , it is necessary to be able to evaluate the systematic uncertainty on the E_T^{miss} scale. The E_T^{miss} , as defined in Section 5.3, is the sum of several terms corresponding to different types of reconstructed objects. The uncertainty on each individual term can be evaluated given the knowledge of the reconstructed objects [8, 23] that are used to build it and this uncertainty can be propagated to E_T^{miss} . The overall systematic uncertainty on the E_T^{miss} scale is then calculated by combining the uncertainties on each term.

The relative impact of the uncertainty of the constituent terms on E_T^{miss} differs from one analysis to another depending on the final state being studied. In particular, in events containing W and Z bosons decaying to leptons, uncertainties on the scale and resolution in the measurements of the charged leptons, together with uncertainties on the jet energy scale, need to be propagated to the systematic uncertainty estimate of E_T^{miss} . Another significant contribution to the E_T^{miss} scale uncertainty in W and Z boson final states comes from the contribution of topoclusters outside reconstructed objects and from soft jets. In the next three subsections, two complementary methods for the evaluation of the systematic uncertainty on the $E_T^{\text{miss, CellOut}}$ and

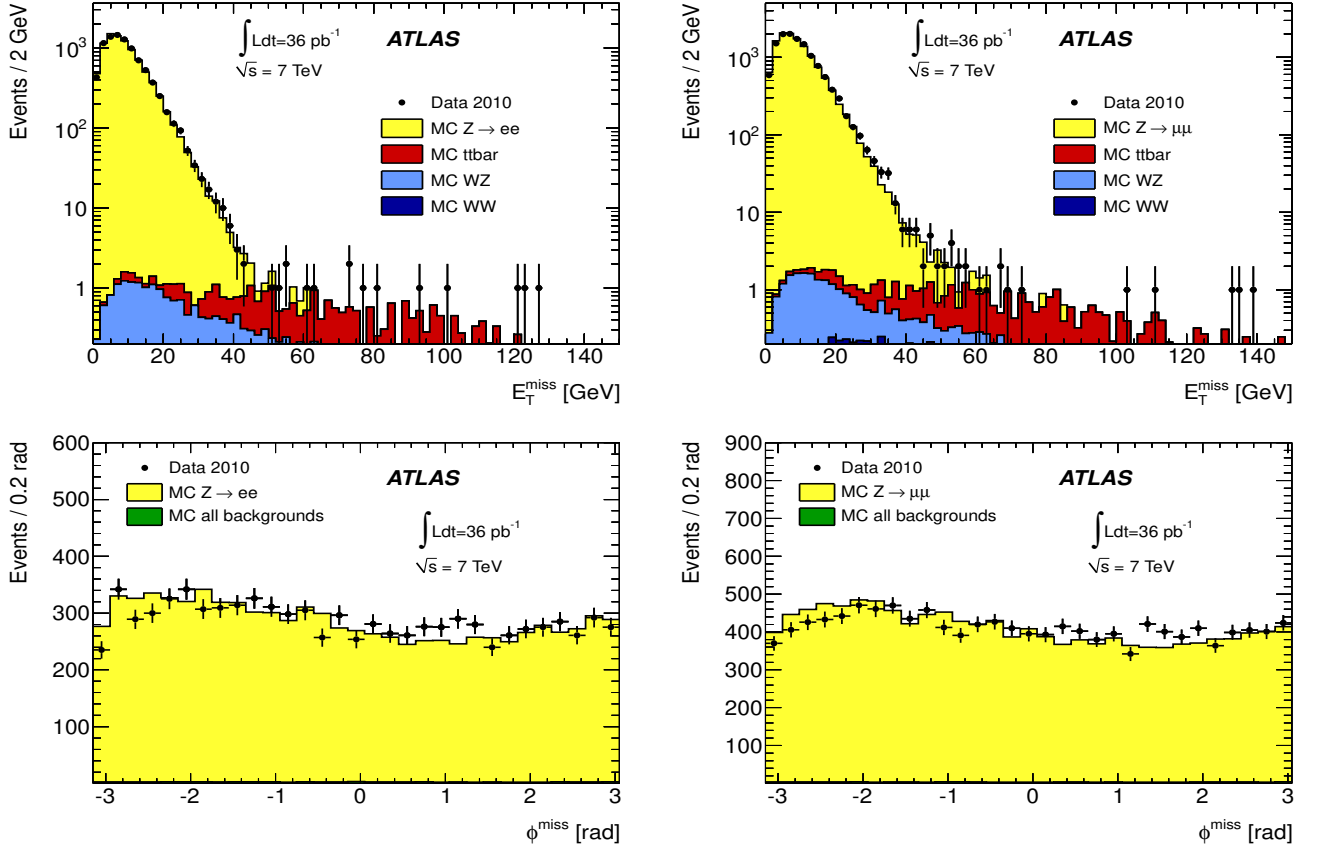


Fig. 5. Distribution of E_T^{miss} (top) and ϕ^{miss} (bottom) as measured in a data sample of $Z \rightarrow ee$ (left) and of $Z \rightarrow \mu\mu$ (right). The expectation from Monte Carlo simulation is superimposed and normalized to data, after each MC sample is weighted with its corresponding cross-section. The sum of all backgrounds is shown in the lower plots.

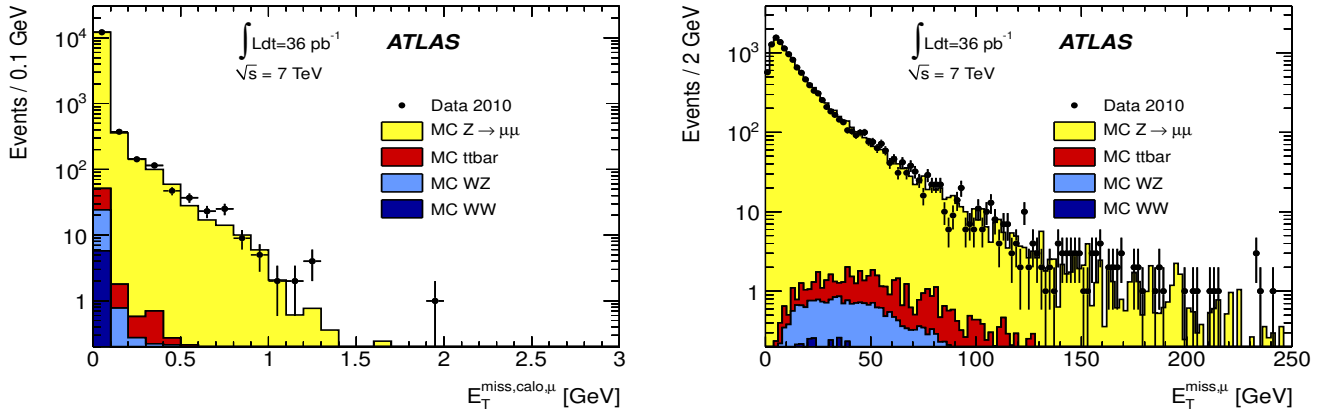


Fig. 6. Distribution of E_T^{miss} computed with calorimeter cells associated to muons ($E_T^{\text{miss,calo},\mu}$) (left) and computed from reconstructed muons ($E_T^{\text{miss},\mu}$) (right) for $Z \rightarrow \mu\mu$ data. The expectation from Monte Carlo simulation is superimposed and normalized to data, after each MC sample is weighted with its corresponding cross-section.

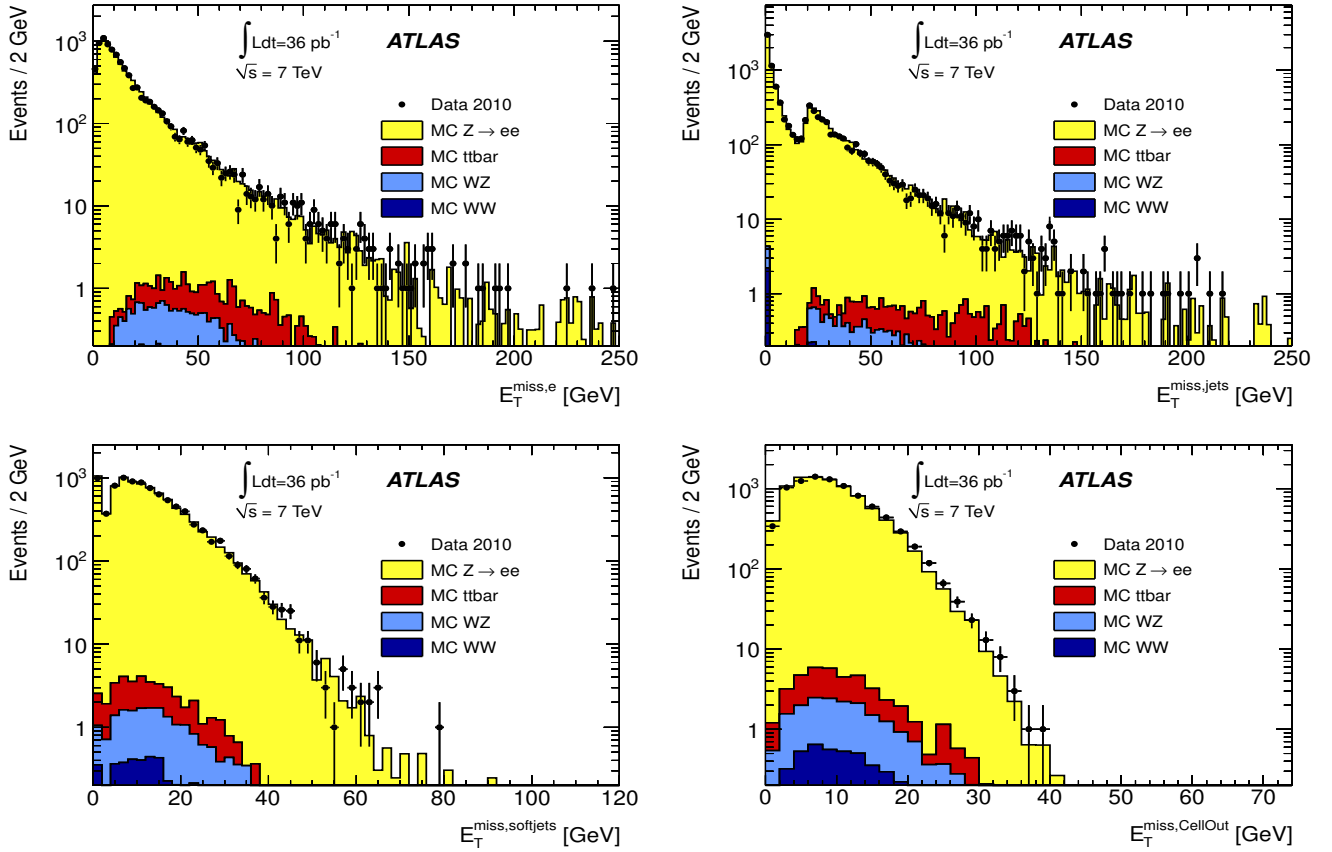


Fig. 7. Distribution of E_T^{miss} computed with cells associated to electrons ($E_T^{\text{miss},e}$) (top left), jets with $p_T > 20$ GeV ($E_T^{\text{miss},\text{jets}}$) (top right), jets with $7 \text{ GeV} < p_T < 20$ GeV ($E_T^{\text{miss},\text{softjets}}$) (bottom left) and from topoclusters outside reconstructed objects ($E_T^{\text{miss},\text{CellOut}}$) (bottom right) for $Z \rightarrow ee$ data. The expectation from Monte Carlo simulation is superimposed and normalized to data, after each MC sample is weighted with its corresponding cross-section.

the $E_T^{\text{miss},\text{softjets}}$ terms are described. Finally the overall E_T^{miss} uncertainty for $W \rightarrow \ell\nu$ events is calculated.

7.1 Evaluation of the systematic uncertainty on the $E_T^{\text{miss},\text{CellOut}}$ scale using Monte Carlo simulation

There are several possible sources of systematic uncertainty in the calculation of $E_T^{\text{miss},\text{CellOut}}$. These sources include inaccuracies in the description of the detector material, the choice of shower model and the model for the underlying event in the simulation. The systematic uncertainty due to each of these sources is estimated with dedicated MC simulations. The MC jet samples, generated with PYTHIA, are those used to assess the systematic uncertainty on the jet energy scale [21]. Table 1 lists the simulation samples considered, referred to in the following as “variations” with respect to the nominal sample.

The estimate of the uncertainty on $E_T^{\text{miss},\text{CellOut}}$ for a variation i is determined by calculating the percentage difference between the mean value of this term for the nominal sample, labelled μ_0 , and that for the variation sample, labelled μ_i . This approach assumes that the variations affect the total scale and none of the variations introduces a shape dependence in the

$E_T^{\text{miss},\text{CellOut}}$ term, as verified in Ref. [24]. In order to cross-check for a possible dependence on the event total transverse energy, the relative difference $R_i = (\mu_i - \mu_0)/\mu_0$ between different variations is computed in bins of $\sum E_T$ for the jet samples. No significant dependence of R_i on $\sum E_T$ is observed. A cross-check on the topology dependence is done using $W \rightarrow \ell\nu$ samples simulated by introducing the variations i . Table 2 shows the R_i values as computed in both the QCD jet samples and the $W \rightarrow \ell\nu$ samples. The results are consistent, showing that the estimated uncertainty does not have a large dependence on the event topology.

A symmetric systematic uncertainty on the $E_T^{\text{miss},\text{CellOut}}$ scale is obtained by summing in quadrature the estimated uncertainties averaged between simulated jet and W events. The total estimated uncertainty⁶ on the $E_T^{\text{miss},\text{CellOut}}$ term is 2.6%.

⁶ In this uncertainty evaluation using MC simulation, the uncertainty on the absolute electromagnetic energy scale in the calorimeters should also be taken into account. For the bulk of the LAr barrel electromagnetic calorimeter a 1.5% uncertainty is found on the cell energy measurement, increasing to 5% for the presampler and 3% for the tile calorimeter [25].

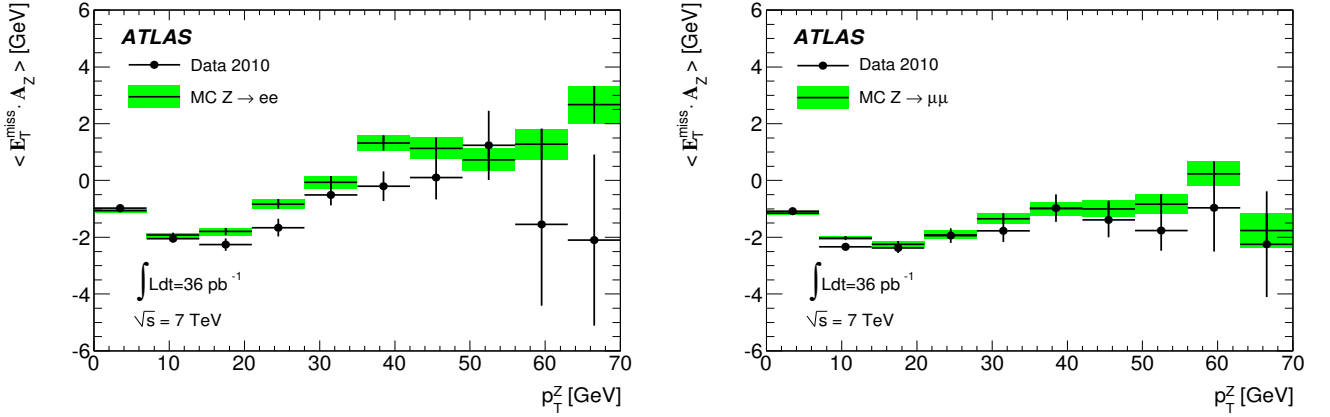


Fig. 8. Mean values of $E_T^{\text{miss}} \cdot A_Z$ as a function of p_T^Z in $Z \rightarrow ee$ (left) and $Z \rightarrow \mu\mu$ (right) events.

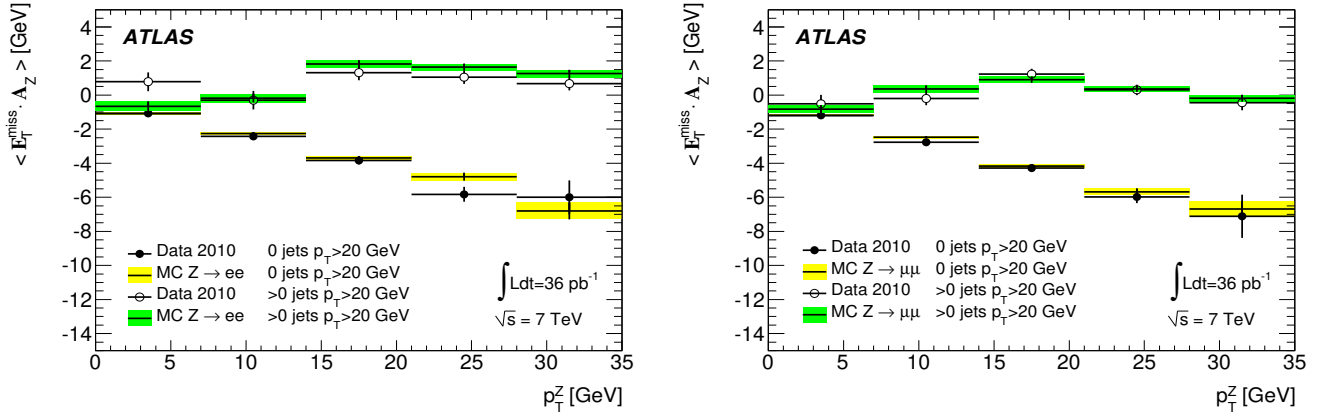


Fig. 9. Mean value of $E_T^{\text{miss}} \cdot A_Z$ as a function of p_T^Z requiring either zero jets with $p_T > 20$ GeV or at least 1 jet with $p_T > 20$ GeV in the event for $Z \rightarrow ee$ (left) and $Z \rightarrow \mu\mu$ (right) events.

Variation	Description
Dead Material	5% increase in the inner detector material 0.1 X_0 in front of the cryostat of the EM barrel calorimeter 0.05 X_0 between presampler and EM barrel calorimeter 0.1 X_0 in the cryostat after the EM barrel calorimeter
FTFP_BERT	density of material in barrel-endcap transition of the EM calorimeter $\times 1.5$
QGSP	An alternative shower model for hadronic interaction in GEANT4
PYTHIA Perugia 2010 tune	An alternative setting of the PYTHIA parameters with increased final state radiation and more soft particles

Table 1. Variations of the default simulation settings used for the estimate of the $E_T^{\text{miss,CellOut}}$ term systematic uncertainty. See Ref. [21] for details of the parameters.

7.2 Evaluation of the systematic uncertainty on the $E_T^{\text{miss,CellOut}}$ scale from the topocluster energy scale uncertainty

The uncertainty on the scale of the $E_T^{\text{miss,CellOut}}$ term, which is built from topoclusters with a correction based on tracks (see Section 5.3.1), can also be calculated from the topocluster energy scale uncertainties. These uncertainties can be estimated from comparisons between data and MC simulation using the

E/p response from single tracks, measured by summing the energies of all calorimeter clusters around a single isolated track [25]. The effects of these uncertainties on the $E_T^{\text{miss,CellOut}}$ term can be evaluated by varying the energy scale of topoclusters that contribute to the $E_T^{\text{miss,CellOut}}$ term in $W \rightarrow e\nu$ MC samples, as was done in Ref. [8].

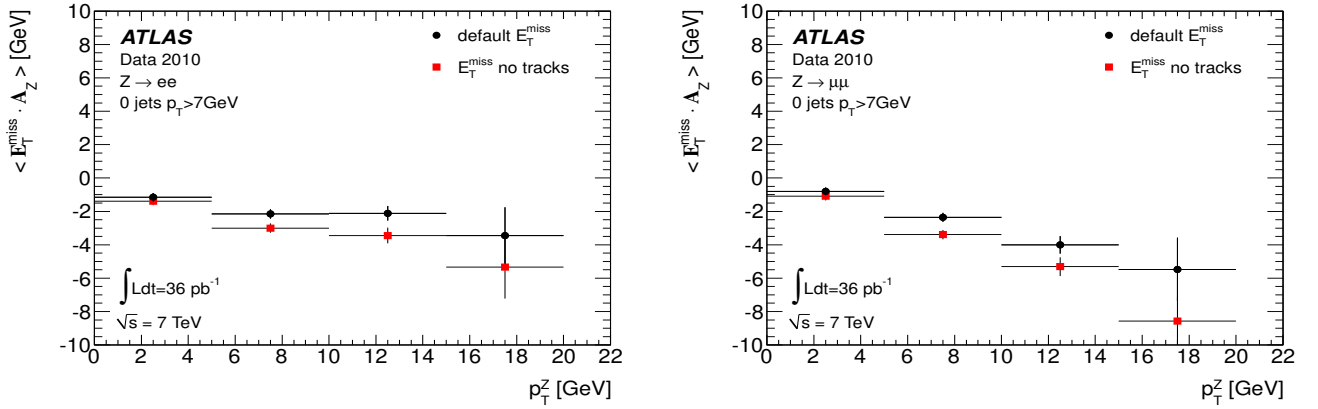


Fig. 10. Mean value of $E_T^{\text{miss}} \cdot A_Z$ as a function of p_T^Z in $Z \rightarrow ee$ (left) and $Z \rightarrow \mu\mu$ (right) for events with no jets with $p_T > 7$ GeV. The default E_T^{miss} is compared with E_T^{miss} calculated in the same way with the exception that the track-cluster matching algorithm is not used for the calculation of $E_T^{\text{miss,CellOut}}$.

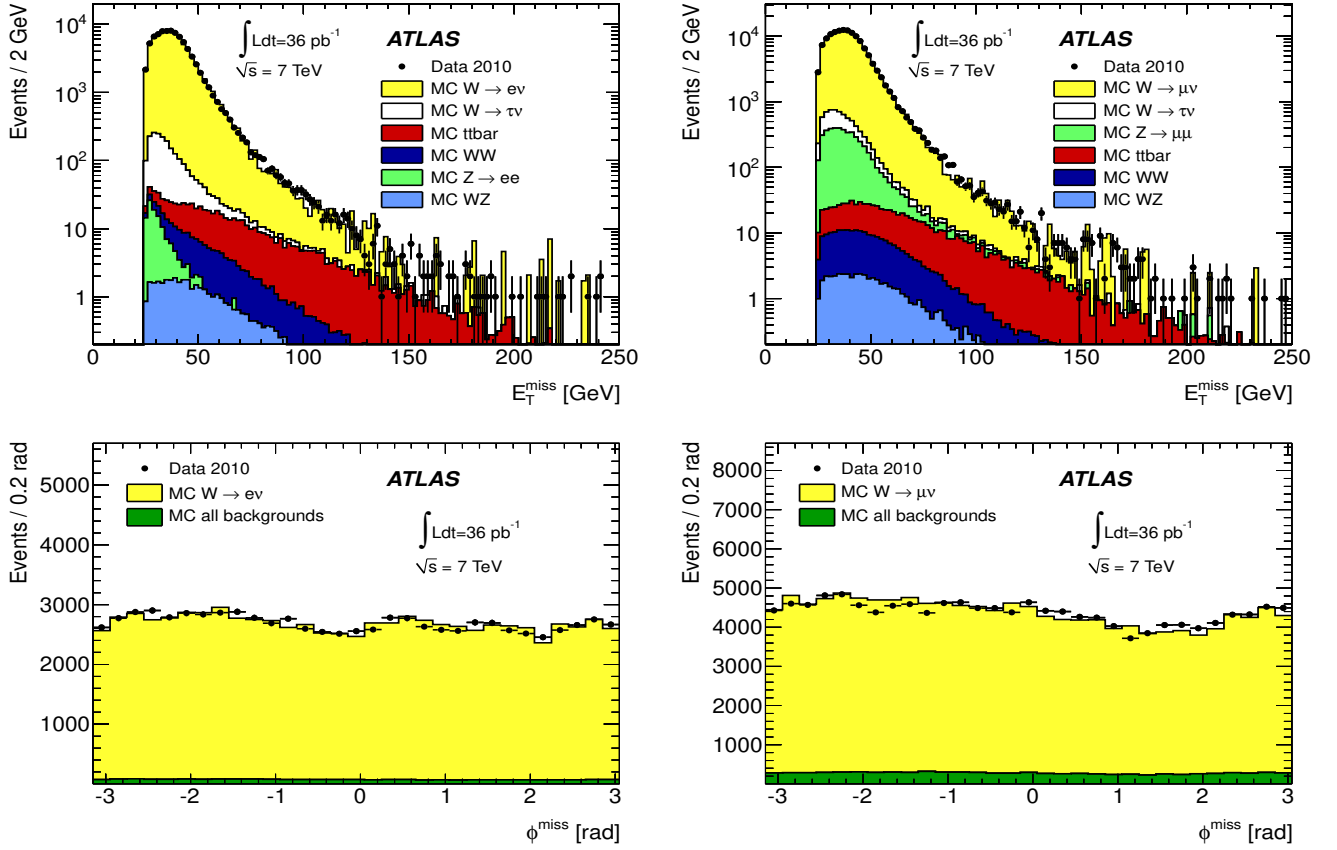


Fig. 11. Distribution of E_T^{miss} (top) and ϕ^{miss} (bottom) as measured in a data sample of $W \rightarrow e\nu$ (left) and $W \rightarrow \mu\nu$ (right) events. The expectation from Monte Carlo simulation is superimposed and normalized to data, after each MC sample is weighted with its corresponding cross-section. The sum of all backgrounds is shown in the lower plots.

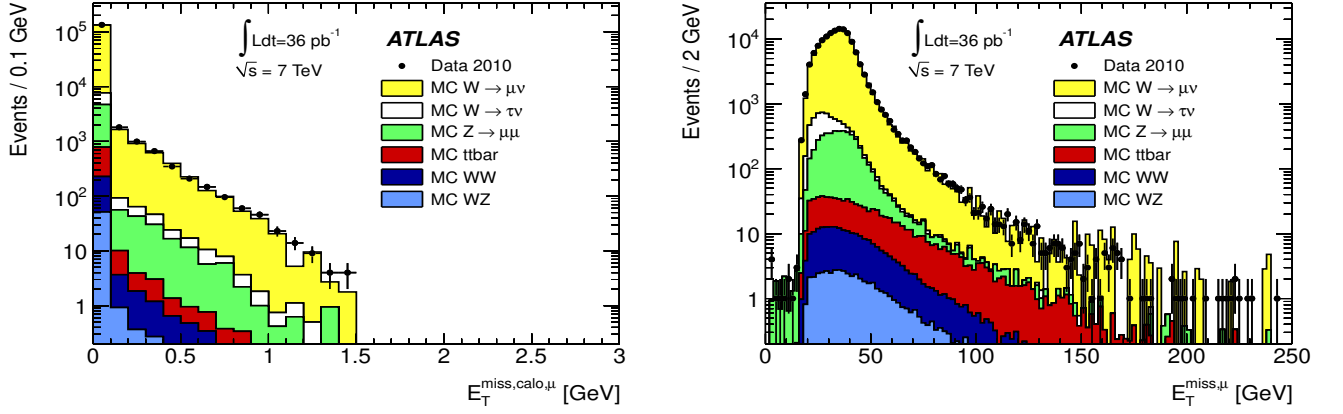


Fig. 12. Distribution of E_T^{miss} computed with cells from muons ($E_T^{\text{miss,calo},\mu}$) (left) and reconstructed muons ($E_T^{\text{miss,muon}}$) (right) for $W \rightarrow \mu\nu$ data. The expectation from Monte Carlo simulation is superimposed and normalized to data, after each MC sample is weighted with its corresponding cross-section.

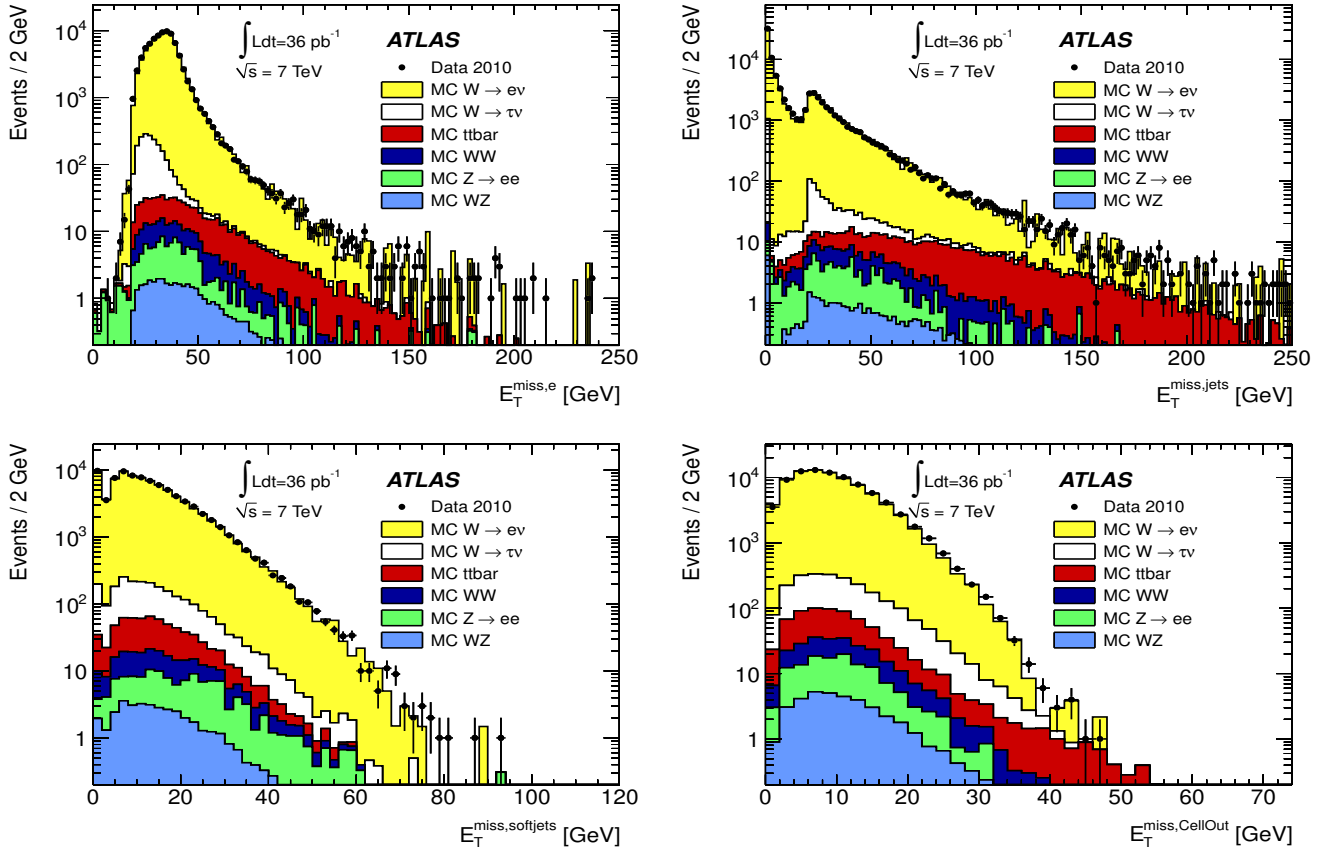


Fig. 13. Distribution of E_T^{miss} computed with cells associated to electrons ($E_T^{\text{miss},e}$) (top left), jets with $p_T > 20$ GeV ($E_T^{\text{miss,jets}}$) (top right), jets with $p_T < 20$ GeV ($E_T^{\text{miss,softjets}}$) (bottom left) and from topoclusters outside reconstructed objects ($E_T^{\text{miss,CellOut}}$) (bottom right) for data. The expectation from Monte Carlo simulation is superimposed and normalized to data, after each MC sample is weighted with its corresponding cross-section.

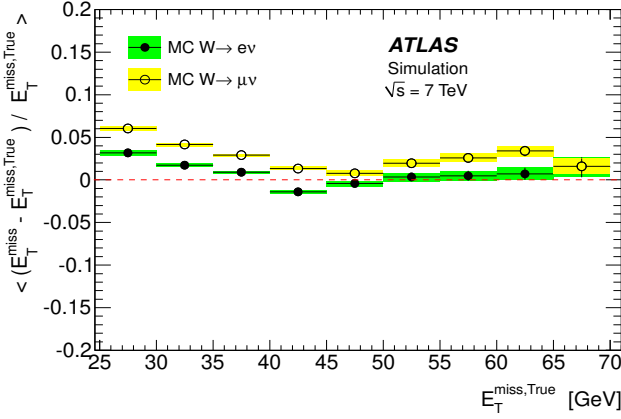


Fig. 14. E_T^{miss} linearity in $W \rightarrow e\nu$ and $W \rightarrow \mu\nu$ MC events as a function of $E_T^{\text{miss, True}}$

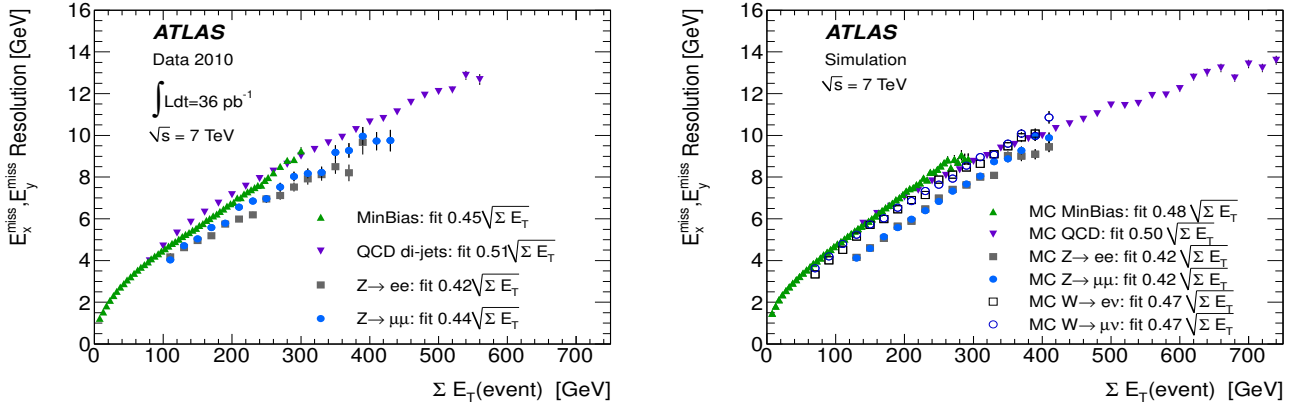


Fig. 15. E_x^{miss} and E_y^{miss} resolution as a function of the total transverse energy in the event calculated by summing the p_T of muons and the total transverse energy in the calorimeter in data at $\sqrt{s} = 7$ TeV (left) and MC (right). The resolution of the two E_T^{miss} components is fitted with a function $\sigma = k \cdot \sqrt{\Sigma E_T}$ and the fitted values of the parameter k , expressed in $\text{GeV}^{1/2}$, are reported in the figure.

Variation	jet events	W production
Dead Material	$(-0.5 \pm 0.1)\%$	$(-0.6 \pm 0.2)\%$
FTFP_BERT	$(0.1 \pm 0.4)\%$	$(0.5 \pm 0.2)\%$
QGSP	$(-1.6 \pm 0.4)\%$	$(-2.2 \pm 0.2)\%$
PYTHIA Perugia 2010 tune	$(-1.7 \pm 0.1)\%$	$(-1.5 \pm 0.2)\%$

Table 2. Systematic uncertainties (R_i) on $E_T^{\text{miss, CellOut}}$ associated with variations in the dead material (all the variations listed in Table 1 are applied at the same time), in the calorimeter shower modelling (FTFP_BERT, QGSP) and in the event generator settings (PYTHIA Perugia 2010 tune).

The shift in the topocluster energy scale is applied by multiplying the topocluster energy by the function:

$$1 \pm a \times (1 + b/p_T) \quad (8)$$

with $a = 3(10)\%$ for $|\eta| < (>) 3.2$ and $b = 1.2$ GeV.

The a parameter in Equation 8 addresses the uncertainty on the cluster energy scale, obtained by comparing the ratio of the cluster energy and the measured track momentum, E/p , in

data and MC simulation [25]. The value in the forward region, where tracks cannot be used to validate the energy scale, is estimated from the transverse momentum balance of one jet in the central region and one jet in the forward region in events with only two jets at high transverse momenta.

The b parameter in Equation 8 addresses the possible change in the clustering efficiency and scale in a non-isolated environment. To go from the response for single isolated particles to the cluster energy scale, possible effects from the noise thresholds in the configuration with nearby particles are taken into account.

Because of threshold effects, more energy is clustered for nearby particles than for isolated ones. In an hypothetical worst case scenario, the environment is so busy that the clustering algorithm is forced to cluster all the deposited energy, with no bias due to the noise thresholds. Therefore, the maximal size of the noise threshold effect can be evaluated by comparing the ratio E_{cell}/p of the total energy E_{cell} deposited into all cells around an isolated track to the track momentum, to the ratio

E/p of the clustered energy E to the track momentum, in data and MC simulation.

The fractional $E_T^{\text{miss,CellOut}}$ uncertainty is evaluated from:

$$(\Delta^{\text{CellOut}+} + \Delta^{\text{CellOut}-}) / (2 \times E_T^{\text{miss,CellOut}}) \quad (9)$$

where

$$\begin{aligned} \Delta^{\text{CellOut}+} &= |E_T^{\text{miss,CellOut}+} - E_T^{\text{miss,CellOut}}| \\ \Delta^{\text{CellOut}-} &= |E_T^{\text{miss,CellOut}-} - E_T^{\text{miss,CellOut}}| \end{aligned} \quad (10)$$

with $E_T^{\text{miss,CellOut}+}$ and $E_T^{\text{miss,CellOut}-}$ obtained by shifting the topocluster energies up and down, respectively, using Equation 8. The value of the fractional $E_T^{\text{miss,CellOut}}$ uncertainty is found to be approximately 13%, decreasing slightly with increasing $\sum E_T^{\text{CellOut}}$. This uncertainty is much larger than the uncertainty due to the detector description estimated from the first three lines of Table 2. The main reason is that the values of a and b which enter into Equation 8 are conservative, to include the effects described above. In particular the cluster energy uncertainty in the forward region is conservatively estimated, since the uncertainty cannot be evaluated using tracks. Moreover, the procedure does not take into account the fact that when the clusters are shifted up in p_T , some of them can form jets above threshold and they are therefore included in the soft jet term in E_T^{miss} . These clusters should be removed from the $E_T^{\text{miss,CellOut}}$, they are in fact kept and this increases the uncertainty. It should also be noted that in the calculation of $E_T^{\text{miss,CellOut}}$ the track momentum is used instead of the topocluster energy when there is a track-topocluster matching (see Section 5.3.1). This would result in a reduced uncertainty due to the more precise measurement of the track momentum, which is not taken into account here. Further study is expected to provide a reduction in this uncertainty in future, by considering the described effects in detail.

To give an estimate of the $E_T^{\text{miss,CellOut}}$ systematic uncertainty, the calorimeter contribution can be taken from Section 7.2, and the uncertainty from the event generator settings from Section 7.1 (PYTHIA Perugia 2010 tune). This results in a total systematic uncertainty on the scale of $E_T^{\text{miss,CellOut}}$ of about 13%, which slightly decreases when $\sum E_T^{\text{CellOut}}$ increases.

7.3 Evaluation of the systematic uncertainty on the $E_T^{\text{miss,softjets}}$ scale

The same procedure described in the previous sections is used to assess the systematic uncertainty on the E_T^{miss} term calculated from soft jets (see Section 5.1).

Using the MC approach described in Section 7.1, it is found that the uncertainty on $E_T^{\text{miss,softjets}}$ does not exhibit a large dependence on the event $\sum E_T$, as was also found for the uncertainty on the $E_T^{\text{miss,CellOut}}$ scale. The results are consistent between the QCD jet samples and the W samples, as can be seen from Table 3 which gives the systematic uncertainties R_i as computed in jet samples and in $W \rightarrow \ell\nu$ samples.

A total, symmetric, systematic uncertainty of about 3.3% on the $E_T^{\text{miss,softjets}}$ term is obtained by combining the results

Variation	jet events	W production
Dead Material	$(-1.5 \pm 0.1)\%$	$(-1.5 \pm 0.2)\%$
FTFP_BERT	$(0.3 \pm 0.4)\%$	$(0.8 \pm 0.2)\%$
QGSP	$(-2.6 \pm 0.4)\%$	$(-2.5 \pm 0.2)\%$
PYTHIA Perugia 2010 tune	$(-1.4 \pm 0.1)\%$	$(-1.0 \pm 0.2)\%$

Table 3. Systematic uncertainties (R_i) on $E_T^{\text{miss,softjets}}$ associated with variations in the dead material (all the variations listed in Table 1 are applied at the same time), in the calorimeter shower modelling (FTFP_BERT, QGSP) and in the event generator settings (PYTHIA Perugia 2010 tune).

in Table 3, as was done in Section 7.1. With the same data-driven approach utilising the uncertainty on the topocluster energy scale described in Section 7.2, the systematic uncertainty on $E_T^{\text{miss,softjets}}$ is evaluated to be about 10%.

As for $E_T^{\text{miss,CellOut}}$, the uncertainty on the $E_T^{\text{miss,softjets}}$ scale found by shifting the topocluster energies is larger than the uncertainty estimated from MC simulation. To give an estimate of the systematic uncertainty on $E_T^{\text{miss,softjets}}$, the contribution from the calorimeter response can be taken from the data-driven evaluation and the contribution from the event generator settings from Table 3. This results in an overall systematic uncertainty of about 10% on $E_T^{\text{miss,softjets}}$, slightly increasing as $\sum E_T$ increases.

7.4 Evaluation of the overall systematic uncertainty on the E_T^{miss} scale in $W \rightarrow e\nu$ and $W \rightarrow \mu\nu$ events

Using as inputs the systematic uncertainties on the different reconstructed objects [8, 21] and on $E_T^{\text{miss,CellOut}}$ and $E_T^{\text{miss,softjets}}$ evaluated in the previous sections, the overall E_T^{miss} systematic uncertainty in $W \rightarrow e\nu$ and $W \rightarrow \mu\nu$ events is estimated. The same method can be applied to any final state event topology. Figure 16 shows, for both $W \rightarrow e\nu$ and $W \rightarrow \mu\nu$ events, the systematic uncertainties on each of the terms $E_T^{\text{miss},e}$ ($E_T^{\text{miss},\mu}$), $E_T^{\text{miss,jets}}$, $E_T^{\text{miss,softjets}}$ and $E_T^{\text{miss,CellOut}}$ as a function of their individual contribution to $\sum E_T$ labelled $\sum E_T^{\text{term}}$. All the uncertainties are calculated with the formulae in Equations 9 and 10. In the same figure the uncertainty on E_T^{miss} due to the uncertainties on the different terms is also shown as a function of the total $\sum E_T$, together with the overall uncertainty on E_T^{miss} , obtained by combining the partial terms. The uncertainties on $E_T^{\text{miss,softjets}}$ and $E_T^{\text{miss,CellOut}}$ are considered to be fully correlated. In $W \rightarrow e\nu$ and $W \rightarrow \mu\nu$ events, selected as described in Section 3.3, the overall uncertainty on the E_T^{miss} scale increases with $\sum E_T$ from $\sim 1\%$ to $\sim 7\%$. It is estimated to be, on average, about 2.6% for both channels.

The E_T^{miss} scale uncertainty depends on the event topology because the contribution of a given E_T^{miss} term can vary for different final states.

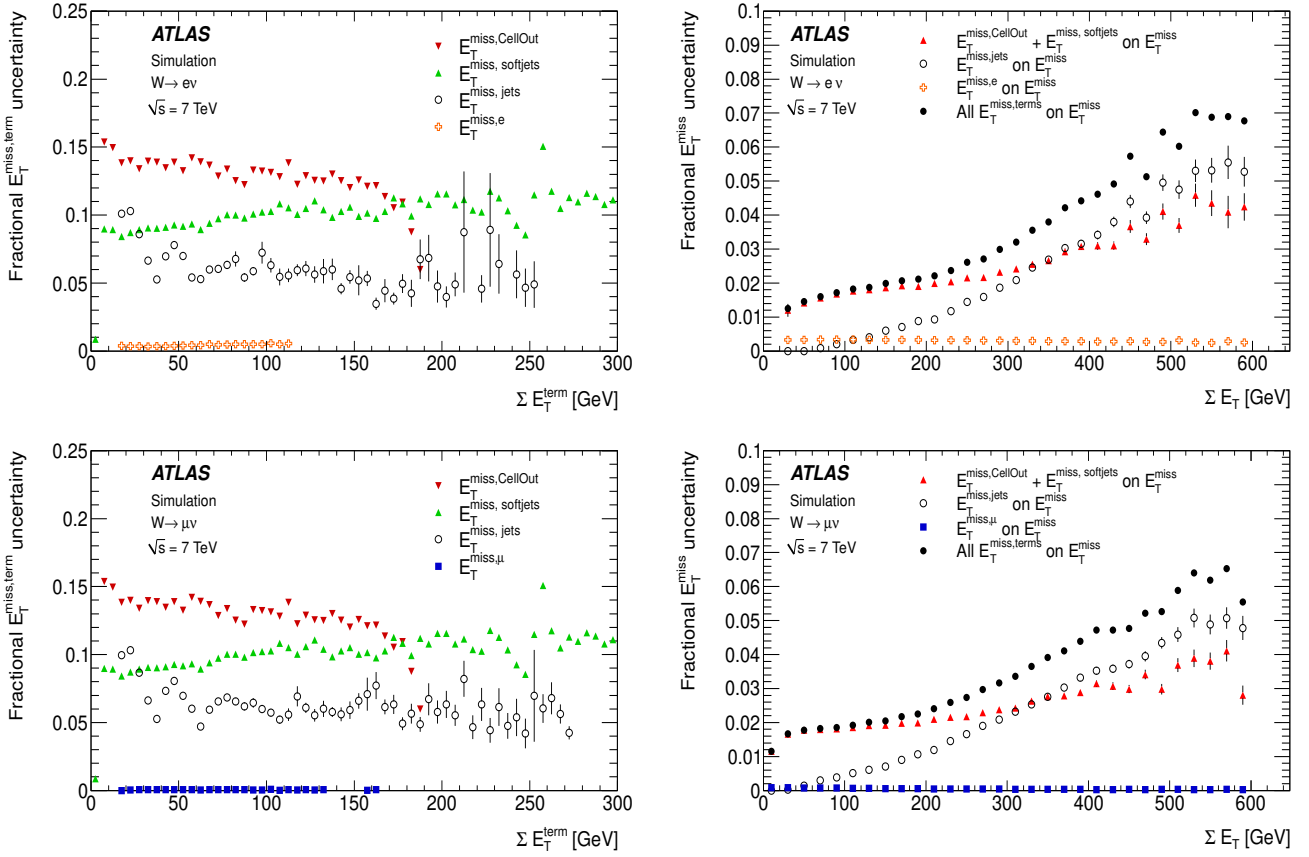


Fig. 16. Fractional systematic uncertainty (calculated as in Equations 9 and 10) on different E_T^{miss} terms as a function of respective ΣE_T^{term} (left) and contributions of different term uncertainties on E_T^{miss} uncertainty as a function of ΣE_T (right) in MC $W \rightarrow e\nu$ events (top) and $W \rightarrow \mu\nu$ events (bottom). The overall systematic uncertainty on the E_T^{miss} scale, obtained combining the various contributions is shown in the right plots (filled circles). The uncertainties on $E_T^{\text{miss,softjets}}$ and $E_T^{\text{miss,CellOut}}$ are considered to be fully correlated.

8 Determination of the E_T^{miss} scale from $W \rightarrow \ell\nu$ events

The determination of the absolute E_T^{miss} scale is important in a range of analyses involving E_T^{miss} measurements, ranging from precision measurements to searches for new physics.

In this section two complementary methods to determine the absolute scale of E_T^{miss} using $W \rightarrow \ell\nu$ events are described. The first method uses a fit to the distribution of the transverse mass, m_T , of the lepton- E_T^{miss} system, and is sensitive both to the scale and the resolution of E_T^{miss} . The second method uses the interdependence of the neutrino and lepton momenta in the $W \rightarrow e\nu$ channel, and the E_T^{miss} scale is determined as a function of the reconstructed electron transverse momentum. Both methods allow checks on the agreement between data and MC simulation for the E_T^{miss} scale.

8.1 Reconstructed transverse mass method

The method described in this section uses the shape of the m_T distribution and is sensitive to both the E_T^{miss} resolution and

scale. The lepton transverse momentum, p_T^ℓ , and the E_T^{miss} are used to calculate m_T as:

$$m_T = \sqrt{2p_T^\ell E_T^{\text{miss}}(1 - \cos\phi)} \quad (11)$$

where ϕ is the azimuthal angle between the lepton momentum and E_T^{miss} directions. The true m_T is reconstructed from the simulation under the hypothesis that E_T^{miss} is entirely due to the neutrino momentum, p_T^ν . Template histograms of the m_T distributions are generated by convoluting the true transverse mass distribution with a Gaussian function:

$$E_{x(y)}^{\text{miss,smeared}} = \alpha E_{x(y)}^{\text{miss,True}} * \text{Gauss}(0, k \cdot \sqrt{\Sigma E_T}) \quad (12)$$

where the parameters α and k are the E_T^{miss} scale and resolution respectively.

The α and k parameters are determined through a fit of the m_T distribution to data using a linear combination of signal and background m_T distributions obtained from simulation. All the backgrounds, with the exception of the jet background, are evaluated from the same MC samples used in Section 6.3 and the normalization is fixed according to their cross-sections. The

shape of the jet background is also evaluated from MC simulation and its normalization is obtained from the fit, in addition to α and k .

To select $W \rightarrow \mu\nu$ events, the same criteria as described in Section 3.3 are used, with the exception that no cut on E_T^{miss} is applied and a looser cut, $m_T > 30$ GeV, is applied in order that the background normalization can be fitted. The α and k parameters obtained from the fit are shown in Table 4, together with the numbers of events for the signal and backgrounds and the χ^2/ndof of the fit. In the table, instead of the values of α , the values of $\alpha - 1 = \langle (E_{x(y)}^{\text{miss}} - E_{x(y)}^{\text{miss, True}}) / E_{x(y)}^{\text{miss, True}} \rangle$ are reported, in order to compare with the result in Sections 6.3.1 and 8.2. The results for the α and k parameters using the m_T distribution of the simulated signal are also shown in Table 4, and they are in good agreement with the results from data. The result of the fit to data and MC simulation is shown in Figure 17.

To select $W \rightarrow e\nu$ events, the selection described in Section 3.3 is used with the addition of tighter cuts. A cut $E_T^{\text{miss}} > 36$ GeV is applied to exclude the region where the E_T^{miss} response is not linear (see Figure 14). A cut $m_T > 40$ GeV is also applied. The α and k parameters obtained from the fit are shown in Table 4, together with the results obtained from the MC, which are in good agreement with data. The result of the fit to data and MC simulation is shown in Figure 17.

The results obtained with this method are compatible, at the few percent level, with the results shown in Figure 14 and Figure 15, which were derived using only simulation. From those figures, for the $W \rightarrow \mu\nu$ channel $\alpha - 1$ has values up to 3% and the resolution is $0.47\sqrt{\sum E_T}$; for the $W \rightarrow e\nu$ channel $\alpha - 1$ is close to zero for high E_T^{miss} values and the resolution is $0.47\sqrt{\sum E_T}$.

The uncertainty due to background subtraction is already included in the uncertainty reported in Table 4. The systematic uncertainty on $\alpha - 1$ is determined to be about 1% for each channel, by checking the stability of the results using different cuts on E_T^{miss} and using a different generator, MC@NLO. In summary, with this method the E_T^{miss} absolute scale is determined from $W \rightarrow \ell\nu$ events, in a data sample corresponding to an integrated luminosity of about 36 pb^{-1} , with an uncertainty (adding the uncertainties reported in Table 4 with the systematic uncertainty) of about 1.5% and about 2% for the $W \rightarrow \mu\nu$ and $W \rightarrow e\nu$ decay channels, respectively.

8.2 Method based on the correlation between electron and neutrino transverse momenta in $W \rightarrow e\nu$

In this section the correlation between the transverse momenta of charged and neutral leptons from W boson decays is used to determine the E_T^{miss} scale. The mean measured E_T^{miss} is compared to the mean true E_T^{miss} from signal MC events. The relative bias in the reconstructed E_T^{miss} , $(\langle E_T^{\text{miss}} \rangle - \langle E_T^{\text{miss, True}} \rangle) / \langle E_T^{\text{miss, True}} \rangle$, is studied as a function of p_T^e because the MC simulation of the electron response is more accurate than that for hadrons.

This method is shown for $W \rightarrow e\nu$ events by applying selection criteria similar to the ones described in Section 3.3, but with isolation requirements both on the electron track and

calorimeter signal. The E_T^{miss} is required to be greater than 20 GeV and no cut is applied on m_T .

MC samples are generated with MC@NLO [15]. A next-to-leading-order (NLO) generator is used for this study because in this approach the E_T^{miss} scale is validated on the basis of the known decay properties of the W boson. The correlation between p_T^e and p_T^e is important for this study, and is poorly described by leading-order generators such as PYTHIA, whereas it is much improved in MC@NLO. The MC events are weighted such that the true W boson transverse momentum, p_T^W , and pseudorapidity η^W agree with that generated using the RESBOS [26] generator which is more accurate in describing p_T^W at low values. Finally, an additional smearing is applied to the reconstructed electron momentum in the MC samples, to match the electron resolution measured in data, and the correction is propagated to E_T^{miss} .

A data-driven technique is used to estimate the impact of jet background, which is small (see Figure 18 left) and concentrated at low p_T^e . $W \rightarrow \tau\nu$ events, where the τ decays to an electron, are the second largest background, but the impact on the mean value of E_T^{miss} is found to be negligible.

The distribution of p_T^e is shown in Figure 18. The distribution from data after event selection is fitted by varying the normalization of signal MC and QCD background distributions. A satisfactory description of data is achieved except for the first bin, which is excluded from the fit. For each p_T^e bin, the corrected distribution of E_T^{miss} is obtained by subtracting that of the background sample (after normalizing it according to the fit) from the data distribution. The largest impact of background corresponds to $p_T^e = 20$ GeV, with an effect of about 2 GeV on the mean value of E_T^{miss} ; the effect decreases quickly to 0.2 GeV at $p_T^e = 30$ GeV.

Since a cut on E_T^{miss} is used for the event selection and the E_T^{miss} resolution is finite, the results are biased. To correct for the bias in signal MC events the requirement of reconstructed $E_T^{\text{miss}} > 20$ GeV is replaced by a cut on true $E_T^{\text{miss}} > 20$ GeV.

The mean measured E_T^{miss} , corrected for background and for the event selection bias, is used to calculate the relative bias in the reconstructed E_T^{miss} , $(\langle E_T^{\text{miss}} \rangle - \langle E_T^{\text{miss, True}} \rangle) / \langle E_T^{\text{miss, True}} \rangle$, which is shown in Figure 18 as a function of p_T^e . The figure shows that the E_T^{miss} scale is correct at low values of p_T^e while it is overestimated at high values of p_T^e .

The bias on E_T^{miss} is on the percent level between 25 and 35 GeV, then it rises up to 7% and it is $2 \pm 0.1\%$ on average. For comparison, if the entire calculation is performed on signal MC events alone, the resulting average bias in E_T^{miss} is $2.9 \pm 0.1\%$. The method relies on simulation to derive the correlation between $E_T^{\text{miss, True}}$ and p_T^e , so it can be sensitive to details of the simulation. In particular, the jet factorization and renormalization scales, as well as the choice of PDF, can affect the results, but all these also change the p_T^W distribution. Therefore the shape of the p_T^W distribution was distorted by $\pm 10\%$, justified by the comparison of a recent measurement of the p_T^Z distribution [27] with RESBOS predictions, and the relative bias was calculated again. A systematic uncertainty on the relative E_T^{miss} scale bias of $\pm 2\%$ is evaluated. The results for the average E_T^{miss} scale are summarized in Table 5. These

Channel	$\alpha - 1$ (%)	k	Signal	EW(fixed)	QCD	χ^2/ndof
$W \rightarrow \mu\nu$ data	5.1 ± 0.8	0.52 ± 0.01	164920 ± 840	14760	24870 ± 840	68/87
$W \rightarrow \mu\nu$ MC	5.5 ± 0.8	0.50 ± 0.01				70/78
$W \rightarrow e\nu$ data	-0.8 ± 1.6	0.49 ± 0.01	75660 ± 180	1210	980 ± 180	54/75
$W \rightarrow e\nu$ MC	1.8 ± 1.7	0.50 ± 0.01				38/54

Table 4. Results of m_T fit in $W \rightarrow \ell\nu$ events. The second and third columns show the scale and resolution parameters obtained. The numbers of events for the signal, the electroweak and QCD backgrounds obtained from the fit are shown in the fourth, fifth and sixth columns for data. In the last column the χ^2/ndof of the fit is reported. The errors are statistical and take into account background subtraction uncertainties and correlations.

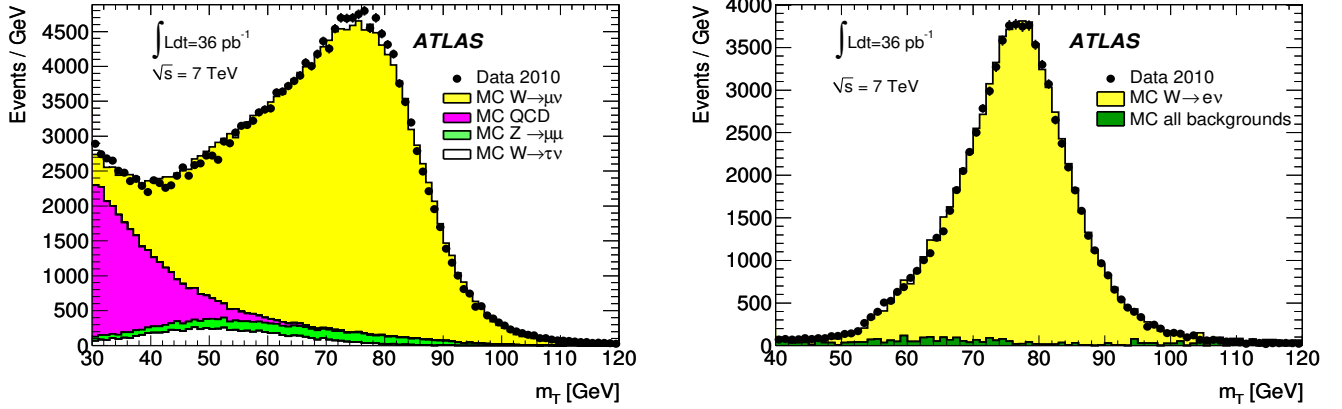


Fig. 17. Distributions of the transverse mass, m_T , of the muon- E_T^{miss} system (left) and of the electron- E_T^{miss} system (right) for data. The m_T distributions from Monte Carlo simulation are superimposed, after each background sample is weighted as explained in the text. The main backgrounds are shown for $W \rightarrow \mu\nu$, the sum of all backgrounds is shown for $W \rightarrow e\nu$. The $W \rightarrow \ell\nu$ MC signal histogram is obtained using the true E_T^{miss} smeared as in Equation (12) with the scale and resolution parameters obtained from the fit.

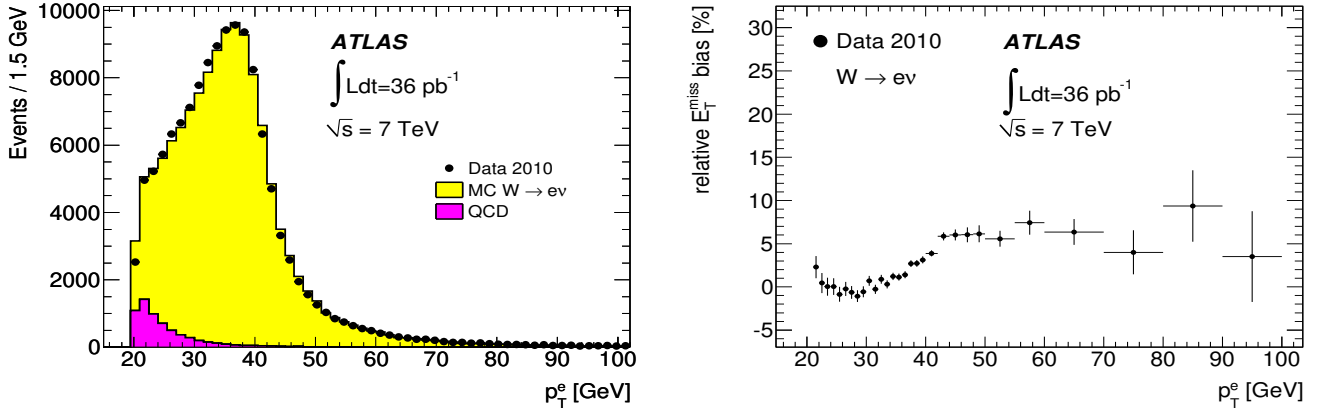


Fig. 18. Transverse momentum distribution of electron candidates in data, in signal MC with nominal event selection and with reversed cuts for background (QCD) from data (left). Relative bias in the reconstructed E_T^{miss} (right). Only statistical uncertainties are shown.

results agree within errors with the values of $\alpha - 1$ shown in Table 4.

9 Conclusion

The missing transverse momentum (E_T^{miss}) has been measured in minimum bias, di-jet, $Z \rightarrow \ell\ell$ and $W \rightarrow \ell\nu$ events in 7 TeV pp collisions recorded with the ATLAS detector in 2010.

The value of E_T^{miss} is reconstructed from calorimeter cells in topological clusters, with the exception of electrons and photons for which a different clustering algorithm is used, and from reconstructed muons. The cells are calibrated according to their parent particle type. The scheme yielding the best performance is evaluated to be that in which electrons are calibrated with the default electron calibration and photons are used at the EM scale, the τ -jets and jets are calibrated with the local hadronic calibration (LCW), the jets with p_T greater than 20 GeV are scaled to the jet energy scale, and the contri-

source	scale bias (%)
data	$2.0 \pm 0.1 \pm 2.0$
MC	2.9 ± 0.1

Table 5. Average relative E_T^{miss} scale bias obtained from data and MC simulation from the electron-neutrino correlation method. The statistical and the systematic uncertainties are given for data.

bution from topoclusters not associated to high- p_T objects is calculated with LCW calibration combined with tracking information.

Monte Carlo simulation is found to describe the data in general rather well. No large tails are observed in the E_T^{miss} distribution in minimum bias, di-jet and $Z \rightarrow \ell\ell$ events, where no significant E_T^{miss} is expected. The tails are not completely well described by MC simulation especially in di-jets events, where there are more events in the tail in data.

There is some difference observed between data and MC simulation for the reconstructed total transverse energy. The precise difference is dependent on the model used to simulate soft-physics processes.

The E_T^{miss} resolution is similar in the different channels studied and in agreement with the resolution in the MC simulation. The resolution follows a function $\sigma = k \cdot \sqrt{\Sigma E_T}$, where the parameter k is about $0.5 \text{ GeV}^{1/2}$.

The linearity of the E_T^{miss} measurement in $W \rightarrow \ell\nu$ events is studied in MC simulation as a function of the true E_T^{miss} . Except for the bias observed at small true E_T^{miss} values (visible up to 40 GeV), due to the finite E_T^{miss} resolution, the linearity is better than 1% in $W \rightarrow e\nu$ events, while a small non-linearity up to about 3% is observed in $W \rightarrow \mu\nu$ events.

The E_T^{miss} projected along the Z direction in $Z \rightarrow \ell\ell$ events is observed to have a bias up to 6 GeV at large values of p_T^Z in events with no jets, suggesting that some improvements are still needed in the calibration of low- p_T objects.

The overall systematic uncertainty on E_T^{miss} scale, calculated by combining the uncertainties on the various terms entering the full E_T^{miss} calculation, is estimated to be, on average, 2.6% in events with a W decaying to a lepton (electron or muon) and neutrino. The uncertainty is larger at large ΣE_T .

Two methods are used for determining the E_T^{miss} scale from $W \rightarrow \ell\nu$ events in data, giving results in agreement with that evaluated using MC simulation. The resulting uncertainty on the E_T^{miss} scale determined in-situ with 36 pb^{-1} of data is, on average, about 2%.

10 Acknowledgements

We thank CERN for the very successful operation of the LHC, as well as the support staff from our institutions without whom ATLAS could not be operated efficiently.

We acknowledge the support of ANPCyT, Argentina; YerPhI, Armenia; ARC, Australia; BMWF, Austria; ANAS, Azerbaijan; SSTC, Belarus; CNPq and FAPESP, Brazil; NSERC, NRC and CFI, Canada; CERN; CONICYT, Chile; CAS, MOST and NSFC, China; COLCIENCIAS, Colombia; MSMT CR, MPO CR and VSC CR, Czech Republic; DNRF, DNSRC and

Lundbeck Foundation, Denmark; ARTEMIS, European Union; IN2P3-CNRS, CEA-DSM/IRFU, France; GNAS, Georgia; BMBF, DFG, HGF, MPG and AvH Foundation, Germany; GSRT, Greece; ISF, MINERVA, GIF, DIP and Benoziyo Center, Israel; INFN, Italy; MEXT and JSPS, Japan; CNRST, Morocco; FOM and NWO, Netherlands; RCN, Norway; MNiSW, Poland; GRICES and FCT, Portugal; MERYS (MECTS), Romania; MES of Russia and ROSATOM, Russian Federation; JINR; MSTB, Serbia; MSSR, Slovakia; ARRS and MVZT, Slovenia; DST/NRF, South Africa; MICINN, Spain; SRC and Wallenberg Foundation, Sweden; SER, SNSF and Cantons of Bern and Geneva, Switzerland; NSC, Taiwan; TAEK, Turkey; STFC, the Royal Society and Leverhulme Trust, United Kingdom; DOE and NSF, United States of America.

The crucial computing support from all WLCG partners is acknowledged gratefully, in particular from CERN and the ATLAS Tier-1 facilities at TRIUMF (Canada), NDGF (Denmark, Norway, Sweden), CC-IN2P3 (France), KIT/GridKA (Germany), INFN-CNAF (Italy), NL-T1 (Netherlands), PIC (Spain), ASGC (Taiwan), RAL (UK) and BNL (USA) and in the Tier-2 facilities worldwide.

References

1. The ATLAS Collaboration, *The ATLAS Experiment at the CERN Large Hadron Collider*, JINST **3** (2008) S08003.
2. The ATLAS Collaboration, *Performance of the ATLAS detector using first collision data*, JHEP **09** (2010) 056.
3. The ATLAS Collaboration, *Search for squarks and gluinos using final states with jets and missing transverse momentum with the ATLAS detector in 7 TeV proton-proton collisions*, Phys. Lett. B **701** (2011) 186.
4. The ATLAS Collaboration, *Properties of jets and inputs to jets reconstruction and calibration with the ATLAS detector using proton-proton collisions at $\sqrt{s} = 7$ TeV*, ATLAS-CONF-2010-053.
5. M. Cacciari, G. P. Salam, and G. Soyez, *The anti- k_t jet clustering algorithm*, JHEP **05** (2008) 063, arXiv:0802.1189.
6. The ATLAS Collaboration, *Luminosity Determination in pp Collisions at 7 TeV using the ATLAS Detector at the LHC*, EPJC **071** (2011) 1630, arXiv:1101.2185.
7. The ATLAS Collaboration, *Updated Luminosity Determination in pp Collisions at $\sqrt{s}=7$ TeV using the ATLAS Detector*, ATLAS-CONF-2011-011.
8. The ATLAS Collaboration, *Measurement of the $W \rightarrow l\nu$ and $Z \rightarrow ll$ production cross sections in proton-proton collisions at $\sqrt{s} = 7$ TeV with the ATLAS detector*, JHEP **12** (2010) 060, arXiv:1010.2130.
9. The ATLAS Collaboration, *Charged-particle multiplicities in pp interactions measured with the ATLAS detector at the LHC*, New J. Phys. **13** (2011) 053033.
10. The ATLAS Collaboration, *Muon Reconstruction Performance*, ATLAS-CONF-2010-064.
11. The ATLAS Collaboration, *Electron and photon reconstruction and identification in ATLAS: expected performance at high energy and results at 900 GeV*, ATLAS-CONF-2010-005.
12. T. Sjostrand, S. Mrenna, and P. Skands, *PYTHIA 6.4 Physics and Manual*, JHEP **05** (2006) 026.
13. The ATLAS Collaboration, *Charged particle multiplicities in pp interactions at $\sqrt{s} = 0.9$ and 7 TeV in a diffractive limited phase-space measured with the ATLAS detector at the LHC and new PYTHIA6 tune*, ATLAS-CONF-2010-031.

14. S. Agostinelli et al., *GEANT4: A simulation toolkit*, NIM A **506** (2003) 250.
15. S. Frixione and B. R. Webber, *Matching NLO QCD computations and parton shower simulations*, JHEP **06** (2002) 029.
16. T. Sjostrand, S. Mrenna, and P. Skands, *Brief Introduction to PYTHIA8.1*, Comput. Phys. Comm. **178** (2008) 852, [arXiv:0710.3820](#).
17. The ATLAS Collaboration, *Expected Performance of the ATLAS Experiment - Detector, Trigger and Physics (Jet and E_T^{miss} chapter)*, [arXiv:0901.0512](#).
18. W. Lampl et al., *Calorimeter clustering algorithms: Description and performance*, ATL-LARG-PUB-2008-002.
19. The ATLAS Collaboration, *Tau Reconstruction and Identification Performance in ATLAS*, ATLAS-CONF-2010-086.
20. T. Barillari et al., *Local Hadron Calibration Properties*, ATL-LARG-PUB-2009-001.
21. The ATLAS Collaboration, *Jet energy scale and its systematic uncertainty in proton-proton collisions at $\sqrt{s} = 7$ TeV in ATLAS 2010 data*, ATLAS-CONF-2011-032.
22. R. Corke and T. Sjostrand, *Interleaved Parton Showers and Tuning Prospects*, JHEP **032** (2011) 1103, [arXiv:1011.1759](#).
23. The ATLAS Collaboration, *Measurement of inclusive jet and dijet cross sections in proton-proton collisions at 7 TeV centre-of-mass energy with the ATLAS detector*, Eur. Phys. J. C **71** (2011) 1512, [arXiv:1009.5908](#).
24. The ATLAS Collaboration, *Reconstruction and Calibration of Missing Transverse Energy and Performance in Z and W events in ATLAS Proton-Proton Collisions at $\sqrt{s} = 7$ TeV*, ATLAS-CONF-2011-080.
25. The ATLAS Collaboration, *ATLAS Calorimeter Response to Single Isolated Hadrons and Estimation of the Calorimeter Jet Scale Uncertainty*, ATLAS-CONF-2011-028.
26. C. Balazs and C. P. Yuan, *Soft gluon effects on lepton pairs at hadron colliders*, Phys. Rev. D **56** (1997) 55585583.
27. The ATLAS Collaboration, *Measurement of the transverse momentum distribution of Z/ γ bosons in proton-proton collisions at $\sqrt{s} = 7$ TeV with the ATLAS detector*, submitted to Phys. Lett. B, [arXiv:1107.2381](#).

The ATLAS Collaboration

G. Aad⁴⁸, B. Abbott¹¹¹, J. Abdallah¹¹, A.A. Abdelalim⁴⁹, A. Abdesselam¹¹⁸, O. Abidinov¹⁰, B. Abi¹¹², M. Abolins⁸⁸, H. Abramowicz¹⁵³, H. Abreu¹¹⁵, E. Acerbi^{89a,89b}, B.S. Acharya^{164a,164b}, D.L. Adams²⁴, T.N. Addy⁵⁶, J. Adelman¹⁷⁵, M. Aderholz⁹⁹, S. Adomeit⁹⁸, P. Adragna⁷⁵, T. Adye¹²⁹, S. Aefsky²², J.A. Aguilar-Saavedra^{124b,a}, M. Aharrouche⁸¹, S.P. Ahlen²¹, F. Ahles⁴⁸, A. Ahmad¹⁴⁸, M. Ahsan⁴⁰, G. Aielli^{133a,133b}, T. Akdogan^{18a}, T.P.A. Åkesson⁷⁹, G. Akimoto¹⁵⁵, A.V. Akimov⁹⁴, A. Akiyama⁶⁷, M.S. Alam¹, M.A. Alam⁷⁶, J. Albert¹⁶⁹, S. Albrand⁵⁵, M. Aleksa²⁹, I.N. Aleksandrov⁶⁵, F. Alessandria^{89a}, C. Alexa^{25a}, G. Alexander¹⁵³, G. Alexandre⁴⁹, T. Alexopoulos⁹, M. Alhroob²⁰, M. Aliev¹⁵, G. Alimonti^{89a}, J. Alison¹²⁰, M. Aliyev¹⁰, P.P. Allport⁷³, S.E. Allwood-Spiers⁵³, J. Almond⁸², A. Aloisio^{102a,102b}, R. Alon¹⁷¹, A. Alonso⁷⁹, M.G. Alvigi^{102a,102b}, K. Amako⁶⁶, P. Amaral²⁹, C. Amelung²², V.V. Ammosov¹²⁸, A. Amorim^{124a,b}, G. Amorós¹⁶⁷, N. Amram¹⁵³, C. Anastopoulos²⁹, L.S. Ancu¹⁶, N. Andari¹¹⁵, T. Andeen³⁴, C.F. Anders²⁰, G. Anders^{58a}, K.J. Anderson³⁰, A. Andreazza^{89a,89b}, V. Andrei^{58a}, M.-L. Andrieux⁵⁵, X.S. Anduaga⁷⁰, A. Angerami³⁴, F. Anghinolfi²⁹, N. Anjos^{124a}, A. Annovi⁴⁷, A. Antonaki⁸, M. Antonelli⁴⁷, A. Antonov⁹⁶, J. Antos^{144b}, F. Anulli^{132a}, S. Aoun⁸³, L. Aperio Bella⁴, R. Apolle^{118,c}, G. Arabidze⁸⁸, I. Aracena¹⁴³, Y. Arai⁶⁶, A.T.H. Arce⁴⁴, J.P. Archambault²⁸, S. Arfaoui^{29,d}, J.-F. Arguin¹⁴, E. Arik^{18a,*}, M. Arik^{18a}, A.J. Armbruster⁸⁷, O. Arnaez⁸¹, C. Arnault¹¹⁵, A. Artamonov⁹⁵, G. Artoni^{132a,132b}, D. Arutinov²⁰, S. Asai¹⁵⁵, R. Asfandiyarov¹⁷², S. Ask²⁷, B. Åsman^{146a,146b}, L. Asquith⁵, K. Assamagan²⁴, A. Astbury¹⁶⁹, A. Astvatsaturov⁵², G. Atoian⁹, B. Aubert⁴, B. Auerbach¹⁷⁵, E. Auge¹¹⁵, K. Augsten¹²⁷, M. Aurousseau^{145a}, N. Austin⁷³, G. Avolio¹⁶³, R. Avramidou⁹, D. Axen¹⁶⁸, C. Ay⁵⁴, G. Azuelos^{93,e}, Y. Azuma¹⁵⁵, M.A. Baak²⁹, G. Baccaglioni^{89a}, C. Bacci^{134a,134b}, A.M. Bach¹⁴, H. Bachacou¹³⁶, K. Bachas²⁹, G. Bachy²⁹, M. Backes⁴⁹, M. Backhaus²⁰, E. Badescu^{25a}, P. Baggaia^{132a,132b}, S. Bahinipati², Y. Bai^{32a}, D.C. Bailey¹⁵⁸, T. Bain¹⁵⁸, J.T. Baines¹²⁹, O.K. Baker¹⁷⁵, M.D. Baker²⁴, S. Baker⁷⁷, E. Banas³⁸, P. Banerjee⁹³, Sw. Banerjee¹⁷², D. Banfi²⁹, A. Bangert¹³⁷, V. Bansal¹⁶⁹, H.S. Bansil¹⁷, L. Barak¹⁷¹, S.P. Baranov⁹⁴, A. Barashkou⁶⁵, A. Barbaro Galtieri¹⁴, T. Barber²⁷, E.L. Barberio⁸⁶, D. Barberis^{50a,50b}, M. Barbero²⁰, D.Y. Bardin⁶⁵, T. Barillari⁹⁹, M. Barisonzi¹⁷⁴, T. Barklow¹⁴³, N. Barlow²⁷, B.M. Barnett¹²⁹, R.M. Barnett¹⁴, A. Baroncelli^{134a}, G. Barone⁴⁹, A.J. Barr¹¹⁸, F. Barreiro⁸⁰, J. Barreiro Guimarães da Costa⁵⁷, P. Barrillon¹¹⁵, R. Bartoldus¹⁴³, A.E. Barton⁷¹, D. Bartsch²⁰, V. Bartsch¹⁴⁹, R.L. Bates⁵³, L. Batkova^{144a}, J.R. Batley²⁷, A. Battaglia¹⁶, M. Battistin²⁹, G. Battistoni^{89a}, F. Bauer¹³⁶, H.S. Bawa^{143,f}, B. Beare¹⁵⁸, T. Beau⁷⁸, P.H. Beauchemin¹¹⁸, R. Beccherle^{50a}, P. Bechtel⁴¹, H.P. Beck¹⁶, M. Beckingham⁴⁸, K.H. Becks¹⁷⁴, A.J. Beddall^{18c}, A. Beddall^{18c}, S. Bedikian¹⁷⁵, V.A. Bednyakov⁶⁵, C.P. Bee⁸³, M. Begel²⁴, S. Behar Harpaz¹⁵², P.K. Behera⁶³, M. Beimforde⁹⁹, C. Belanger-Champagne⁸⁵, P.J. Bell⁴⁹, W.H. Bell⁴⁹, G. Bella¹⁵³, L. Bellagamba^{19a}, F. Bellina²⁹, M. Bellomo²⁹, A. Belloni⁵⁷, O. Beloborodova¹⁰⁷, K. Belotskiy⁹⁶, O. Beltramello²⁹, S. Ben Ami¹⁵², O. Benary¹⁵³, D. Benckroun^{135a}, C. Benchouk⁸³, M. Bendel⁸¹, N. Benekos¹⁶⁵, Y. Benhammou¹⁵³, D.P. Benjamin⁴⁴, M. Benoit¹¹⁵, J.R. Bensinger²², K. Benslama¹³⁰, S. Bentvelsen¹⁰⁵, D. Berge²⁹, E. Bergeas Kuutmann⁴¹, N. Berger⁴, F. Berghaus¹⁶⁹, E. Berglund⁴⁹, J. Beringer¹⁴, K. Bernardet⁸³, P. Bernat⁷⁷, R. Bernhard⁴⁸, C. Bernius²⁴, T. Berry⁷⁶, A. Bertin^{19a,19b}, F. Bertinelli²⁹, F. Bertolucci^{122a,122b}, M.I. Besana^{89a,89b}, N. Besson¹³⁶, S. Bethke⁹⁹, W. Bhimji⁴⁵, R.M. Bianchi²⁹, M. Bianco^{72a,72b}, O. Biebel⁹⁸, S.P. Bieniek⁷⁷, K. Bierwagen⁵⁴, J. Biesiada¹⁴, M. Biglietti^{134a,134b}, H. Bilokon⁴⁷, M. Bindi^{19a,19b}, S. Binet¹¹⁵, A. Bingul^{18c}, C. Bini^{132a,132b}, C. Biscarat¹⁷⁷, U. Bitenc⁴⁸, K.M. Black²¹, R.E. Blair⁵, J.-B. Blanchard¹¹⁵, G. Blanchot²⁹, T. Blazek^{144a}, C. Blocker²², J. Blocki³⁸, A. Blondel⁴⁹, W. Blum⁸¹, U. Blumenschein⁵⁴, G.J. Bobbink¹⁰⁵, V.B. Bobrovnikov¹⁰⁷, S.S. Bocchetta⁷⁹, A. Bocci⁴⁴, C.R. Boddy¹¹⁸, M. Boehler⁴¹, J. Boek¹⁷⁴, N. Boelaert³⁵, S. Böser⁷⁷, J.A. Bogaerts²⁹, A. Bogdanchikov¹⁰⁷, A. Bogouch^{90,*}, C. Bohm^{146a}, V. Boisvert⁷⁶, T. Bold^{163,g}, V. Boldea^{25a}, N.M. Bolnet¹³⁶, M. Bona⁷⁵, V.G. Bondarenko⁹⁶, M. Boonekamp¹³⁶, G. Boorman⁷⁶, C.N. Booth¹³⁹, S. Bordon⁷⁸, C. Borer¹⁶, A. Borisov¹²⁸, G. Borissov⁷¹, I. Borjanovic^{12a}, S. Borroni^{132a,132b}, K. Bos¹⁰⁵, D. Boscherini^{19a}, M. Bosman¹¹, H. Boterenbrood¹⁰⁵, D. Botterill¹²⁹, J. Bouchami⁹³, J. Boudreau¹²³, E.V. Bouhova-Thacker⁷¹, C. Bourdarios¹¹⁵, N. Bousson⁸³, A. Boveia³⁰, J. Boyd²⁹, I.R. Boyko⁶⁵, N.I. Bozhko¹²⁸, I. Bozovic-Jelisavcic^{12b}, J. Bracinik¹⁷, A. Braem²⁹, P. Branchini^{134a}, G.W. Brandenburg⁵⁷, A. Brandt⁷, G. Brandt¹⁵, O. Brandt⁵⁴, U. Bratzler¹⁵⁶, B. Brau⁸⁴, J.E. Brau¹¹⁴, H.M. Braun¹⁷⁴, B. Brelief¹⁵⁸, J. Bremer²⁹, R. Brenner¹⁶⁶, S. Bressler¹⁵², D. Breton¹¹⁵, D. Britton⁵³, F.M. Brochu²⁷, I. Brock²⁰, R. Brock⁸⁸, T.J. Brodbeck⁷¹, E. Brodet¹⁵³, F. Broggi^{89a}, C. Bromberg⁸⁸, G. Brooijmans³⁴, W.K. Brooks^{31b}, G. Brown⁸², H. Brown⁷, P.A. Bruckman de Renstrom³⁸, D. Bruncko^{144b}, R. Bruneliere⁴⁸, S. Brunet⁶¹, A. Bruni^{19a}, G. Bruni^{19a}, M. Bruschi^{19a}, T. Buanes¹³, F. Bucci⁴⁹, J. Buchanan¹¹⁸, N.J. Buchanan², P. Buchholz¹⁴¹, R.M. Buckingham¹¹⁸, A.G. Buckley⁴⁵, S.I. Buda^{25a}, I.A. Budagov⁶⁵, B. Budick¹⁰⁸, V. Büscher⁸¹, L. Bugge¹¹⁷, D. Buiria-Clark¹¹⁸, O. Bulekov⁹⁶, M. Bunse⁴², T. Buran¹¹⁷, H. Burckhart²⁹, S. Burdin⁷³, T. Burgess¹³, S. Burke¹²⁹, E. Busato³³, P. Bussey⁵³, C.P. Buszello¹⁶⁶, F. Butin²⁹, B. Butler¹⁴³, J.M. Butler²¹, C.M. Buttar⁵³, J.M. Butterworth⁷⁷, W. Buttinger²⁷, T. Byatt⁷⁷, S. Cabrera Urbán¹⁶⁷, D. Caforio^{19a,19b}, O. Cakir^{3a}, P. Calafiura¹⁴, G. Calderini⁷⁸, P. Calfayan⁹⁸, R. Calkins¹⁰⁶, L.P. Caloba^{23a}, R. Caloi^{132a,132b}, D. Calvet³³, S. Calvet³³, R. Camacho Toro³³, P. Camarri^{133a,133b}, M. Cambiaghi^{119a,119b}, D. Cameron¹¹⁷, S. Campana²⁹, M. Campanelli⁷⁷, V. Canale^{102a,102b}, F. Canelli³⁰, A. Canepa^{159a}, J. Cantero⁸⁰, L. Capasso^{102a,102b}, M.D.M. Capeans Garrido²⁹, I. Caprini^{25a}, M. Caprini^{25a}, D. Capriotti⁹⁹, M. Capua^{36a,36b}, R. Caputo¹⁴⁸, C. Caramarcu^{25a}, R. Cardarelli^{133a}, T. Carli²⁹, G. Carlino^{102a}, L. Carminati^{89a,89b}, B. Caron^{159a}, S. Caron⁴⁸, G.D. Carrillo Montoya¹⁷², A.A. Carter⁷⁵, J.R. Carter²⁷, J. Carvalho^{124a,h}, D. Casadei¹⁰⁸, M.P. Casado¹¹, M. Cascella^{122a,122b}, C. Caso^{50a,50b,*}, A.M. Castaneda Hernandez¹⁷², E. Castaneda-Miranda¹⁷², V. Castillo Gimenez¹⁶⁷, N.F. Castro^{124a}, G. Cataldi^{72a}, F. Cataneo²⁹, A. Catinaccio²⁹, J.R. Catmore⁷¹, A. Cattai²⁹, G. Cattani^{133a,133b}, S. Caughron⁸⁸, D. Cauz^{164a,164c}, P. Cavalleri⁷⁸, D. Cavalli^{89a}, M. Cavalli-Sforza¹¹, V. Cavaiani^{122a,122b}, F. Ceradini^{134a,134b}, A.S. Cerqueira^{23a}, A. Cerri²⁹, L. Cerrito⁷⁵, F. Cerutti⁴⁷, S.A. Cetin^{18b}, F. Cevenini^{102a,102b}, A. Chafaq^{135a}, D. Chakraborty¹⁰⁶, K. Chan², B. Chapleau⁸⁵, J.D. Chapman²⁷, J.W. Chapman⁸⁷, E. Chareyre⁷⁸, D.G. Charlton¹⁷, V. Chavda⁸²,

C.A. Chavez Barajas²⁹, S. Cheatham⁸⁵, S. Chekanov⁵, S.V. Chekulaev^{159a}, G.A. Chelkov⁶⁵, M.A. Chelstowska¹⁰⁴, C. Chen⁶⁴, H. Chen²⁴, S. Chen^{32c}, T. Chen^{32c}, X. Chen¹⁷², S. Cheng^{32a}, A. Cheplakov⁶⁵, V.F. Chepurinov⁶⁵, R. Cherkaoui El Moursli^{135e}, V. Chernyatin²⁴, E. Cheu⁶, S.L. Cheung¹⁵⁸, L. Chevalier¹³⁶, G. Chiefari^{102a,102b}, L. Chikovani⁵¹, J.T. Childers^{58a}, A. Chilingarov⁷¹, G. Chiodini^{72a}, M.V. Chizhov⁶⁵, G. Choudalakis³⁰, S. Chouridou¹³⁷, I.A. Christidi⁷⁷, A. Christov⁴⁸, D. Chromek-Burckhart²⁹, M.L. Chu¹⁵¹, J. Chudoba¹²⁵, G. Ciapetti^{132a,132b}, K. Ciba³⁷, A.K. Ciftci^{3a}, R. Ciftci^{3a}, D. Cinca³³, V. Cindro⁷⁴, M.D. Ciobotaru¹⁶³, C. Ciocca^{19a,19b}, A. Ciochio¹⁴, M. Cirilli⁸⁷, M. Ciubancan^{25a}, A. Clark⁴⁹, P.J. Clark⁴⁵, W. Cleland¹²³, J.C. Clemens⁸³, B. Clement⁵⁵, C. Clement^{146a,146b}, R.W. Clift¹²⁹, Y. Coadou⁸³, M. Cobal^{164a,164c}, A. Coccaro^{50a,50b}, J. Cochran⁶⁴, P. Coe¹¹⁸, J.G. Cogan¹⁴³, J. Coggeshall¹⁶⁵, E. Cogneras¹⁷⁷, C.D. Cojocaru²⁸, J. Colas⁴, A.P. Colijn¹⁰⁵, C. Collard¹¹⁵, N.J. Collins¹⁷, C. Collins-Tooth⁵³, J. Collot⁵⁵, G. Colon⁸⁴, P. Conde Muiño^{124a}, E. Coniavitis¹¹⁸, M.C. Conidi¹¹, M. Consonni¹⁰⁴, V. Consorti⁴⁸, S. Constantinescu^{25a}, C. Conta^{119a,119b}, F. Conventi^{102a,i}, J. Cook²⁹, M. Cooke¹⁴, B.D. Cooper⁷⁷, A.M. Cooper-Sarkar¹¹⁸, N.J. Cooper-Smith⁷⁶, K. Copic³⁴, T. Cornelissen^{50a,50b}, M. Corradi^{19a}, F. Corriveau^{85,j}, A. Cortes-Gonzalez¹⁶⁵, G. Cortiana⁹⁹, G. Costa^{89a}, M.J. Costa¹⁶⁷, D. Costanzo¹³⁹, T. Costin³⁰, D. Côté²⁹, R. Coura Torres^{23a}, L. Courneyea¹⁶⁹, G. Cowan⁷⁶, C. Cowden²⁷, B.E. Cox⁸², K. Cranmer¹⁰⁸, F. Crescioli^{122a,122b}, M. Cristinziani²⁰, G. Crosetti^{36a,36b}, R. Crupi^{72a,72b}, S. Crépe-Renaudin⁵⁵, C.-M. Cuciuc^{25a}, C. Cuenca Almenar¹⁷⁵, T. Cuhadar Donszelmann¹³⁹, M. Curatolo⁴⁷, C.J. Curtis¹⁷, P. Cwetanski⁶¹, H. Czirr¹⁴¹, Z. Czynszula¹¹⁷, S. D'Auria⁵³, M. D'Onofrio⁷³, A. D'Orazio^{132a,132b}, P.V.M. Da Silva^{23a}, C. Da Via⁸², W. Dabrowski³⁷, T. Dai⁸⁷, C. Dallapiccola⁸⁴, M. Dam³⁵, M. Dameri^{50a,50b}, D.S. Damiani¹³⁷, H.O. Danielsson²⁹, D. Dannheim⁹⁹, V. Dao⁴⁹, G. Darbo^{50a}, G.L. Darlea^{25b}, C. Daum¹⁰⁵, J.P. Dauvergne²⁹, W. Davey⁸⁶, T. Davidek¹²⁶, N. Davidson⁸⁶, R. Davidson⁷¹, E. Davies^{118,c}, M. Davies⁹³, A.R. Davison⁷⁷, Y. Davygora^{58a}, E. Dawe¹⁴², I. Dawson¹³⁹, J.W. Dawson^{5,*}, R.K. Daya³⁹, K. De⁷, R. de Asmundis^{102a}, S. De Castro^{19a,19b}, P.E. de Castro Faria Salgado²⁴, S. De Cecco⁷⁸, J. de Graat⁹⁸, N. De Groot¹⁰⁴, P. de Jong¹⁰⁵, C. De La Taille¹¹⁵, H. De la Torre⁸⁰, B. De Lotto^{164a,164c}, L. De Mora⁷¹, L. De Noij¹⁰⁵, M. De Oliveira Branco²⁹, D. De Pedis^{132a}, A. De Salvo^{132a}, U. De Sanctis^{164a,164c}, A. De Santo¹⁴⁹, J.B. De Vivie De Regie¹¹⁵, S. Dean⁷⁷, D.V. Dedovich⁶⁵, J. Degenhardt¹²⁰, M. Dehchar¹¹⁸, C. Del Papa^{164a,164c}, J. Del Peso⁸⁰, T. Del Prete^{122a,122b}, M. Deliyergiyev⁷⁴, A. Dell'Acqua²⁹, L. Dell'Asta^{89a,89b}, M. Della Pietra^{102a,i}, D. della Volpe^{102a,102b}, M. Delmastro²⁹, P. Delpierre⁸³, N. Delruelle²⁹, P.A. Delsart⁵⁵, C. Deluca¹⁴⁸, S. Demers¹⁷⁵, M. Demichev⁶⁵, B. Demirköz^{11,k}, J. Deng¹⁶³, S.P. Denisov¹²⁸, D. Derendarz³⁸, J.E. Derkaoui^{135d}, F. Derue⁷⁸, P. Dervan⁷³, K. Desch²⁰, E. Devetak¹⁴⁸, P.O. Deviveiros¹⁵⁸, A. Dewhurst¹²⁹, B. DeWilde¹⁴⁸, S. Dhaliwal¹⁵⁸, R. Dhullipudi^{24,l}, A. Di Ciaccio^{133a,133b}, L. Di Ciaccio⁴, A. Di Girolamo²⁹, B. Di Girolamo²⁹, S. Di Luise^{134a,134b}, A. Di Mattia⁸⁸, B. Di Micco²⁹, R. Di Nardo^{133a,133b}, A. Di Simone^{133a,133b}, R. Di Sipio^{19a,19b}, M.A. Diaz^{31a}, F. Diblen^{18c}, E.B. Diehl⁸⁷, J. Dietrich⁴¹, T.A. Dietzsch^{58a}, S. Diglio¹¹⁵, K. Dindar Yagci³⁹, J. Dingfelder²⁰, C. Dionisi^{132a,132b}, P. Dita^{25a}, S. Dita^{25a}, F. Dittus²⁹, F. Djama⁸³, T. Djobava⁵¹, M.A.B. do Vale^{23a}, A. Do Valle Wemans^{124a}, T.K.O. Doan⁴, M. Dobbs⁸⁵, R. Dobinson^{29,*}, D. Dobos⁴², E. Dobson²⁹, M. Dobson¹⁶³, J. Dodd³⁴, C. Doglioni¹¹⁸, T. Doherty⁵³, Y. Doi^{66,*}, J. Dolejsi¹²⁶, I. Dolenc⁷⁴, Z. Dolezal¹²⁶, B.A. Dolgoshein^{96,*}, T. Dohmae¹⁵⁵, M. Donadelli^{23d}, M. Donega¹²⁰, J. Donini⁵⁵, J. Dopke²⁹, A. Doria^{102a}, A. Dos Anjos¹⁷², M. Dosil¹¹, A. Dotti^{122a,122b}, M.T. Dova⁷⁰, J.D. Dowell¹⁷, A.D. Doxiadis¹⁰⁵, A.T. Doyle⁵³, Z. Drasal¹²⁶, J. Drees¹⁷⁴, N. Dressnandt¹²⁰, H. Drevermann²⁹, C. Driouichi³⁵, M. Dris⁹, J. Dubbert⁹⁹, T. Dubbs¹³⁷, S. Dube¹⁴, E. Duchovni¹⁷¹, G. Duckeck⁹⁸, A. Dudarev²⁹, F. Dudziak⁶⁴, M. Dührssen²⁹, I.P. Duerdoth⁸², L. Dufloc¹¹⁵, M.-A. Dufour⁸⁵, M. Dunford²⁹, H. Duran Yildiz^{3b}, R. Duxfield¹³⁹, M. Dwuznik³⁷, F. Dydak²⁹, D. Dzahini⁵⁵, M. Düren⁵², W.L. Ebenstein⁴⁴, J. Ebke⁹⁸, S. Eckert⁴⁸, S. Eckweiler⁸¹, K. Edmonds⁸¹, C.A. Edwards⁷⁶, N.C. Edwards⁵³, W. Ehrenfeld⁴¹, T. Ehrich⁹⁹, T. Eifert²⁹, G. Eigen¹³, K. Einsweiler¹⁴, E. Eisenhandler⁷⁵, T. Ekelof¹⁶⁶, M. El Kacimi^{135c}, M. Ellert¹⁶⁶, S. Elles⁴, F. Ellinghaus⁸¹, K. Ellis⁷⁵, N. Ellis²⁹, J. Elmsheuser⁹⁸, M. Elsing²⁹, D. Emelianov¹²⁹, R. Engelmann¹⁴⁸, A. Engl⁹⁸, B. Epp⁶², A. Eppig⁸⁷, J. Erdmann⁵⁴, A. Ereditato¹⁶, D. Eriksson^{146a}, J. Ernst¹, M. Ernst²⁴, J. Ernwein¹³⁶, D. Errede¹⁶⁵, S. Errede¹⁶⁵, E. Ertel⁸¹, M. Escalier¹¹⁵, C. Escobar¹⁶⁷, X. Espinal Curull¹¹, B. Esposito⁴⁷, F. Etienne⁸³, A.I. Etienne¹³⁶, E. Etzion¹⁵³, D. Evangelakou⁵⁴, H. Evans⁶¹, L. Fabbri^{19a,19b}, C. Fabre²⁹, R.M. Fakhruddinov¹²⁸, S. Falciano^{132a}, Y. Fang¹⁷², M. Fanti^{89a,89b}, A. Farbin⁷, A. Farilla^{134a}, J. Farley¹⁴⁸, T. Farooque¹⁵⁸, S.M. Farrington¹¹⁸, P. Farthouat²⁹, P. Fassnacht²⁹, D. Fassouliotis⁸, B. Fathollahzadeh¹⁵⁸, A. Favareto^{89a,89b}, L. Fayard¹¹⁵, S. Fazio^{36a,36b}, R. Febbraro³³, P. Federic^{144a}, O.L. Fedin¹²¹, W. Fedorko⁸⁸, M. Fehling-Kaschek⁴⁸, L. Feligioni⁸³, D. Fellmann⁵, C.U. Felzmann⁸⁶, C. Feng^{32d}, E.J. Feng³⁰, A.B. Fenyyuk¹²⁸, J. Ferencei^{144b}, J. Ferland⁹³, W. Fernando¹⁰⁹, S. Ferrag⁵³, J. Ferrando⁵³, V. Ferrara⁴¹, A. Ferrari¹⁶⁶, P. Ferrari¹⁰⁵, R. Ferrari^{119a}, A. Ferrer¹⁶⁷, M.L. Ferrer⁴⁷, D. Ferrere⁴⁹, C. Ferretti⁸⁷, A. Ferretto Parodi^{50a,50b}, M. Fiascaris³⁰, F. Fiedler⁸¹, A. Filipčič⁷⁴, A. Filippas⁹, F. Filthaut¹⁰⁴, M. Fincke-Keeler¹⁶⁹, M.C.N. Fiolhais^{124a,h}, L. Fiorini¹⁶⁷, A. Firan³⁹, G. Fischer⁴¹, P. Fischer²⁰, M.J. Fisher¹⁰⁹, S.M. Fisher¹²⁹, M. Flechl⁴⁸, I. Fleck¹⁴¹, J. Fleckner⁸¹, P. Fleischmann¹⁷³, S. Fleischmann¹⁷⁴, T. Flick¹⁷⁴, L.R. Flores Castillo¹⁷², M.J. Flowerdew⁹⁹, M. Fokitis⁹, T. Fonseca Martin¹⁶, D.A. Forbush¹³⁸, A. Formica¹³⁶, A. Forti⁸², D. Fortin^{159a}, J.M. Foster⁸², D. Fournier¹¹⁵, A. Foussat²⁹, A.J. Fowler⁴⁴, K. Fowler¹³⁷, H. Fox⁷¹, P. Francavilla^{122a,122b}, S. Franchino^{119a,119b}, D. Francis²⁹, T. Frank¹⁷¹, M. Franklin⁵⁷, S. Franz²⁹, M. Fraternali^{119a,119b}, S. Fratina¹²⁰, S.T. French²⁷, F. Friedrich⁴³, R. Froeschl²⁹, D. Froidevaux²⁹, J.A. Frost²⁷, C. Fukunaga¹⁵⁶, E. Fullana Torregrosa²⁹, J. Fuster¹⁶⁷, C. Gabaldon²⁹, O. Gabizon¹⁷¹, T. Gadfort²⁴, S. Gadomski⁴⁹, G. Gagliardi^{50a,50b}, P. Gagnon⁶¹, C. Galea⁹⁸, E.J. Gallas¹¹⁸, M.V. Gallas²⁹, V. Gallo¹⁶, B.J. Gallop¹²⁹, P. Gallus¹²⁵, E. Galyaev⁴⁰, K.K. Gan¹⁰⁹, Y.S. Gao^{143,f}, V.A. Gapienko¹²⁸, A. Gaponenko¹⁴, F. Garbersson¹⁷⁵, M. Garcia-Sciveres¹⁴, C. García¹⁶⁷, J.E. García Navarro⁴⁹, R.W. Gardner³⁰, N. Garelli²⁹, H. Garitaonandia¹⁰⁵, V. Garonne²⁹, J. Garvey¹⁷, C. Gatti⁴⁷, G. Gaudio^{119a}, O. Gaumer⁴⁹, B. Gaur¹⁴¹, L. Gauthier¹³⁶, I.L. Gavrilenko⁹⁴, C. Gay¹⁶⁸, G. Gaycken²⁰, J.-C. Gayde²⁹, E.N. Gazis⁹, P. Ge^{32d}, C.N.P. Gee¹²⁹, D.A.A. Geerts¹⁰⁵, Ch. Geich-Gimbel²⁰, K. Gellerstedt^{146a,146b},

C. Gemme^{50a}, A. Gemmell⁵³, M.H. Genest⁹⁸, S. Gentile^{132a,132b}, M. George⁵⁴, S. George⁷⁶, P. Gerlach¹⁷⁴, A. Gershon¹⁵³, C. Geweniger^{58a}, H. Ghazlane^{135b}, P. Ghez⁴, N. Ghodbane³³, B. Giacobbe^{19a}, S. Giagu^{132a,132b}, V. Giakoumopoulou⁸, V. Giangiobbe^{122a,122b}, F. Gianotti²⁹, B. Gibbard²⁴, A. Gibson¹⁵⁸, S.M. Gibson²⁹, L.M. Gilbert¹¹⁸, M. Gilchriese¹⁴, V. Gilevsky⁹¹, D. Gillberg²⁸, A.R. Gillman¹²⁹, D.M. Gingrich^{2,e}, J. Ginzburg¹⁵³, N. Giokaris⁸, R. Giordano^{102a,102b}, F.M. Giorgi¹⁵, P. Giovannini⁹⁹, P.F. Giraud¹³⁶, D. Giugni^{89a}, M. Giunta^{132a,132b}, P. Giusti^{19a}, B.K. Gjelsten¹¹⁷, L.K. Gladilin⁹⁷, C. Glasman⁸⁰, J. Glatzer⁴⁸, A. Glazov⁴¹, K.W. Glitza¹⁷⁴, G.L. Glonti⁶⁵, J. Godfrey¹⁴², J. Godlewski²⁹, M. Goebel⁴¹, T. Göpfert⁴³, C. Goeringer⁸¹, C. Gössling⁴², T. Göttfert⁹⁹, S. Goldfarb⁸⁷, D. Goldin³⁹, T. Golling¹⁷⁵, S.N. Golovnia¹²⁸, A. Gomes^{124a,b}, L.S. Gomez Fajardo⁴¹, R. Gonçalo⁷⁶, J. Goncalves Pinto Firmino Da Costa⁴¹, L. Gonella²⁰, A. Gonidec²⁹, S. Gonzalez¹⁷², S. González de la Hoz¹⁶⁷, M.L. Gonzalez Silva²⁶, S. Gonzalez-Sevilla⁴⁹, J.J. Goodson¹⁴⁸, L. Goossens²⁹, P.A. Gorbounov⁹⁵, H.A. Gordon²⁴, I. Gorelov¹⁰³, G. Gorfine¹⁷⁴, B. Gorini²⁹, E. Gorini^{72a,72b}, A. Gorišek⁷⁴, E. Gornicki³⁸, S.A. Gorokhov¹²⁸, V.N. Goryachev¹²⁸, B. Gosdzik⁴¹, M. Gosselink¹⁰⁵, M.I. Gostkin⁶⁵, I. Gough Eschrich¹⁶³, M. Goughri^{135a}, D. Goujdami^{135c}, M.P. Goulette⁴⁹, A.G. Goussiou¹³⁸, C. Goy⁴, I. Grabowska-Bold^{163,g}, V. Grabski¹⁷⁶, P. Grafström²⁹, C. Grah¹⁷⁴, K.-J. Grah⁴¹, F. Grancagnolo^{72a}, S. Grancagnolo¹⁵, V. Grassi¹⁴⁸, V. Gratchev¹²¹, N. Grau³⁴, H.M. Gray²⁹, J.A. Gray¹⁴⁸, E. Graziani^{134a}, O.G. Grebenyuk¹²¹, D. Greenfield¹²⁹, T. Greenshaw⁷³, Z.D. Greenwood^{24,l}, K. Gregersen³⁵, I.M. Gregor⁴¹, P. Grenier¹⁴³, J. Griffiths¹³⁸, N. Grigalashvili⁶⁵, A.A. Grillo¹³⁷, S. Grinstein¹¹, Y.V. Grishkevich⁹⁷, J.-F. Grivaz¹¹⁵, J. Grognuz²⁹, M. Groh⁹⁹, E. Gross¹⁷¹, J. Grosse-Knetter⁵⁴, J. Groth-Jensen¹⁷¹, K. Grybel¹⁴¹, V.J. Guarino⁵, D. Guest¹⁷⁵, C. Guicheney³³, A. Guida^{72a,72b}, T. Guillemin⁴, S. Guindon⁵⁴, H. Guler^{85,m}, J. Gunther¹²⁵, B. Guo¹⁵⁸, J. Guo³⁴, A. Gupta³⁰, Y. Gusakov⁶⁵, V.N. Gushchin¹²⁸, A. Gutierrez⁹³, P. Gutierrez¹¹¹, N. Guttman¹⁵³, O. Gutzwiller¹⁷², C. Guyot¹³⁶, C. Gwenlan¹¹⁸, C.B. Gwilliam⁷³, A. Haas¹⁴³, S. Haas²⁹, C. Haber¹⁴, R. Hackenberg²⁴, H.K. Hadavand³⁹, D.R. Hadley¹⁷, P. Haefner⁹⁹, F. Hahn²⁹, S. Haider²⁹, Z. Hajduk³⁸, H. Hakobyan¹⁷⁶, J. Haller⁵⁴, K. Hamacher¹⁷⁴, P. Hamal¹¹³, A. Hamilton⁴⁹, S. Hamilton¹⁶¹, H. Han^{32a}, L. Han^{32b}, K. Hanagaki¹¹⁶, M. Hance¹²⁰, C. Handel⁸¹, P. Hanke^{58a}, J.R. Hansen³⁵, J.B. Hansen³⁵, J.D. Hansen³⁵, P.H. Hansen³⁵, P. Hansson¹⁴³, K. Hara¹⁶⁰, G.A. Hare¹³⁷, T. Harenberg¹⁷⁴, S. Harkusha⁹⁰, D. Harper⁸⁷, R.D. Harrington²¹, O.M. Harris¹³⁸, K. Harrison¹⁷, J. Hartert⁴⁸, F. Hartjes¹⁰⁵, T. Haruyama⁶⁶, A. Harvey⁵⁶, S. Hasegawa¹⁰¹, Y. Hasegawa¹⁴⁰, S. Hassani¹³⁶, M. Hatch²⁹, D. Hauff⁹⁹, S. Haug¹⁶, M. Hauschild²⁹, R. Hauser⁸⁸, M. Havranek²⁰, B.M. Hawes¹¹⁸, C.M. Hawkes¹⁷, R.J. Hawkins²⁹, D. Hawkins¹⁶³, T. Hayakawa⁶⁷, D. Hayden⁷⁶, H.S. Hayward⁷³, S.J. Haywood¹²⁹, E. Hazen²¹, M. He^{32d}, S.J. Head¹⁷, V. Hedberg⁷⁹, L. Heelan⁷, S. Heim⁸⁸, B. Heinemann¹⁴, S. Heisterkamp³⁵, L. Helary⁴, M. Heller¹¹⁵, S. Hellman^{146a,146b}, D. Hellmich²⁰, C. Helsens¹¹, R.C.W. Henderson⁷¹, M. Henke^{58a}, A. Henrichs⁵⁴, A.M. Henriques Correia²⁹, S. Henrot-Versille¹¹⁵, F. Henry-Couannier⁸³, C. Hensel⁵⁴, T. Henß¹⁷⁴, C.M. Hernandez⁷, Y. Hernández Jiménez¹⁶⁷, R. Herrberg¹⁵, A.D. Hershenhorn¹⁵², G. Herten⁴⁸, R. Hertenberger⁹⁸, L. Hervás²⁹, N.P. Hessey¹⁰⁵, A. Hidvegi^{146a}, E. Higón-Rodríguez¹⁶⁷, D. Hill^{5,*}, J.C. Hill²⁷, N. Hill⁵, K.H. Hiller⁴¹, S. Hillert²⁰, S.J. Hillier¹⁷, I. Hinchliffe¹⁴, E. Hines¹²⁰, M. Hirose¹¹⁶, F. Hirsch⁴², D. Hirschbuehl¹⁷⁴, J. Hobbs¹⁴⁸, N. Hod¹⁵³, M.C. Hodgkinson¹³⁹, P. Hodgson¹³⁹, A. Hoecker²⁹, M.R. Hoferkamp¹⁰³, J. Hoffman³⁹, D. Hoffmann⁸³, M. Hohlfield⁸¹, M. Holder¹⁴¹, S.O. Holmgren^{146a}, T. Holy¹²⁷, J.L. Holzbauer⁸⁸, Y. Homma⁶⁷, T.M. Hong¹²⁰, L. Hooft van Huysduynen¹⁰⁸, T. Horazdovsky¹²⁷, C. Horn¹⁴³, S. Horner⁴⁸, K. Horton¹¹⁸, J.-Y. Hostachy⁵⁵, S. Hou¹⁵¹, M.A. Houlden⁷³, A. Hoummada^{135a}, J. Howarth⁸², D.F. Howell¹¹⁸, I. Hristova¹⁵, J. Hrivnac¹¹⁵, I. Hruska¹²⁵, T. Hryn'ova⁴, P.J. Hsu¹⁷⁵, S.-C. Hsu¹⁴, G.S. Huang¹¹¹, Z. Hubacek¹²⁷, F. Hubaut⁸³, F. Huegging²⁰, T.B. Huffman¹¹⁸, E.W. Hughes³⁴, G. Hughes⁷¹, R.E. Hughes-Jones⁸², M. Huhtinen²⁹, P. Hurst⁵⁷, M. Hurwitz¹⁴, U. Husemann⁴¹, N. Huseynov^{65,n}, J. Huston⁸⁸, J. Huth⁵⁷, G. Iacobucci⁴⁹, G. Iakovidis⁹, M. Ibbotson⁸², I. Ibragimov¹⁴¹, R. Ichimiya⁶⁷, L. Iconomidou-Fayard¹¹⁵, J. Idarraga¹¹⁵, M. Idzik³⁷, P. Iengo^{102a,102b}, O. Igonkina¹⁰⁵, Y. Ikegami⁶⁶, M. Ikeno⁶⁶, Y. Ilchenko³⁹, D. Iliadis¹⁵⁴, N. Ilic¹⁵⁸, D. Imbault⁷⁸, M. Imhaeuser¹⁷⁴, M. Imori¹⁵⁵, T. Ince²⁰, J. Inigo-Golfín²⁹, P. Ioannou⁸, M. Iodice^{134a}, G. Ionescu⁴, A. Irls Quiles¹⁶⁷, K. Ishii⁶⁶, A. Ishikawa⁶⁷, M. Ishino⁶⁸, R. Ishmukhametov³⁹, C. Issever¹¹⁸, S. Istin^{18a}, A.V. Ivashin¹²⁸, W. Iwanski³⁸, H. Iwasaki⁶⁶, J.M. Izen⁴⁰, V. Izzo^{102a}, B. Jackson¹²⁰, J.N. Jackson⁷³, P. Jackson¹⁴³, M.R. Jaekel²⁹, V. Jain⁶¹, K. Jakobs⁴⁸, S. Jakobsen³⁵, J. Jakubek¹²⁷, D.K. Jana¹¹¹, E. Jankowski¹⁵⁸, E. Jansen⁷⁷, A. Jantsch⁹⁹, M. Janus²⁰, G. Jarlskog⁷⁹, L. Jeanty⁵⁷, K. Jelen³⁷, I. Jen-La Plante³⁰, P. Jenni²⁹, A. Jeremie⁴, P. Jež³⁵, S. Jézéquel⁴, M.K. Jha^{19a}, H. Ji¹⁷², W. Ji⁸¹, J. Jia¹⁴⁸, Y. Jiang^{32b}, M. Jimenez Belenguer⁴¹, G. Jin^{32b}, S. Jin^{32a}, O. Jinnouchi¹⁵⁷, M.D. Joergensen³⁵, D. Joffe³⁹, L.G. Johansen¹³, M. Johansen^{146a,146b}, K.E. Johansson^{146a}, P. Johansson¹³⁹, S. Johnert⁴¹, K.A. Johns⁶, K. Jon-And^{146a,146b}, G. Jones⁸², R.W.L. Jones⁷¹, T.W. Jones⁷³, T.J. Jones⁷³, O. Jonsson²⁹, C. Joram²⁹, P.M. Jorge^{124a,b}, J. Joseph¹⁴, T. Jovin^{12b}, X. Ju¹³⁰, V. Juranek¹²⁵, P. Jussel⁶², A. Juste Rozas¹¹, V.V. Kabachenko¹²⁸, S. Kabana¹⁶, M. Kaci¹⁶⁷, A. Kaczmarska³⁸, P. Kadlecik³⁵, M. Kado¹¹⁵, H. Kagan¹⁰⁹, M. Kagan⁵⁷, S. Kaiser⁹⁹, E. Kajomovitz¹⁵², S. Kalinin¹⁷⁴, L.V. Kalinovskaya⁶⁵, S. Kama³⁹, N. Kanaya¹⁵⁵, M. Kaneda²⁹, T. Kanno¹⁵⁷, V.A. Kantserov⁹⁶, J. Kanzaki⁶⁶, B. Kaplan¹⁷⁵, A. Kapliy³⁰, J. Kaplon²⁹, D. Kar⁴³, M. Karagoz¹¹⁸, M. Karnevskiy⁴¹, K. Karr⁵, V. Kartvelishvili⁷¹, A.N. Karyukhin¹²⁸, L. Kashif¹⁷², A. Kasmi³⁹, R.D. Kass¹⁰⁹, A. Kastanas¹³, M. Kataoka⁴, Y. Kataoka¹⁵⁵, E. Katsoufis⁹, J. Katzy⁴¹, V. Kaushik⁶, K. Kawagoe⁶⁷, T. Kawamoto¹⁵⁵, G. Kawamura⁸¹, M.S. Kayl¹⁰⁵, V.A. Kazanin¹⁰⁷, M.Y. Kazarinov⁶⁵, J.R. Keates⁸², R. Keeler¹⁶⁹, R. Kehoe³⁹, M. Keil⁵⁴, G.D. Kekelidze⁶⁵, M. Kelly⁸², J. Kennedy⁹⁸, C.J. Kenney¹⁴³, M. Kenyon⁵³, O. Kepka¹²⁵, N. Kerschen²⁹, B.P. Kerševan⁷⁴, S. Kersten¹⁷⁴, K. Kessoku¹⁵⁵, C. Ketterer⁴⁸, J. Keung¹⁵⁸, M. Khakzad²⁸, F. Khalil-zada¹⁰, H. Khandanyan¹⁶⁵, A. Khanov¹¹², D. Kharchenko⁶⁵, A. Khodinov⁹⁶, A.G. Kholodenko¹²⁸, A. Khomich^{58a}, T.J. Khoo²⁷, G. Khorauli²⁰, A. Khoroshilov¹⁷⁴, N. Khovanskii⁶⁵, V. Khovanskii⁹⁵, E. Khramov⁶⁵, J. Khubua⁵¹, H. Kim⁷, M.S. Kim², P.C. Kim¹⁴³, S.H. Kim¹⁶⁰, N. Kimura¹⁷⁰, O. Kind¹⁵, B.T. King⁷³, M. King⁶⁷, R.S.B. King¹¹⁸, J. Kirk¹²⁹, G.P. Kirsch¹¹⁸, L.E. Kirsch²², A.E. Kiryunin⁹⁹, T. Kishimoto⁶⁷, D. Kisielewska³⁷, T. Kittelmann¹²³, A.M. Kiver¹²⁸, H. Kiyamura⁶⁷, E. Kladiva^{144b}, J. Klaiber-Lodewigs⁴², M. Klein⁷³, U. Klein⁷³, K. Kleinknecht⁸¹, M. Klemetti⁸⁵, A. Klier¹⁷¹, A. Klimentov²⁴,

R. Klingenberg⁴², E.B. Klinkby³⁵, T. Klioutchnikova²⁹, P.F. Klok¹⁰⁴, S. Klous¹⁰⁵, E.-E. Kluge^{58a}, T. Kluge⁷³, P. Kluit¹⁰⁵, S. Kluth⁹⁹, N.S. Knecht¹⁵⁸, E. Kneringer⁶², J. Knobloch²⁹, E.B.F.G. Knoops⁸³, A. Knue⁵⁴, B.R. Ko⁴⁴, T. Kobayashi¹⁵⁵, M. Kobel⁴³, M. Kocian¹⁴³, A. Kocnar¹¹³, P. Kodys¹²⁶, K. Köneke²⁹, A.C. König¹⁰⁴, S. Koenig⁸¹, L. Köpke⁸¹, F. Koetsveld¹⁰⁴, P. Koevesarki²⁰, T. Koffas²⁹, E. Koffeman¹⁰⁵, F. Kohn⁵⁴, Z. Kohout¹²⁷, T. Kohriki⁶⁶, T. Koi¹⁴³, T. Kokott²⁰, G.M. Kolachev¹⁰⁷, H. Kolanoski¹⁵, V. Kolesnikov⁶⁵, I. Koletsou^{89a}, J. Koll⁸⁸, D. Kollar²⁹, M. Kollefrath⁴⁸, S.D. Kolya⁸², A.A. Komar⁹⁴, J.R. Komaragiri¹⁴², Y. Komori¹⁵⁵, T. Kondo⁶⁶, T. Kono^{41,o}, A.I. Kononov⁴⁸, R. Konoplich^{108,p}, N. Konstantinidis⁷⁷, A. Kootz¹⁷⁴, S. Koperny³⁷, S.V. Kopikov¹²⁸, K. Korcyl³⁸, K. Kordas¹⁵⁴, V. Koreshev¹²⁸, A. Korn¹⁴, A. Korol¹⁰⁷, I. Korolkov¹¹, E.V. Korolkova¹³⁹, V.A. Korotkov¹²⁸, O. Kortner⁹⁹, S. Kortner⁹⁹, V.V. Kostyukhin²⁰, M.J. Kotamäki²⁹, S. Kotov⁹⁹, V.M. Kotov⁶⁵, A. Kotwal⁴⁴, C. Kourkoumelis⁸, V. Kouskoura¹⁵⁴, A. Koutsman¹⁰⁵, R. Kowalewski¹⁶⁹, T.Z. Kowalski³⁷, W. Kozanecki¹³⁶, A.S. Kozhin¹²⁸, V. Kral¹²⁷, V.A. Kramarenko⁹⁷, G. Kramberger⁷⁴, M.W. Krasny⁷⁸, A. Krasznahorkay¹⁰⁸, J. Kraus⁸⁸, A. Kreisel¹⁵³, F. Krejci¹²⁷, J. Kretschmar⁷³, N. Krieger⁵⁴, P. Krieger¹⁵⁸, K. Kroeninger⁵⁴, H. Kroha⁹⁹, J. Kroll¹²⁰, J. Kroseberg²⁰, J. Krstic^{12a}, U. Kruchonak⁶⁵, H. Krüger²⁰, T. Kruker¹⁶, Z.V. Krumshteyn⁶⁵, A. Kruth²⁰, T. Kubota⁸⁶, S. Kuehn⁴⁸, A. Kugel^{58c}, T. Kuhl⁴¹, D. Kuhn⁶², V. Kukhtin⁶⁵, Y. Kulchitsky⁹⁰, S. Kuleshov^{31b}, C. Kummer⁹⁸, M. Kuna⁷⁸, N. Kundu¹¹⁸, J. Kunkle¹²⁰, A. Kupco¹²⁵, H. Kurashige⁶⁷, M. Kurata¹⁶⁰, Y.A. Kurochkin⁹⁰, V. Kus¹²⁵, W. Kuykendall¹³⁸, M. Kuze¹⁵⁷, P. Kuzhir⁹¹, J. Kvita²⁹, R. Kwee¹⁵, A. La Rosa¹⁷², L. La Rotonda^{36a,36b}, L. Labarga⁸⁰, J. Labbe⁴, S. Lablak^{135a}, C. Lacasta¹⁶⁷, F. Lacava^{132a,132b}, H. Lacker¹⁵, D. Lacour⁷⁸, V.R. Lacuesta¹⁶⁷, E. Ladygin⁶⁵, R. Lafaye⁴, B. Laforge⁷⁸, T. Lagouri⁸⁰, S. Lai⁴⁸, E. Laisne⁵⁵, M. Lamanna²⁹, C.L. Lampen⁶, W. Lampl⁶, E. Lancon¹³⁶, U. Landgraf⁴⁸, M.P.J. Landon⁷⁵, H. Landsman¹⁵², J.L. Lane⁸², C. Lange⁴¹, A.J. Lankford¹⁶³, F. Lanni²⁴, K. Lantzsche²⁹, S. Laplace⁷⁸, C. Lapoire²⁰, J.F. Laporte¹³⁶, T. Lari^{89a}, A.V. Laronov¹²⁸, A. Lerner¹¹⁸, C. Lasseur²⁹, M. Lassnig²⁹, P. Laurelli⁴⁷, A. Lavorato¹¹⁸, W. Lavrijsen¹⁴, P. Laycock⁷³, A.B. Lazarev⁶⁵, O. Le Dortz⁷⁸, E. Le Guirrec⁸³, C. Le Maner¹⁵⁸, E. Le Meneu¹³⁶, C. Leibel⁹³, T. LeCompte⁵, F. Ledroit-Guillon⁵⁵, H. Lee¹⁰⁵, J.S.H. Lee¹⁵⁰, S.C. Lee¹⁵¹, L. Lee¹⁷⁵, M. Lefebvre¹⁶⁹, M. Legendre¹³⁶, A. Leger⁴⁹, B.C. LeGeyt¹²⁰, F. Legger⁹⁸, C. Leggett¹⁴, M. Lehmann²⁰, G. Lehmann Miotto²⁹, X. Lei⁶, M.A.L. Leite^{23d}, R. Leitner¹²⁶, D. Lellouch¹⁷¹, M. Leltchouk³⁴, B. Lemmer⁵⁴, V. Lendermann^{58a}, K.J.C. Leney^{145b}, T. Lenz¹⁰⁵, G. Lenzen¹⁷⁴, B. Lenzi²⁹, K. Leonhardt⁴³, S. Leontsinis⁹, C. Leroy⁹³, J.-R. Lessard¹⁶⁹, J. Lesser^{146a}, C.G. Lester²⁷, A. Leung Fook Cheong¹⁷², J. Levêque⁴, D. Levin⁸⁷, L.J. Levinson¹⁷¹, M.S. Levitski¹²⁸, M. Lewandowska²¹, A. Lewis¹¹⁸, G.H. Lewis¹⁰⁸, A.M. Leyko²⁰, M. Leyton¹⁵, B. Li⁸³, H. Li¹⁷², S. Li^{32b,d}, X. Li⁸⁷, Z. Liang³⁹, Z. Liang^{118,q}, B. Liberti^{133a}, P. Lichard²⁹, M. Lichtnecker⁹⁸, K. Lie¹⁶⁵, W. Liebig¹³, R. Lifshitz¹⁵², J.N. Lilley¹⁷, C. Limbach²⁰, A. Limosani⁸⁶, M. Limper⁶³, S.C. Lin^{151,r}, F. Linde¹⁰⁵, J.T. Linnemann⁸⁸, E. Lipeles¹²⁰, L. Lipinsky¹²⁵, A. Lipniacka¹³, T.M. Liss¹⁶⁵, D. Lissauer²⁴, A. Lister⁴⁹, A.M. Litke¹³⁷, C. Liu²⁸, D. Liu^{151,s}, H. Liu⁸⁷, J.B. Liu⁸⁷, M. Liu^{32b}, S. Liu², Y. Liu^{32b}, M. Livan^{119a,119b}, S.S.A. Livermore¹¹⁸, A. Lleres⁵⁵, J. Llorente Merino⁸⁰, S.L. Lloyd⁷⁵, E. Lobodzinska⁴¹, P. Loch⁶, W.S. Lockman¹³⁷, S. Lockwitz¹⁷⁵, T. Loddenkoetter²⁰, F.K. Loebinger⁸², A. Loginov¹⁷⁵, C.W. Loh¹⁶⁸, T. Lohse¹⁵, K. Lohwasser⁴⁸, M. Lokajicek¹²⁵, J. Loken¹¹⁸, V.P. Lombardo⁴, R.E. Long⁷¹, L. Lopes^{124a,b}, D. Lopez Mateos⁵⁷, M. Losada¹⁶², P. Loscutoff¹⁴, F. Lo Sterzo^{132a,132b}, M.J. Losty^{159a}, X. Lou⁴⁰, A. Lounis¹¹⁵, K.F. Loureiro¹⁶², J. Love²¹, P.A. Love⁷¹, A.J. Lowe^{143,f}, F. Lu^{32a}, H.J. Lubatti¹³⁸, C. Luci^{132a,132b}, A. Lucotte⁵⁵, A. Ludwig⁴³, D. Ludwig⁴¹, I. Ludwig⁴⁸, J. Ludwig⁴⁸, F. Luehring⁶¹, G. Luijckx¹⁰⁵, D. Lumb⁴⁸, L. Luminari^{132a}, E. Lund¹¹⁷, B. Lund-Jensen¹⁴⁷, B. Lundberg⁷⁹, J. Lundberg^{146a,146b}, J. Lundquist³⁵, M. Lungwitz⁸¹, A. Lupi^{122a,122b}, G. Lutz⁹⁹, D. Lynn²⁴, J. Lys¹⁴, E. Lytken⁷⁹, H. Ma²⁴, L.L. Ma¹⁷², J.A. Macana Goia⁹³, G. Maccarrone⁴⁷, A. Macchiolo⁹⁹, B. Maček⁷⁴, J. Machado Miguens^{124a}, R. Mackeprang³⁵, R.J. Madaras¹⁴, W.F. Mader⁴³, R. Maenner^{58c}, T. Maeno²⁴, P. Mättig¹⁷⁴, S. Mättig⁴¹, P.J. Magalhaes Martins^{124a,h}, L. Magnoni²⁹, E. Magradze⁵⁴, Y. Mahalalel¹⁵³, K. Mahboubi⁴⁸, G. Mahout¹⁷, C. Maiani^{132a,132b}, C. Maidantchik^{23a}, A. Maio^{124a,b}, S. Majewski²⁴, Y. Makida⁶⁶, N. Makovec¹¹⁵, P. Mal⁶, Pa. Malecki³⁸, P. Malecki³⁸, V.P. Maleev¹²¹, F. Malek⁵⁵, U. Mallik⁶³, D. Malon⁵, S. Maltezos⁹, V. Malyshev¹⁰⁷, S. Malyukov²⁹, R. Mameghani⁹⁸, J. Mamuzic^{12b}, A. Manabe⁶⁶, L. Mandelli^{89a}, I. Mandić⁷⁴, R. Mandrysch¹⁵, J. Maneira^{124a}, P.S. Mangeard⁸⁸, I.D. Manjavidze⁶⁵, A. Mann⁵⁴, P.M. Manning¹³⁷, A. Manousakis-Katsikakis⁸, B. Mansoulie¹³⁶, A. Manz⁹⁹, A. Mapelli²⁹, L. Mapelli²⁹, L. March⁸⁰, J.F. Marchand²⁹, F. Marchese^{133a,133b}, G. Marchiori⁷⁸, M. Marcisovsky¹²⁵, A. Marin^{21,*}, C.P. Marino⁶¹, F. Marroquim^{23a}, R. Marshall⁸², Z. Marshall²⁹, F.K. Martens¹⁵⁸, S. Marti-Garcia¹⁶⁷, A.J. Martin¹⁷⁵, B. Martin²⁹, B. Martin⁸⁸, F.F. Martin¹²⁰, J.P. Martin⁹³, Ph. Martin⁵⁵, T.A. Martin¹⁷, B. Martin dit Latour⁴⁹, S. Martin-Haugh¹⁴⁹, M. Martinez¹¹, V. Martinez Outschoorn⁵⁷, A.C. Martyniuk⁸², M. Marx⁸², F. Marzano^{132a}, A. Marzin¹¹¹, L. Masetti⁸¹, T. Mashimo¹⁵⁵, R. Mashinistov⁹⁴, J. Masik⁸², A.L. Maslennikov¹⁰⁷, I. Massa^{19a,19b}, G. Massaro¹⁰⁵, N. Massol⁴, P. Mastrandrea^{132a,132b}, A. Mastroberardino^{36a,36b}, T. Masubuchi¹⁵⁵, M. Mathes²⁰, P. Matricon¹¹⁵, H. Matsumoto¹⁵⁵, H. Matsunaga¹⁵⁵, T. Matsushita⁶⁷, C. Mattheis^{118,c}, J.M. Maugain²⁹, S.J. Maxfield⁷³, D.A. Maximov¹⁰⁷, E.N. May⁵, A. Mayne¹³⁹, R. Mazini¹⁵¹, M. Mazur²⁰, M. Mazzanti^{89a}, E. Mazzoni^{122a,122b}, S.P. Mc Kee⁸⁷, A. McCarn¹⁶⁵, R.L. McCarthy¹⁴⁸, T.G. McCarthy²⁸, N.A. McCubbin¹²⁹, K.W. McFarlane⁵⁶, J.A. McFayden¹³⁹, H. McGlone⁵³, G. Mchedlize⁵¹, R.A. McLaren²⁹, T. McLaughlan¹⁷, S.J. McMahon¹²⁹, R.A. McPherson^{169,j}, A. Meade⁸⁴, J. Mechnich¹⁰⁵, M. Mechtel¹⁷⁴, M. Medinnis⁴¹, R. Meera-Lebbai¹¹¹, T. Meguro¹¹⁶, R. Mehdiyev⁹³, S. Mehlhase³⁵, A. Mehta⁷³, K. Meier^{58a}, J. Meinhardt⁴⁸, B. Meirose⁷⁹, C. Melachrinou³⁰, B.R. Mellado Garcia¹⁷², L. Mendoza Navas¹⁶², Z. Meng^{151,s}, A. Mengarelli^{19a,19b}, S. Menke⁹⁹, C. Menot²⁹, E. Meoni¹¹, K.M. Mercurio⁵⁷, P. Mermod¹¹⁸, L. Merola^{102a,102b}, C. Meroni^{89a}, F.S. Merritt³⁰, A. Messina²⁹, J. Metcalfe¹⁰³, A.S. Mete⁶⁴, S. Meuser²⁰, C. Meyer⁸¹, J.-P. Meyer¹³⁶, J. Meyer¹⁷³, J. Meyer⁵⁴, T.C. Meyer²⁹, W.T. Meyer⁶⁴, J. Miao^{32d}, S. Michal²⁹, L. Micu^{25a}, R.P. Middleton¹²⁹, P. Miele²⁹, S. Migas⁷³, L. Mijović⁴¹, G. Mikenberg¹⁷¹, M. Mikestikova¹²⁵, M. Mikuž⁷⁴, D.W. Miller¹⁴³, R.J. Miller⁸⁸, W.J. Mills¹⁶⁸, C. Mills⁵⁷, A. Milov¹⁷¹, D.A. Milstead^{146a,146b}, D. Milstein¹⁷¹, A.A. Minaenko¹²⁸, M. Miñano¹⁶⁷, I.A. Minashvili⁶⁵, A.I. Mincer¹⁰⁸, B. Mindur³⁷, M. Mineev⁶⁵, Y. Ming¹³⁰,

L.M. Mir¹¹, G. Mirabelli^{132a}, L. Miralles Verge¹¹, A. Misiejuk⁷⁶, J. Mitrevski¹³⁷, G.Y. Mitrofanov¹²⁸, V.A. Mitsou¹⁶⁷, S. Mitsui⁶⁶, P.S. Miyagawa¹³⁹, K. Miyazaki⁶⁷, J.U. Mjörnmark⁷⁹, T. Moa^{146a,146b}, P. Mockett¹³⁸, S. Moed⁵⁷, V. Moeller²⁷, K. Mönig⁴¹, N. Möser²⁰, S. Mohapatra¹⁴⁸, W. Mohr⁴⁸, S. Mohrdieck-Möck⁹⁹, A.M. Moiseev^{128,*}, R. Moles-Valls¹⁶⁷, J. Molina-Perez²⁹, J. Monk⁷⁷, E. Monnier⁸³, S. Montesano^{89a,89b}, F. Monticelli⁷⁰, S. Monzani^{19a,19b}, R.W. Moore², G.F. Moorhead⁸⁶, C. Mora Herrera⁴⁹, A. Moraes⁵³, N. Morange¹³⁶, J. Morel⁵⁴, G. Morello^{36a,36b}, D. Moreno⁸¹, M. Moreno Llácer¹⁶⁷, P. Morettini^{50a}, M. Morii⁵⁷, J. Morin⁷⁵, Y. Morita⁶⁶, A.K. Morley²⁹, G. Mornacchi²⁹, S.V. Morozov⁹⁶, J.D. Morris⁷⁵, L. Morvaj¹⁰¹, H.G. Moser⁹⁹, M. Mosidze⁵¹, J. Moss¹⁰⁹, R. Mount¹⁴³, E. Mountricha¹³⁶, S.V. Mouraviev⁹⁴, E.J.W. Moyse⁸⁴, M. Mudrinic^{12b}, F. Mueller^{58a}, J. Mueller¹²³, K. Mueller²⁰, T.A. Müller⁹⁸, D. Muenstermann²⁹, A. Muir¹⁶⁸, Y. Munwes¹⁵³, W.J. Murray¹²⁹, I. Mussche¹⁰⁵, E. Musto^{102a,102b}, A.G. Myagkov¹²⁸, M. Myska¹²⁵, J. Nadal¹¹, K. Nagai¹⁶⁰, K. Nagano⁶⁶, Y. Nagasaka⁶⁰, A.M. Nairz²⁹, Y. Nakahama²⁹, K. Nakamura¹⁵⁵, I. Nakano¹¹⁰, G. Nanava²⁰, A. Napier¹⁶¹, M. Nash^{77,c}, N.R. Nation²¹, T. Nattermann²⁰, T. Naumann⁴¹, G. Navarro¹⁶², H.A. Neal⁸⁷, E. Nebot⁸⁰, P.Yu. Nechaeva⁹⁴, A. Negri^{119a,119b}, G. Negri²⁹, S. Nektarijevic⁴⁹, S. Nelson¹⁴³, T.K. Nelson¹⁴³, S. Nemecek¹²⁵, P. Nemethy¹⁰⁸, A.A. Nepomuceno^{23a}, M. Nessi^{29,t}, S.Y. Nesterov¹²¹, M.S. Neubauer¹⁶⁵, A. Neusiedl⁸¹, R.M. Neves¹⁰⁸, P. Nevski²⁴, P.R. Newman¹⁷, V. Nguyen Thi Hong¹³⁶, R.B. Nickerson¹¹⁸, R. Nicolaidou¹³⁶, L. Nicolas¹³⁹, B. Nicquevert²⁹, F. Niedercorn¹¹⁵, J. Nielsen¹³⁷, T. Niinikoski²⁹, N. Nikiporou³⁴, A. Nikiporov¹⁵, V. Nikolaenko¹²⁸, K. Nikolaev⁶⁵, I. Nikolic-Audit⁷⁸, K. Nikolics⁴⁹, K. Nikolopoulos²⁴, H. Nilsen⁴⁸, P. Nilsson⁷, Y. Ninomiya¹⁵⁵, A. Nisati^{132a}, T. Nishiyama⁶⁷, R. Nisius⁹⁹, L. Nodulman⁵, M. Nomachi¹¹⁶, I. Nomidis¹⁵⁴, M. Nordberg²⁹, B. Nordkvist^{146a,146b}, P.R. Norton¹²⁹, J. Novakova¹²⁶, M. Nozaki⁶⁶, M. Nožička⁴¹, L. Nozka¹¹³, I.M. Nugent^{159a}, A.-E. Nuncio-Quiroz²⁰, G. Nunes Hanninger⁸⁶, T. Nunnemann⁹⁸, E. Nurse⁷⁷, T. Nyman²⁹, B.J. O'Brien⁴⁵, S.W. O'Neale^{17,*}, D.C. O'Neil¹⁴², V. O'Shea⁵³, F.G. Oakham^{28,e}, H. Oberlack⁹⁹, J. Ocariz⁷⁸, A. Ochi⁶⁷, S. Oda¹⁵⁵, S. Odaka⁶⁶, J. Odier⁸³, H. Ogren⁶¹, A. Oh⁸², S.H. Oh⁴⁴, C.C. Ohm^{146a,146b}, T. Ohshima¹⁰¹, H. Ohshita¹⁴⁰, T.K. Ohska⁶⁶, T. Ohsugi⁵⁹, S. Okada⁶⁷, H. Okawa¹⁶³, Y. Okumura¹⁰¹, T. Okuyama¹⁵⁵, M. Olcese^{50a}, A.G. Olchevski⁶⁵, M. Oliveira^{124a,h}, D. Oliveira Damazio²⁴, E. Oliver Garcia¹⁶⁷, D. Olivito¹²⁰, A. Olszewski³⁸, J. Olszowska³⁸, C. Omachi⁶⁷, A. Onofre^{124a,u}, P.U.E. Onyisi³⁰, C.J. Oram^{159a}, M.J. Oreglia³⁰, Y. Oren¹⁵³, D. Orestano^{134a,134b}, I. Orlov¹⁰⁷, C. Oropeza Barrera⁵³, R.S. Orr¹⁵⁸, B. Osculati^{50a,50b}, R. Ospanov¹²⁰, C. Osuna¹¹, G. Otero y Garzon²⁶, J.P. Ottersbach¹⁰⁵, M. Ouchrif^{135d}, F. Ould-Saada¹¹⁷, A. Ouraou¹³⁶, Q. Ouyang^{32a}, M. Owen⁸², S. Owen¹³⁹, V.E. Ozcan^{18a}, N. Ozturk⁷, A. Pacheco Pages¹¹, C. Padilla Aranda¹¹, S. Pagan Griso¹⁴, E. Paganis¹³⁹, F. Paige²⁴, K. Pajchel¹¹⁷, G. Palacino^{159b}, C.P. Palestini²⁹, D. Pallin³³, A. Palma^{124a,b}, J.D. Palmer¹⁷, Y.B. Pan¹⁷², E. Panagiotopoulou⁹, B. Panes^{31a}, N. Panikashvili⁸⁷, S. Panitkin²⁴, D. Pantea^{25a}, M. Panuskova¹²⁵, V. Paolone¹²³, A. Papadelis^{146a}, Th.D. Papadopoulos⁹, A. Paramonov⁵, W. Park^{24,v}, M.A. Parker²⁷, F. Parodi^{50a,50b}, J.A. Parsons³⁴, U. Parzefall⁴⁸, E. Pasqualucci^{132a}, A. Passeri^{134a}, F. Pastore^{134a,134b}, Fr. Pastore²⁹, G. Pásztor^{49,w}, S. Pataria¹⁷², N. Patel¹⁵⁰, J.R. Pater⁸², S. Patricelli^{102a,102b}, T. Pauly²⁹, M. Pecsý^{144a}, M.I. Pedraza Morales¹⁷², S.V. Peleganchuk¹⁰⁷, H. Peng^{32b}, R. Pengo²⁹, A. Penson³⁴, J. Penwell⁶¹, M. Perantoni^{23a}, K. Perez^{34,x}, T. Perez Cavalcanti⁴¹, E. Perez Codina¹¹, M.T. Pérez García-Están¹⁶⁷, V. Perez Reale³⁴, L. Perini^{89a,89b}, H. Pernegger²⁹, R. Perrino^{72a}, P. Perrodo⁴, S. Persema^{3a}, V.D. Peshekhonov⁶⁵, B.A. Petersen²⁹, J. Petersen²⁹, T.C. Petersen³⁵, E. Petit⁸³, A. Petridis¹⁵⁴, C. Petridou¹⁵⁴, E. Petrolo^{132a}, F. Petrucci^{134a,134b}, D. Petschull⁴¹, M. Petteni¹⁴², R. Pezoa^{31b}, A. Phan⁸⁶, A.W. Phillips²⁷, P.W. Phillips¹²⁹, G. Piacquadio²⁹, E. Piccaro⁷⁵, M. Piccinini^{19a,19b}, A. Pickford⁵³, S.M. Piec⁴¹, R. Piegaia²⁶, J.E. Pilcher³⁰, A.D. Pilkington⁸², J. Pina^{124a,b}, M. Pinamonti^{164a,164c}, A. Pinder¹¹⁸, J.L. Pinfold², J. Ping^{32c}, B. Pinto^{124a,b}, O. Pirotte²⁹, C. Pizio^{89a,89b}, R. Placakyte⁴¹, M. Plamondon¹⁶⁹, W.G. Plano⁸², M.-A. Pleier²⁴, A.V. Pleskach¹²⁸, A. Poblaguev²⁴, S. Poddar^{58a}, F. Podlisky³³, L. Poggioli¹¹⁵, T. Poghosyan²⁰, M. Pohl⁴⁹, F. Polci⁵⁵, G. Polesello^{119a}, A. Policicchio¹³⁸, A. Polini^{19a}, J. Poll⁷⁵, V. Polychronakos²⁴, D.M. Pomarede¹³⁶, D. Pomeroy²², K. Pommès²⁹, L. Pontecorvo^{132a}, B.G. Pope⁸⁸, G.A. Popeneciu^{25a}, D.S. Popovic^{12a}, A. Poppleton²⁹, X. Portell Bueso²⁹, R. Porter¹⁶³, C. Posch²¹, G.E. Pospelov⁹⁹, S. Pospisil¹²⁷, I.N. Potrap⁹⁹, C.J. Potter¹⁴⁹, C.T. Potter¹¹⁴, G. Poulard²⁹, J. Poveda¹⁷², R. Prabhu⁷⁷, P. Pralavorio⁸³, S. Prasad⁵⁷, R. Pravahan⁷, S. Prell⁶⁴, K. Pretzl¹⁶, L. Pribyl²⁹, D. Price⁶¹, L.E. Price⁵, M.J. Price²⁹, P.M. Prichard⁷³, D. Prieur¹²³, M. Primavera^{72a}, K. Prokofiev¹⁰⁸, F. Prokoshin^{31b}, S. Protopopescu²⁴, J. Proudfoot⁵, X. Prudent⁴³, H. Przysiezniak⁴, S. Psoroulas²⁰, E. Ptacek¹¹⁴, E. Pueschel⁸⁴, J. Purdham⁸⁷, M. Purohit^{24,v}, P. Puzo¹¹⁵, Y. Pylypchenko¹¹⁷, J. Qian⁸⁷, Z. Qian⁸³, Z. Qin⁴¹, A. Quadri⁵⁴, D.R. Quarrie¹⁴, W.B. Quayle¹⁷², F. Quinonez^{31a}, M. Raas¹⁰⁴, V. Radescu^{58b}, B. Radics²⁰, T. Rador^{18a}, F. Ragusa^{89a,89b}, G. Rahal¹⁷⁷, A.M. Rahimi¹⁰⁹, D. Rahm²⁴, S. Rajagopalan²⁴, M. Rammensee⁴⁸, M. Rammes¹⁴¹, M. Ramstedt^{146a,146b}, A.S. Randle-Conde³⁹, K. Randrianarivony²⁸, P.N. Ratoff⁷¹, F. Rauscher⁹⁸, E. Rauter⁹⁹, M. Raymond²⁹, A.L. Read¹¹⁷, D.M. Rebuzzi^{119a,119b}, A. Redelbach¹⁷³, G. Redlinger²⁴, R. Reece¹²⁰, K. Reeves⁴⁰, A. Reichold¹⁰⁵, E. Reinherz-Aronis¹⁵³, A. Reinsch¹¹⁴, I. Reisinger⁴², D. Reljic^{12a}, C. Rembser²⁹, Z.L. Ren¹⁵¹, A. Renaud¹¹⁵, P. Renkel³⁹, M. Rescigno^{132a}, S. Resconi^{89a}, B. Resende¹³⁶, P. Reznicek⁹⁸, R. Rezvani¹⁵⁸, A. Richards⁷⁷, R. Richter⁹⁹, E. Richter-Was^{38,y}, M. Ridel⁷⁸, S. Rieke⁸¹, M. Rijpsma¹⁰⁵, M. Rijssenbeek¹⁴⁸, A. Rimoldi^{119a,119b}, L. Rinaldi^{19a}, R.R. Rios³⁹, I. Riu¹¹, G. Rivoltella^{89a,89b}, F. Rizatdinova¹¹², E. Rizvi⁷⁵, S.H. Robertson^{85,j}, A. Robichaud-Veronneau⁴⁹, D. Robinson²⁷, J.E.M. Robinson⁷⁷, M. Robinson¹¹⁴, A. Robson⁵³, J.G. Rocha de Lima¹⁰⁶, C. Roda^{122a,122b}, D. Roda Dos Santos²⁹, S. Rodier⁸⁰, D. Rodriguez¹⁶², A. Roe⁵⁴, S. Roe²⁹, O. Røhne¹¹⁷, V. Rojo¹, S. Rolli¹⁶¹, A. Romaniouk⁹⁶, V.M. Romanov⁶⁵, G. Romeo²⁶, L. Roos⁷⁸, E. Ros¹⁶⁷, S. Rosati^{132a,132b}, K. Rosbach⁴⁹, A. Rose¹⁴⁹, M. Rose⁷⁶, G.A. Rosenbaum¹⁵⁸, E.I. Rosenberg⁶⁴, P.L. Rosendahl¹³, O. Rosenthal¹⁴¹, L. Rosselet⁴⁹, V. Rossetti¹¹, E. Rossi^{102a,102b}, L.P. Rossi^{50a}, L. Rossi^{89a,89b}, M. Rotaru^{25a}, I. Roth¹⁷¹, J. Rothberg¹³⁸, D. Rousseau¹¹⁵, C.R. Royon¹³⁶, A. Rozanov⁸³, Y. Rozen¹⁵², X. Ruan¹¹⁵, I. Rubinskiy⁴¹, B. Ruckert⁹⁸, N. Ruckstuhl¹⁰⁵, V.I. Rud⁹⁷, C. Rudolph⁴³, G. Rudolph⁶², F. Rühr⁶, F. Ruggieri^{134a,134b}, A. Ruiz-Martinez⁶⁴, E. Rulikowska-Zarebska³⁷, V. Rumiantsev^{91,*}, L. Rumyantsev⁶⁵, K. Runge⁴⁸, O. Runolfsson²⁰, Z. Rurikova⁴⁸,

N.A. Rusakov⁶⁵, D.R. Rust⁶¹, J.P. Rutherford⁶, C. Ruwiedel¹⁴, P. Ruzicka¹²⁵, Y.F. Ryabov¹²¹, V. Ryadovikov¹²⁸, P. Ryan⁸⁸, M. Rybar¹²⁶, G. Rybkin¹¹⁵, N.C. Ryder¹¹⁸, S. Rzaeva¹⁰, A.F. Saavedra¹⁵⁰, I. Sadeh¹⁵³, H.F.-W. Sadrozinski¹³⁷, R. Sadykov⁶⁵, F. Safai Tehrani^{132a,132b}, H. Sakamoto¹⁵⁵, G. Salamanna⁷⁵, A. Salamon^{133a}, M. Saleem¹¹¹, D. Salihagic⁹⁹, A. Salnikov¹⁴³, J. Salt¹⁶⁷, B.M. Salvachua Ferrando⁵, D. Salvatore^{36a,36b}, F. Salvatore¹⁴⁹, A. Salvucci¹⁰⁴, A. Salzburger²⁹, D. Sampsonidis¹⁵⁴, B.H. Samset¹¹⁷, A. Sanchez^{102a,102b}, H. Sandaker¹³, H.G. Sander⁸¹, M.P. Sanders⁹⁸, M. Sandhoff¹⁷⁴, T. Sandoval²⁷, C. Sandoval¹⁶², R. Sandstroem⁹⁹, S. Sandvoss¹⁷⁴, D.P.C. Sankey¹²⁹, A. Sansoni⁴⁷, C. Santamarina Rios⁸⁵, C. Santoni³³, R. Santonico^{133a,133b}, H. Santos^{124a}, J.G. Saraiva^{124a,b}, T. Sarangi¹⁷², E. Sarkisyan-Grinbaum⁷, F. Sarri^{122a,122b}, G. Sartisohn¹⁷⁴, O. Sasaki⁶⁶, T. Sasaki⁶⁶, N. Sasao⁶⁸, I. Satsounkevitch⁹⁰, G. Sauvage⁴, E. Sauvan⁴, J.B. Sauvan¹¹⁵, P. Savard^{158,e}, V. Savinov¹²³, D.O. Savu²⁹, P. Savva⁹, L. Sawyer^{24,l}, D.H. Saxon⁵³, L.P. Says³³, C. Sbarra^{19a,19b}, A. Sbrizzi^{19a,19b}, O. Scallan⁹³, D.A. Scannicchio¹⁶³, J. Schaarschmidt¹¹⁵, P. Schacht⁹⁹, U. Schäfer⁸¹, S. Schaepe²⁰, S. Schaezel^{58b}, A.C. Schaffer¹¹⁵, D. Schaile⁹⁸, R.D. Schamberger¹⁴⁸, A.G. Schamov¹⁰⁷, V. Scharf^{58a}, V.A. Schegelsky¹²¹, D. Scheirich⁸⁷, M. Schernau¹⁶³, M.I. Scherzer¹⁴, C. Schiavi^{50a,50b}, J. Schieck⁹⁸, M. Schioppa^{36a,36b}, S. Schlenker²⁹, J.L. Schlereth⁵, E. Schmidt⁴⁸, K. Schmieden²⁰, C. Schmitt⁸¹, S. Schmitt^{58b}, M. Schmitz²⁰, A. Schöning^{58b}, M. Schott²⁹, D. Schouten¹⁴², J. Schovancova¹²⁵, M. Schram⁸⁵, C. Schroeder⁸¹, N. Schroer^{58c}, S. Schuh²⁹, G. Schuler²⁹, J. Schultes¹⁷⁴, H.-C. Schultz-Coulon^{58a}, H. Schulz¹⁵, J.W. Schumacher²⁰, M. Schumacher⁴⁸, B.A. Schumm¹³⁷, Ph. Schune¹³⁶, C. Schwanenberger⁸², A. Schwartzman¹⁴³, Ph. Schwemling⁷⁸, R. Schwienhorst⁸⁸, R. Schwierz⁴³, J. Schwindling¹³⁶, T. Schwindt²⁰, W.G. Scott¹²⁹, J. Searcy¹¹⁴, E. Sedykh¹²¹, E. Segura¹¹, S.C. Seidel¹⁰³, A. Seiden¹³⁷, F. Seifert⁴³, J.M. Seixas^{23a}, G. Sekhniaidze^{102a}, D.M. Seliverstov¹²¹, B. Sellden^{146a}, G. Sellers⁷³, M. Seman^{144b}, N. Semprini-Cesari^{19a,19b}, C. Serfon⁹⁸, L. Serin¹¹⁵, R. Seuster⁹⁹, H. Severini¹¹¹, M.E. Sevier⁸⁶, A. Sfyrila²⁹, E. Shabalina⁵⁴, M. Shamim¹¹⁴, L.Y. Shan^{32a}, J.T. Shank²¹, Q.T. Shao⁸⁶, M. Shapiro¹⁴, P.B. Shatalov⁹⁵, L. Shaver⁶, K. Shaw^{164a,164c}, D. Sherman¹⁷⁵, P. Sherwood⁷⁷, A. Shibata¹⁰⁸, H. Shichi¹⁰¹, S. Shimizu²⁹, M. Shimojima¹⁰⁰, T. Shin⁵⁶, A. Shmeleva⁹⁴, M.J. Shochet³⁰, D. Short¹¹⁸, M.A. Shupe⁶, P. Sicho¹²⁵, A. Sidoti^{132a,132b}, A. Siebel¹⁷⁴, F. Siegert⁴⁸, J. Siegrist¹⁴, Dj. Sijacki^{12a}, O. Silbert¹⁷¹, J. Silva^{124a,b}, Y. Silver¹⁵³, D. Silverstein¹⁴³, S.B. Silverstein^{146a}, V. Simak¹²⁷, O. Simard¹³⁶, Lj. Simic^{12a}, S. Simion¹¹⁵, B. Simmons⁷⁷, R. Simoniello^{89a,89b}, M. Simonyan³⁵, P. Sinervo¹⁵⁸, N.B. Sinev¹¹⁴, V. Sipica¹⁴¹, G. Siragusa¹⁷³, A. Sircar²⁴, A.N. Sisakyan⁶⁵, S.Yu. Sivoklokov⁹⁷, J. Sjölin^{146a,146b}, T.B. Sjrursen¹³, L.A. Skinnari¹⁴, K. Skovpen¹⁰⁷, P. Skubic¹¹¹, N. Skvorodnev²², M. Slater¹⁷, T. Slavicek¹²⁷, K. Sliwa¹⁶¹, T.J. Sloan⁷¹, J. Sloper²⁹, V. Smakhtin¹⁷¹, S.Yu. Smirnov⁹⁶, L.N. Smirnova⁹⁷, O. Smirnova⁷⁹, B.C. Smith⁵⁷, D. Smith¹⁴³, K.M. Smith⁵³, M. Smizanska⁷¹, K. Smolek¹²⁷, A.A. Snesarev⁹⁴, S.W. Snow⁸², J. Snow¹¹¹, J. Snuverink¹⁰⁵, S. Snyder²⁴, M. Soares^{124a}, R. Sobie^{169,j}, J. Sodomka¹²⁷, A. Soffer¹⁵³, C.A. Solans¹⁶⁷, M. Solar¹²⁷, J. Solc¹²⁷, E. Soldatov⁹⁶, U. Soldevila¹⁶⁷, E. Solfaroli Camillocci^{132a,132b}, A.A. Solodkov¹²⁸, O.V. Solovyanov¹²⁸, J. Sondericker²⁴, N. Soni², V. Sopko¹²⁷, B. Sopko¹²⁷, M. Sorbi^{89a,89b}, M. Sosebee⁷, A. Soukharev¹⁰⁷, S. Spagnolo^{72a,72b}, F. Spanò⁷⁶, R. Spighi^{19a}, G. Spigo²⁹, F. Spila^{132a,132b}, E. Spiriti^{134a}, R. Spiwoks²⁹, M. Spousta¹²⁶, T. Spreitzer¹⁵⁸, B. Spurlock⁷, R.D. St. Denis⁵³, T. Stahl¹⁴¹, J. Stahlman¹²⁰, R. Stamen^{58a}, E. Stanecka²⁹, R.W. Stanek⁵, C. Stancu^{134a}, S. Stapnes¹¹⁷, E.A. Starchenko¹²⁸, J. Stark⁵⁵, P. Staroba¹²⁵, P. Starovoitov⁹¹, A. Staude⁹⁸, P. Stavina^{144a}, G. Stavropoulos¹⁴, G. Steele⁵³, P. Steinbach⁴³, P. Steinberg²⁴, I. Stekl¹²⁷, B. Stelzer¹⁴², H.J. Stelzer⁸⁸, O. Stelzer-Chilton^{159a}, H. Stenzel⁵², K. Stevenson⁷⁵, G.A. Stewart²⁹, J.A. Stillings²⁰, T. Stockmanns²⁰, M.C. Stockton²⁹, K. Stoerig⁴⁸, G. Stoicea^{25a}, S. Stojek⁹⁹, P. Strachota¹²⁶, A.R. Stradling⁷, A. Straessner⁴³, J. Strandberg¹⁴⁷, S. Strandberg^{146a,146b}, A. Strandlie¹¹⁷, M. Strang¹⁰⁹, E. Strauss¹⁴³, M. Strauss¹¹¹, P. Strizenec^{144b}, R. Ströhmer¹⁷³, D.M. Strom¹¹⁴, J.A. Strong^{76,*}, R. Stroynowski³⁹, J. Strube¹²⁹, B. Stugu¹³, I. Stumer^{24,*}, J. Stupak¹⁴⁸, P. Sturm¹⁷⁴, D.A. Soh^{151,q}, D. Su¹⁴³, H.S. Subramania², A. Succurro¹¹, Y. Sugaya¹¹⁶, T. Sugimoto¹⁰¹, C. Suhr¹⁰⁶, K. Suita⁶⁷, M. Suk¹²⁶, V.V. Sulin⁹⁴, S. Sultansoy^{3d}, T. Sumida²⁹, X. Sun⁵⁵, J.E. Sundermann⁴⁸, K. Suruliz¹³⁹, S. Sushkov¹¹, G. Susinno^{36a,36b}, M.R. Sutton¹⁴⁹, Y. Suzuki⁶⁶, Y. Suzuki⁶⁷, M. Svatos¹²⁵, Yu.M. Sviridov¹²⁸, S. Swedish¹⁶⁸, I. Sykora^{144a}, T. Sykora¹²⁶, B. Szeless²⁹, J. Sánchez¹⁶⁷, D. Ta¹⁰⁵, K. Tackmann⁴¹, A. Taffard¹⁶³, R. Tahirout^{159a}, A. Taga¹¹⁷, N. Taiblum¹⁵³, Y. Takahashi¹⁰¹, H. Takai²⁴, R. Takashima⁶⁹, H. Takeda⁶⁷, T. Takeshita¹⁴⁰, M. Talby⁸³, A. Talyshev¹⁰⁷, M.C. Tamsett²⁴, J. Tanaka¹⁵⁵, R. Tanaka¹¹⁵, S. Tanaka¹³¹, S. Tanaka⁶⁶, Y. Tanaka¹⁰⁰, K. Tani⁶⁷, N. Tannoury⁸³, G.P. Tappern²⁹, S. Tapprogge⁸¹, D. Tardif¹⁵⁸, S. Tarem¹⁵², F. Tarrade²⁸, G.F. Tartarelli^{89a}, P. Tas¹²⁶, M. Tasevsky¹²⁵, E. Tassi^{36a,36b}, M. Tatarkhanov¹⁴, C. Taylor⁷⁷, F.E. Taylor⁹², G.N. Taylor⁸⁶, W. Taylor^{159b}, M. Teinturier¹¹⁵, M. Teixeira Dias Castanheira⁷⁵, P. Teixeira-Dias⁷⁶, K.K. Temming⁴⁸, H. Ten Kate²⁹, P.K. Teng¹⁵¹, S. Terada⁶⁶, K. Terashi¹⁵⁵, J. Terron⁸⁰, M. Terwort^{41,o}, M. Testa⁴⁷, R.J. Teuscher^{158,j}, J. Thadome¹⁷⁴, J. Therhaag²⁰, T. Theveneaux-Pelzer⁷⁸, M. Thioye¹⁷⁵, S. Thoma⁴⁸, J.P. Thomas¹⁷, E.N. Thompson⁸⁴, P.D. Thompson¹⁷, P.D. Thompson¹⁵⁸, A.S. Thompson⁵³, E. Thomson¹²⁰, M. Thomson²⁷, R.P. Thun⁸⁷, F. Tian³⁴, T. Tic¹²⁵, V.O. Tikhomirov⁹⁴, Y.A. Tikhonov¹⁰⁷, C.J.W.P. Timmermans¹⁰⁴, P. Tipton¹⁷⁵, F.J. Tique Aires Viegas²⁹, S. Tisserant⁸³, J. Tobias⁴⁸, B. Toczec³⁷, T. Todorov⁴, S. Todorova-Nova¹⁶¹, B. Toggerson¹⁶³, J. Tojo⁶⁶, S. Tokár^{144a}, K. Tokunaga⁶⁷, K. Tokushuku⁶⁶, K. Tollefson⁸⁸, M. Tomoto¹⁰¹, L. Tompkins¹⁴, K. Toms¹⁰³, G. Tong^{32a}, A. Tonoyan¹³, C. Topfel¹⁶, N.D. Topilin⁶⁵, I. Torchiani²⁹, E. Torrence¹¹⁴, H. Torres⁷⁸, E. Torró Pastor¹⁶⁷, J. Toth^{83,w}, F. Touchard⁸³, D.R. Tovey¹³⁹, D. Traynor⁷⁵, T. Trefzger¹⁷³, L. Tremblet²⁹, A. Tricoli²⁹, I.M. Trigger^{159a}, S. Trincas-Duvold⁷⁸, T.N. Trinh⁷⁸, M.F. Tripiana⁷⁰, W. Trischuk¹⁵⁸, A. Trivedi^{24,v}, B. Trocme⁵⁵, C. Troncon^{89a}, M. Trottier-McDonald¹⁴², A. Trzupek³⁸, C. Tsarouchas²⁹, J.C.-L. Tseng¹¹⁸, M. Tsiakiris¹⁰⁵, P.V. Tsiarehka⁹⁰, D. Tsionou⁴, G. Tsipolitis⁹, V. Tsiskaridze⁴⁸, E.G. Tskhadadze⁵¹, I.I. Tsukerman⁹⁵, V. Tsulaia¹⁴, J.-W. Tsung²⁰, S. Tsuno⁶⁶, D. Tsybychev¹⁴⁸, A. Tua¹³⁹, J.M. Tuggle³⁰, M. Turala³⁸, D. Turecek¹²⁷, I. Turk Cakir^{3e}, E. Turlay¹⁰⁵, R. Turra^{89a,89b}, P.M. Tuts³⁴, A. Tykhonov⁷⁴, M. Tylnad^{146a,146b}, M. Tyndel¹²⁹, H. Tyrvalinen²⁹, G. Tzanakos⁸, K. Uchida²⁰, I. Ueda¹⁵⁵, R. Ueno²⁸, M. Ugland¹³, M. Uhlenbrock²⁰, M. Uhrmacher⁵⁴, F. Ukegawa¹⁶⁰, G. Unal²⁹, D.G. Underwood⁵, A. Undrus²⁴,

G. Unel¹⁶³, Y. Unno⁶⁶, D. Urbaniec³⁴, E. Urkovsky¹⁵³, P. Urrejola^{31a}, G. Usai⁷, M. Uslenghi^{119a,119b}, L. Vacavant⁸³, V. Vacek¹²⁷, B. Vachon⁸⁵, S. Vahsen¹⁴, J. Valenta¹²⁵, P. Valente^{132a}, S. Valentini^{19a,19b}, S. Valkar¹²⁶, E. Valladolid Gallego¹⁶⁷, S. Vallecorsa¹⁵², J.A. Valls Ferrer¹⁶⁷, H. van der Graaf¹⁰⁵, E. van der Kraaij¹⁰⁵, R. Van Der Leeuw¹⁰⁵, E. van der Poel¹⁰⁵, D. van der Ster²⁹, B. Van Eijk¹⁰⁵, N. van Eldik⁸⁴, P. van Gemmeren⁵, Z. van Kesteren¹⁰⁵, I. van Vulpen¹⁰⁵, W. Vandelli²⁹, G. Vandoni²⁹, A. Vaniachine⁵, P. Vankov⁴¹, F. Vannucci⁷⁸, F. Varela Rodriguez²⁹, R. Vari^{132a}, E.W. Varnes⁶, D. Varouchas¹⁴, A. Vartapetian⁷, K.E. Varvell¹⁵⁰, V.I. Vassilakopoulos⁵⁶, F. Vazeille³³, G. Vegni^{89a,89b}, J.J. Veillet¹¹⁵, C. Vellidis⁸, F. Veloso^{124a}, R. Veness²⁹, S. Veneziano^{132a}, A. Ventura^{72a,72b}, D. Ventura¹³⁸, M. Venturi⁴⁸, N. Venturi¹⁶, V. Vercesi^{119a}, M. Verducci¹³⁸, W. Verkerke¹⁰⁵, J.C. Vermeulen¹⁰⁵, A. Vest⁴³, M.C. Vetterli^{142,e}, I. Vichou¹⁶⁵, T. Vickey^{145b,z}, G.H.A. Viehhauser¹¹⁸, S. Viel¹⁶⁸, M. Villa^{19a,19b}, M. Villaplana Perez¹⁶⁷, E. Vilucchi⁴⁷, M.G. Vinciter²⁸, E. Vinek²⁹, V.B. Vinogradov⁶⁵, M. Virchaux^{136,*}, J. Virzi¹⁴, O. Vitells¹⁷¹, M. Viti⁴¹, I. Vivarelli⁴⁸, F. Vives Vaque¹¹, S. Vlachos⁹, M. Vlasak¹²⁷, N. Vlasov²⁰, A. Vogel²⁰, P. Vokac¹²⁷, G. Volpi⁴⁷, M. Volpi⁸⁶, G. Volpini^{89a}, H. von der Schmitt⁹⁹, J. von Loeben⁹⁹, H. von Radziewski⁴⁸, E. von Toerne²⁰, V. Vorobel¹²⁶, A.P. Vorobiev¹²⁸, V. Vorwerk¹¹, M. Vos¹⁶⁷, R. Voss²⁹, T.T. Voss¹⁷⁴, J.H. Vosseveld⁷³, N. Vranjes^{12a}, M. Vranjes Milosavljevic¹⁰⁵, V. Vrba¹²⁵, M. Vreeswijk¹⁰⁵, T. Vu Anh⁸¹, R. Vuillermet²⁹, I. Vukotic¹¹⁵, W. Wagner¹⁷⁴, P. Wagner¹²⁰, H. Wahlen¹⁷⁴, J. Wakabayashi¹⁰¹, J. Walbersloh⁴², S. Walch⁸⁷, J. Walder⁷¹, R. Walker⁹⁸, W. Walkowiak¹⁴¹, R. Wall¹⁷⁵, P. Waller⁷³, C. Wang⁴⁴, H. Wang¹⁷², H. Wang^{32b,aa}, J. Wang¹⁵¹, J. Wang^{32d}, J.C. Wang¹³⁸, R. Wang¹⁰³, S.M. Wang¹⁵¹, A. Warburton⁸⁵, C.P. Ward²⁷, M. Warsinsky⁴⁸, P.M. Watkins¹⁷, A.T. Watson¹⁷, M.F. Watson¹⁷, G. Watts¹³⁸, S. Watts⁸², A.T. Waugh¹⁵⁰, B.M. Waugh⁷⁷, J. Weber⁴², M. Weber¹²⁹, M.S. Weber¹⁶, P. Weber⁵⁴, A.R. Weidberg¹¹⁸, P. Weigell⁹⁹, J. Weingarten⁵⁴, C. Weiser⁴⁸, H. Wellenstein²², P.S. Wells²⁹, M. Wen⁴⁷, T. Wenaus²⁴, S. Wendler¹²³, Z. Weng^{151,q}, T. Wengler²⁹, S. Wenig²⁹, N. Wermes²⁰, M. Werner⁴⁸, P. Werner²⁹, M. Werth¹⁶³, M. Wessels^{58a}, C. Weydert⁵⁵, K. Whalen²⁸, S.J. Wheeler-Ellis¹⁶³, S.P. Whitaker²¹, A. White⁷, M.J. White⁸⁶, S.R. Whitehead¹¹⁸, D. Whiteson¹⁶³, D. Whittington⁶¹, F. Wicke¹¹⁵, D. Wicke¹⁷⁴, F.J. Wickens¹²⁹, W. Wiedenmann¹⁷², M. Wieler¹²⁹, P. Wienemann²⁰, C. Wigglesworth⁷⁵, L.A.M. Wiik⁴⁸, P.A. Wijeratne⁷⁷, A. Wildauer¹⁶⁷, M.A. Wildt^{41,o}, I. Wilhelm¹²⁶, H.G. Wilkens²⁹, J.Z. Will⁹⁸, E. Williams³⁴, H.H. Williams¹²⁰, W. Willis³⁴, S. Willocq⁸⁴, J.A. Wilson¹⁷, M.G. Wilson¹⁴³, A. Wilson⁸⁷, I. Wingerter-Seez⁴, S. Winkelmann⁴⁸, F. Winklmeier²⁹, M. Wittgen¹⁴³, M.W. Wolter³⁸, H. Wolters^{124a,h}, W.C. Wong⁴⁰, G. Wooden¹¹⁸, B.K. Wosiek³⁸, J. Wotschack²⁹, M.J. Woudstra⁸⁴, K. Wraight⁵³, C. Wright⁵³, B. Wrona⁷³, S.L. Wu¹⁷², X. Wu⁴⁹, Y. Wu^{32b,ab}, E. Wulf³⁴, R. Wunstorf⁴², B.M. Wynne⁴⁵, L. Xaplanteris⁹, S. Xella³⁵, S. Xie⁴⁸, Y. Xie^{32a}, C. Xu^{32b,ac}, D. Xu¹³⁹, G. Xu^{32a}, B. Yabsley¹⁵⁰, S. Yacoob^{145b}, M. Yamada⁶⁶, H. Yamaguchi¹⁵⁵, A. Yamamoto⁶⁶, K. Yamamoto⁶⁴, S. Yamamoto¹⁵⁵, T. Yamamura¹⁵⁵, T. Yamanaka¹⁵⁵, J. Yamaoka⁴⁴, T. Yamazaki¹⁵⁵, Y. Yamazaki⁶⁷, Z. Yan²¹, H. Yang⁸⁷, U.K. Yang⁸², Y. Yang⁶¹, Y. Yang^{32a}, Z. Yang^{146a,146b}, S. Yanush⁹¹, W.-M. Yao¹⁴, Y. Yao¹⁴, Y. Yasu⁶⁶, G.V. Ybeles Smit¹³⁰, J. Ye³⁹, S. Ye²⁴, M. Yilmaz^{3c}, R. Yoosoofmiya¹²³, K. Yorita¹⁷⁰, R. Yoshida⁵, C. Young¹⁴³, S. Youssef²¹, D. Yu²⁴, J. Yu⁷, J. Yu^{32c,ac}, L. Yuan^{32a,ad}, A. Yurkewicz¹⁴⁸, V.G. Zaets¹²⁸, R. Zaidan⁶³, A.M. Zaitsev¹²⁸, Z. Zajacova²⁹, Yo.K. Zalite¹²¹, L. Zanello^{132a,132b}, P. Zarzhitsky³⁹, A. Zaytsev¹⁰⁷, C. Zeitnitz¹⁷⁴, M. Zeller¹⁷⁵, M. Zeman¹²⁵, A. Zemla³⁸, C. Zendler²⁰, O. Zenin¹²⁸, T. Ženiš^{144a}, Z. Zenonos^{122a,122b}, S. Zenz¹⁴, D. Zerwas¹¹⁵, G. Zevi della Porta⁵⁷, Z. Zhan^{32d}, D. Zhang^{32b,aa}, H. Zhang⁸⁸, J. Zhang⁵, X. Zhang^{32d}, Z. Zhang¹¹⁵, L. Zhao¹⁰⁸, T. Zhao¹³⁸, Z. Zhao^{32b}, A. Zhemchugov⁶⁵, S. Zheng^{32a}, J. Zhong^{151,ae}, B. Zhou⁸⁷, N. Zhou¹⁶³, Y. Zhou¹⁵¹, C.G. Zhu^{32d}, H. Zhu⁴¹, J. Zhu⁸⁷, Y. Zhu¹⁷², X. Zhuang⁹⁸, V. Zhuravlov⁹⁹, D. Zieminska⁶¹, R. Zimmermann²⁰, S. Zimmermann²⁰, S. Zimmermann⁴⁸, M. Ziolkowski¹⁴¹, R. Zitoun⁴, L. Živković³⁴, V.V. Zmouchko^{128,*}, G. Zobernig¹⁷², A. Zoccoli^{19a,19b}, Y. Zolnierowski⁴, A. Zsenei²⁹, M. zur Nedden¹⁵, V. Zutshi¹⁰⁶, L. Zwalinski²⁹.

¹ University at Albany, Albany NY, United States of America

² Department of Physics, University of Alberta, Edmonton AB, Canada

³ (a) Department of Physics, Ankara University, Ankara; (b) Department of Physics, Dumlupinar University, Kutahya;

(c) Department of Physics, Gazi University, Ankara; (d) Division of Physics, TOBB University of Economics and Technology, Ankara; (e) Turkish Atomic Energy Authority, Ankara, Turkey

⁴ LAPP, CNRS/IN2P3 and Université de Savoie, Annecy-le-Vieux, France

⁵ High Energy Physics Division, Argonne National Laboratory, Argonne IL, United States of America

⁶ Department of Physics, University of Arizona, Tucson AZ, United States of America

⁷ Department of Physics, The University of Texas at Arlington, Arlington TX, United States of America

⁸ Physics Department, University of Athens, Athens, Greece

⁹ Physics Department, National Technical University of Athens, Zografou, Greece

¹⁰ Institute of Physics, Azerbaijan Academy of Sciences, Baku, Azerbaijan

¹¹ Institut de Física d'Altes Energies and Universitat Autònoma de Barcelona and ICREA, Barcelona, Spain

¹² (a) Institute of Physics, University of Belgrade, Belgrade; (b) Vinca Institute of Nuclear Sciences, Belgrade, Serbia

¹³ Department for Physics and Technology, University of Bergen, Bergen, Norway

¹⁴ Physics Division, Lawrence Berkeley National Laboratory and University of California, Berkeley CA, United States of America

¹⁵ Department of Physics, Humboldt University, Berlin, Germany

¹⁶ Albert Einstein Center for Fundamental Physics and Laboratory for High Energy Physics, University of Bern, Bern, Switzerland

¹⁷ School of Physics and Astronomy, University of Birmingham, Birmingham, United Kingdom

- 18 ^(a)Department of Physics, Bogazici University, Istanbul; ^(b)Division of Physics, Dogus University, Istanbul; ^(c)Department of Physics Engineering, Gaziantep University, Gaziantep; ^(d)Department of Physics, Istanbul Technical University, Istanbul, Turkey
- 19 ^(a)INFN Sezione di Bologna; ^(b)Dipartimento di Fisica, Università di Bologna, Bologna, Italy
- 20 Physikalisches Institut, University of Bonn, Bonn, Germany
- 21 Department of Physics, Boston University, Boston MA, United States of America
- 22 Department of Physics, Brandeis University, Waltham MA, United States of America
- 23 ^(a)Universidade Federal do Rio De Janeiro COPPE/EE/IF, Rio de Janeiro; ^(b)Federal University of Juiz de Fora (UFJF), Juiz de Fora; ^(c)Federal University of Sao Joao del Rei (UFSJ), Sao Joao del Rei; ^(d)Instituto de Fisica, Universidade de Sao Paulo, Sao Paulo, Brazil
- 24 Physics Department, Brookhaven National Laboratory, Upton NY, United States of America
- 25 ^(a)National Institute of Physics and Nuclear Engineering, Bucharest; ^(b)University Politehnica Bucharest, Bucharest; ^(c)West University in Timisoara, Timisoara, Romania
- 26 Departamento de Física, Universidad de Buenos Aires, Buenos Aires, Argentina
- 27 Cavendish Laboratory, University of Cambridge, Cambridge, United Kingdom
- 28 Department of Physics, Carleton University, Ottawa ON, Canada
- 29 CERN, Geneva, Switzerland
- 30 Enrico Fermi Institute, University of Chicago, Chicago IL, United States of America
- 31 ^(a)Departamento de Física, Pontificia Universidad Católica de Chile, Santiago; ^(b)Departamento de Física, Universidad Técnica Federico Santa María, Valparaíso, Chile
- 32 ^(a)Institute of High Energy Physics, Chinese Academy of Sciences, Beijing; ^(b)Department of Modern Physics, University of Science and Technology of China, Anhui; ^(c)Department of Physics, Nanjing University, Jiangsu; ^(d)High Energy Physics Group, Shandong University, Shandong, China
- 33 Laboratoire de Physique Corpusculaire, Clermont Université and Université Blaise Pascal and CNRS/IN2P3, Aubiere Cedex, France
- 34 Nevis Laboratory, Columbia University, Irvington NY, United States of America
- 35 Niels Bohr Institute, University of Copenhagen, Kobenhavn, Denmark
- 36 ^(a)INFN Gruppo Collegato di Cosenza; ^(b)Dipartimento di Fisica, Università della Calabria, Arcavata di Rende, Italy
- 37 Faculty of Physics and Applied Computer Science, AGH-University of Science and Technology, Krakow, Poland
- 38 The Henryk Niewodniczanski Institute of Nuclear Physics, Polish Academy of Sciences, Krakow, Poland
- 39 Physics Department, Southern Methodist University, Dallas TX, United States of America
- 40 Physics Department, University of Texas at Dallas, Richardson TX, United States of America
- 41 DESY, Hamburg and Zeuthen, Germany
- 42 Institut für Experimentelle Physik IV, Technische Universität Dortmund, Dortmund, Germany
- 43 Institut für Kern- und Teilchenphysik, Technical University Dresden, Dresden, Germany
- 44 Department of Physics, Duke University, Durham NC, United States of America
- 45 SUPA - School of Physics and Astronomy, University of Edinburgh, Edinburgh, United Kingdom
- 46 Fachhochschule Wiener Neustadt, Johannes Gutenbergstrasse 3, 2700 Wiener Neustadt, Austria
- 47 INFN Laboratori Nazionali di Frascati, Frascati, Italy
- 48 Fakultät für Mathematik und Physik, Albert-Ludwigs-Universität, Freiburg i.Br., Germany
- 49 Section de Physique, Université de Genève, Geneva, Switzerland
- 50 ^(a)INFN Sezione di Genova; ^(b)Dipartimento di Fisica, Università di Genova, Genova, Italy
- 51 Institute of Physics and HEP Institute, Georgian Academy of Sciences and Tbilisi State University, Tbilisi, Georgia
- 52 II Physikalisches Institut, Justus-Liebig-Universität Giessen, Giessen, Germany
- 53 SUPA - School of Physics and Astronomy, University of Glasgow, Glasgow, United Kingdom
- 54 II Physikalisches Institut, Georg-August-Universität, Göttingen, Germany
- 55 Laboratoire de Physique Subatomique et de Cosmologie, Université Joseph Fourier and CNRS/IN2P3 and Institut National Polytechnique de Grenoble, Grenoble, France
- 56 Department of Physics, Hampton University, Hampton VA, United States of America
- 57 Laboratory for Particle Physics and Cosmology, Harvard University, Cambridge MA, United States of America
- 58 ^(a)Kirchhoff-Institut für Physik, Ruprecht-Karls-Universität Heidelberg, Heidelberg; ^(b)Physikalisches Institut, Ruprecht-Karls-Universität Heidelberg, Heidelberg; ^(c)ZITI Institut für technische Informatik, Ruprecht-Karls-Universität Heidelberg, Mannheim, Germany
- 59 Faculty of Science, Hiroshima University, Hiroshima, Japan
- 60 Faculty of Applied Information Science, Hiroshima Institute of Technology, Hiroshima, Japan
- 61 Department of Physics, Indiana University, Bloomington IN, United States of America
- 62 Institut für Astro- und Teilchenphysik, Leopold-Franzens-Universität, Innsbruck, Austria
- 63 University of Iowa, Iowa City IA, United States of America

- ⁶⁴ Department of Physics and Astronomy, Iowa State University, Ames IA, United States of America
- ⁶⁵ Joint Institute for Nuclear Research, JINR Dubna, Dubna, Russia
- ⁶⁶ KEK, High Energy Accelerator Research Organization, Tsukuba, Japan
- ⁶⁷ Graduate School of Science, Kobe University, Kobe, Japan
- ⁶⁸ Faculty of Science, Kyoto University, Kyoto, Japan
- ⁶⁹ Kyoto University of Education, Kyoto, Japan
- ⁷⁰ Instituto de Física La Plata, Universidad Nacional de La Plata and CONICET, La Plata, Argentina
- ⁷¹ Physics Department, Lancaster University, Lancaster, United Kingdom
- ⁷² ^(a) INFN Sezione di Lecce; ^(b) Dipartimento di Fisica, Università del Salento, Lecce, Italy
- ⁷³ Oliver Lodge Laboratory, University of Liverpool, Liverpool, United Kingdom
- ⁷⁴ Department of Physics, Jožef Stefan Institute and University of Ljubljana, Ljubljana, Slovenia
- ⁷⁵ Department of Physics, Queen Mary University of London, London, United Kingdom
- ⁷⁶ Department of Physics, Royal Holloway University of London, Surrey, United Kingdom
- ⁷⁷ Department of Physics and Astronomy, University College London, London, United Kingdom
- ⁷⁸ Laboratoire de Physique Nucléaire et de Hautes Energies, UPMC and Université Paris-Diderot and CNRS/IN2P3, Paris, France
- ⁷⁹ Fysiska institutionen, Lunds universitet, Lund, Sweden
- ⁸⁰ Departamento de Física Teórica C-15, Universidad Autónoma de Madrid, Madrid, Spain
- ⁸¹ Institut für Physik, Universität Mainz, Mainz, Germany
- ⁸² School of Physics and Astronomy, University of Manchester, Manchester, United Kingdom
- ⁸³ CPPM, Aix-Marseille Université and CNRS/IN2P3, Marseille, France
- ⁸⁴ Department of Physics, University of Massachusetts, Amherst MA, United States of America
- ⁸⁵ Department of Physics, McGill University, Montreal QC, Canada
- ⁸⁶ School of Physics, University of Melbourne, Victoria, Australia
- ⁸⁷ Department of Physics, The University of Michigan, Ann Arbor MI, United States of America
- ⁸⁸ Department of Physics and Astronomy, Michigan State University, East Lansing MI, United States of America
- ⁸⁹ ^(a) INFN Sezione di Milano; ^(b) Dipartimento di Fisica, Università di Milano, Milano, Italy
- ⁹⁰ B.I. Stepanov Institute of Physics, National Academy of Sciences of Belarus, Minsk, Republic of Belarus
- ⁹¹ National Scientific and Educational Centre for Particle and High Energy Physics, Minsk, Republic of Belarus
- ⁹² Department of Physics, Massachusetts Institute of Technology, Cambridge MA, United States of America
- ⁹³ Group of Particle Physics, University of Montreal, Montreal QC, Canada
- ⁹⁴ P.N. Lebedev Institute of Physics, Academy of Sciences, Moscow, Russia
- ⁹⁵ Institute for Theoretical and Experimental Physics (ITEP), Moscow, Russia
- ⁹⁶ Moscow Engineering and Physics Institute (MEPhI), Moscow, Russia
- ⁹⁷ Skobeltsyn Institute of Nuclear Physics, Lomonosov Moscow State University, Moscow, Russia
- ⁹⁸ Fakultät für Physik, Ludwig-Maximilians-Universität München, München, Germany
- ⁹⁹ Max-Planck-Institut für Physik (Werner-Heisenberg-Institut), München, Germany
- ¹⁰⁰ Nagasaki Institute of Applied Science, Nagasaki, Japan
- ¹⁰¹ Graduate School of Science, Nagoya University, Nagoya, Japan
- ¹⁰² ^(a) INFN Sezione di Napoli; ^(b) Dipartimento di Scienze Fisiche, Università di Napoli, Napoli, Italy
- ¹⁰³ Department of Physics and Astronomy, University of New Mexico, Albuquerque NM, United States of America
- ¹⁰⁴ Institute for Mathematics, Astrophysics and Particle Physics, Radboud University Nijmegen/Nikhef, Nijmegen, Netherlands
- ¹⁰⁵ Nikhef National Institute for Subatomic Physics and University of Amsterdam, Amsterdam, Netherlands
- ¹⁰⁶ Department of Physics, Northern Illinois University, DeKalb IL, United States of America
- ¹⁰⁷ Budker Institute of Nuclear Physics (BINP), Novosibirsk, Russia
- ¹⁰⁸ Department of Physics, New York University, New York NY, United States of America
- ¹⁰⁹ Ohio State University, Columbus OH, United States of America
- ¹¹⁰ Faculty of Science, Okayama University, Okayama, Japan
- ¹¹¹ Homer L. Dodge Department of Physics and Astronomy, University of Oklahoma, Norman OK, United States of America
- ¹¹² Department of Physics, Oklahoma State University, Stillwater OK, United States of America
- ¹¹³ Palacký University, RCPTM, Olomouc, Czech Republic
- ¹¹⁴ Center for High Energy Physics, University of Oregon, Eugene OR, United States of America
- ¹¹⁵ LAL, Univ. Paris-Sud and CNRS/IN2P3, Orsay, France
- ¹¹⁶ Graduate School of Science, Osaka University, Osaka, Japan
- ¹¹⁷ Department of Physics, University of Oslo, Oslo, Norway
- ¹¹⁸ Department of Physics, Oxford University, Oxford, United Kingdom
- ¹¹⁹ ^(a) INFN Sezione di Pavia; ^(b) Dipartimento di Fisica Nucleare e Teorica, Università di Pavia, Pavia, Italy
- ¹²⁰ Department of Physics, University of Pennsylvania, Philadelphia PA, United States of America
- ¹²¹ Petersburg Nuclear Physics Institute, Gatchina, Russia

- 122 (a) INFN Sezione di Pisa; (b) Dipartimento di Fisica E. Fermi, Università di Pisa, Pisa, Italy
- 123 Department of Physics and Astronomy, University of Pittsburgh, Pittsburgh PA, United States of America
- 124 (a) Laboratório de Instrumentação e Física Experimental de Partículas - LIP, Lisboa, Portugal; (b) Departamento de Física Teórica y del Cosmos and CAFPE, Universidad de Granada, Granada, Spain
- 125 Institute of Physics, Academy of Sciences of the Czech Republic, Praha, Czech Republic
- 126 Faculty of Mathematics and Physics, Charles University in Prague, Praha, Czech Republic
- 127 Czech Technical University in Prague, Praha, Czech Republic
- 128 State Research Center Institute for High Energy Physics, Protvino, Russia
- 129 Particle Physics Department, Rutherford Appleton Laboratory, Didcot, United Kingdom
- 130 Physics Department, University of Regina, Regina SK, Canada
- 131 Ritsumeikan University, Kusatsu, Shiga, Japan
- 132 (a) INFN Sezione di Roma I; (b) Dipartimento di Fisica, Università La Sapienza, Roma, Italy
- 133 (a) INFN Sezione di Roma Tor Vergata; (b) Dipartimento di Fisica, Università di Roma Tor Vergata, Roma, Italy
- 134 (a) INFN Sezione di Roma Tre; (b) Dipartimento di Fisica, Università Roma Tre, Roma, Italy
- 135 (a) Faculté des Sciences Ain Chock, Réseau Universitaire de Physique des Hautes Energies - Université Hassan II, Casablanca; (b) Centre National de l'Energie des Sciences Techniques Nucleaires, Rabat; (c) Université Cadi Ayyad, Faculté des sciences Semlalia Département de Physique, B.P. 2390 Marrakech 40000; (d) Faculté des Sciences, Université Mohamed Premier and LPTPM, Oujda; (e) Faculté des Sciences, Université Mohammed V, Rabat, Morocco
- 136 DSM/IRFU (Institut de Recherches sur les Lois Fondamentales de l'Univers), CEA Saclay (Commissariat à l'Energie Atomique), Gif-sur-Yvette, France
- 137 Santa Cruz Institute for Particle Physics, University of California Santa Cruz, Santa Cruz CA, United States of America
- 138 Department of Physics, University of Washington, Seattle WA, United States of America
- 139 Department of Physics and Astronomy, University of Sheffield, Sheffield, United Kingdom
- 140 Department of Physics, Shinshu University, Nagano, Japan
- 141 Fachbereich Physik, Universität Siegen, Siegen, Germany
- 142 Department of Physics, Simon Fraser University, Burnaby BC, Canada
- 143 SLAC National Accelerator Laboratory, Stanford CA, United States of America
- 144 (a) Faculty of Mathematics, Physics & Informatics, Comenius University, Bratislava; (b) Department of Subnuclear Physics, Institute of Experimental Physics of the Slovak Academy of Sciences, Kosice, Slovak Republic
- 145 (a) Department of Physics, University of Johannesburg, Johannesburg; (b) School of Physics, University of the Witwatersrand, Johannesburg, South Africa
- 146 (a) Department of Physics, Stockholm University; (b) The Oskar Klein Centre, Stockholm, Sweden
- 147 Physics Department, Royal Institute of Technology, Stockholm, Sweden
- 148 Department of Physics and Astronomy, Stony Brook University, Stony Brook NY, United States of America
- 149 Department of Physics and Astronomy, University of Sussex, Brighton, United Kingdom
- 150 School of Physics, University of Sydney, Sydney, Australia
- 151 Institute of Physics, Academia Sinica, Taipei, Taiwan
- 152 Department of Physics, Technion: Israel Inst. of Technology, Haifa, Israel
- 153 Raymond and Beverly Sackler School of Physics and Astronomy, Tel Aviv University, Tel Aviv, Israel
- 154 Department of Physics, Aristotle University of Thessaloniki, Thessaloniki, Greece
- 155 International Center for Elementary Particle Physics and Department of Physics, The University of Tokyo, Tokyo, Japan
- 156 Graduate School of Science and Technology, Tokyo Metropolitan University, Tokyo, Japan
- 157 Department of Physics, Tokyo Institute of Technology, Tokyo, Japan
- 158 Department of Physics, University of Toronto, Toronto ON, Canada
- 159 (a) TRIUMF, Vancouver BC; (b) Department of Physics and Astronomy, York University, Toronto ON, Canada
- 160 Institute of Pure and Applied Sciences, University of Tsukuba, Ibaraki, Japan
- 161 Science and Technology Center, Tufts University, Medford MA, United States of America
- 162 Centro de Investigaciones, Universidad Antonio Narino, Bogota, Colombia
- 163 Department of Physics and Astronomy, University of California Irvine, Irvine CA, United States of America
- 164 (a) INFN Gruppo Collegato di Udine; (b) ICTP, Trieste; (c) Dipartimento di Fisica, Università di Udine, Udine, Italy
- 165 Department of Physics, University of Illinois, Urbana IL, United States of America
- 166 Department of Physics and Astronomy, University of Uppsala, Uppsala, Sweden
- 167 Instituto de Física Corpuscular (IFIC) and Departamento de Física Atómica, Molecular y Nuclear and Departamento de Ingeniería Electrónica and Instituto de Microelectrónica de Barcelona (IMB-CNM), University of Valencia and CSIC, Valencia, Spain
- 168 Department of Physics, University of British Columbia, Vancouver BC, Canada
- 169 Department of Physics and Astronomy, University of Victoria, Victoria BC, Canada
- 170 Waseda University, Tokyo, Japan

- ¹⁷¹ Department of Particle Physics, The Weizmann Institute of Science, Rehovot, Israel
- ¹⁷² Department of Physics, University of Wisconsin, Madison WI, United States of America
- ¹⁷³ Fakultät für Physik und Astronomie, Julius-Maximilians-Universität, Würzburg, Germany
- ¹⁷⁴ Fachbereich C Physik, Bergische Universität Wuppertal, Wuppertal, Germany
- ¹⁷⁵ Department of Physics, Yale University, New Haven CT, United States of America
- ¹⁷⁶ Yerevan Physics Institute, Yerevan, Armenia
- ¹⁷⁷ Domaine scientifique de la Doua, Centre de Calcul CNRS/IN2P3, Villeurbanne Cedex, France
- ^a Also at Laboratório de Instrumentação e Física Experimental de Partículas - LIP, Lisboa, Portugal
- ^b Also at Faculdade de Ciências and CFNUL, Universidade de Lisboa, Lisboa, Portugal
- ^c Also at Particle Physics Department, Rutherford Appleton Laboratory, Didcot, United Kingdom
- ^d Also at CPPM, Aix-Marseille Université and CNRS/IN2P3, Marseille, France
- ^e Also at TRIUMF, Vancouver BC, Canada
- ^f Also at Department of Physics, California State University, Fresno CA, United States of America
- ^g Also at Faculty of Physics and Applied Computer Science, AGH-University of Science and Technology, Krakow, Poland
- ^h Also at Department of Physics, University of Coimbra, Coimbra, Portugal
- ⁱ Also at Università di Napoli Parthenope, Napoli, Italy
- ^j Also at Institute of Particle Physics (IPP), Canada
- ^k Also at Department of Physics, Middle East Technical University, Ankara, Turkey
- ^l Also at Louisiana Tech University, Ruston LA, United States of America
- ^m Also at Group of Particle Physics, University of Montreal, Montreal QC, Canada
- ⁿ Also at Institute of Physics, Azerbaijan Academy of Sciences, Baku, Azerbaijan
- ^o Also at Institut für Experimentalphysik, Universität Hamburg, Hamburg, Germany
- ^p Also at Manhattan College, New York NY, United States of America
- ^q Also at School of Physics and Engineering, Sun Yat-sen University, Guanzhou, China
- ^r Also at Academia Sinica Grid Computing, Institute of Physics, Academia Sinica, Taipei, Taiwan
- ^s Also at High Energy Physics Group, Shandong University, Shandong, China
- ^t Also at Section de Physique, Université de Genève, Geneva, Switzerland
- ^u Also at Departamento de Física, Universidade de Minho, Braga, Portugal
- ^v Also at Department of Physics and Astronomy, University of South Carolina, Columbia SC, United States of America
- ^w Also at KFKI Research Institute for Particle and Nuclear Physics, Budapest, Hungary
- ^x Also at California Institute of Technology, Pasadena CA, United States of America
- ^y Also at Institute of Physics, Jagiellonian University, Krakow, Poland
- ^z Also at Department of Physics, Oxford University, Oxford, United Kingdom
- ^{aa} Also at Institute of Physics, Academia Sinica, Taipei, Taiwan
- ^{ab} Also at Department of Physics, The University of Michigan, Ann Arbor MI, United States of America
- ^{ac} Also at DSM/IRFU (Institut de Recherches sur les Lois Fondamentales de l'Univers), CEA Saclay (Commissariat à l'Energie Atomique), Gif-sur-Yvette, France
- ^{ad} Also at Laboratoire de Physique Nucléaire et de Hautes Energies, UPMC and Université Paris-Diderot and CNRS/IN2P3, Paris, France
- ^{ae} Also at Department of Physics, Nanjing University, Jiangsu, China
- * Deceased